The role of alveolar macrophages in Influenza A infection

Christina Purnama

2013

Christina Purnama. (2013). The role of alveolar macrophages in Influenza A infection. Doctoral thesis, Nanyang Technological University, Singapore.

https://hdl.handle.net/10356/53722

https://doi.org/10.32657/10356/53722

NANYANG
TECHNOLOGICAL
UNIVERSITY

THE ROLE OF ALVEOLAR MACROPHAGES IN INFLUENZA A INFECTION

CHRISTINA PURNAMA

SCHOOL OF BIOLOGICAL SCIENCES

2013

THE ROLE OF ALVEOLAR MACROPHAGES IN INFLUENZA A INFECTION

CHRISTINA PURNAMA

School of Biological Sciences

A thesis submitted to the Nanyang Technological University
in partial fulfillment of the requirement for the degree of
Doctor of Philosophy

2013

ACKNOWLEDGEMENTS

I would like to express my sincere appreciation to all who have provided help and support throughout the project. They are:

- **Lord Jesus Christ** for His favor and blessing throughout my PhD journey.
- **Prof. Klaus Erik Karjalainen** for his patience, guidance and encouragement throughout the project.
- **Assoc. Prof. Christiane Ruedl** for her kind advices, guidance and great help in organizing resources for this project.
- **Dr. Sivasankar Baalasubramanian, Dr. Matheswaran Kandasamy, Hermi Rizal,** and **Poon Chu Ying** from SICS (Singapore Institute for Clinical Sciences) for their kind help in sharing with us Influenza-related materials and methods.
- **Dr. Piotr Tetlak** and **Arun Kumar** for assisting the microinjection together
- **Dr. Wu Zhihao** and **Loh Shuzk Cheng** for their tremendous help in recombineering related experiments.
- **Lucia Piva, Wang Qi, Ng See Liang, Sheng Jian Peng** for their help in optimizing and performing ES cell, lung staining, influenza, and qPCR experiments.
- **Other lab members**, for their various help. Their presence and encouragement in the lab brightens up my days.
- **My family: Anton Setiawan, Jenardi Purnama, Lie Yen Ling, Herry Setiawan, Rina Soesanty, Jessica Purnama**, **Marcella Purnama**, and **Andri Setiawan** for their support and prayers.
- **My friends: Yenny Effendy, Katsudon KTB members, FA Anda** and **TLG ministry** for their listening ears and encouragements during hard times.
- **To Nanyang Technological University** for the research scholarship, and also to **Ministry of Education** for the Tier1 grant. With these financial supports this research has been made possible.
- Last but not least, those whose names have not been mentioned for their various forms of assistance

TABLE OF CONTENTS

SUMMARY

Macrophages are innate immune cells that function as the first line defense against microorganisms. My project aims to generate transgenic models by which I can ablate macrophages *in vivo* in order to study their contribution in different experimental situations. In particular, I am harnessing Influenza A mouse model to better elucidate the roles of specific immune cell subsets.

I am exploiting bacterial artificial chromosome transgenesis approach to incorporate the gene coding for human diphtheria toxin receptor (DTR) under the control of specific myeloid subset marker. The construct was then electroporated into BALB/c embryonic stem cells, from which transgenic mice were derived. Diphtheria toxin injection into the transgenic mice will deplete specific subsets where the myeloid marker of interest is expressed. I selected CD169 (also known as Siglec1 or Sialoadhesin) as the targeted marker due to its macrophage-specific expression patterns. CD169 is a sialic acid binding Ig-like lectin which mediates macrophage adhesive function. This molecule is strongly expressed by specific populations of tissue macrophages in the spleen and lymph node; namely by marginal zone metallophilic macrophages and subcapsular sinus macrophages, respectively. Recent data highlights the importance of CD169 macrophages in concentrating pathogens to prevent systemic spread, eliciting Interferon-I responses upon viral infection, and even presentation of antigen to B cells in the lymph nodes. Hence, CD169-DTR mouse is an attractive tool to study role of tissue macrophage subsets in numerous settings.

Currently, I have tested and characterized CD169-DTR mice generated in our laboratory. Intra-peritoneal administration of DT ablates tissue macrophages in different lymphoid and peripheral organs such as spleen, lymph nodes, bone marrow, and lungs. Lung and broncho-alveolar lavage analysis reveals >90% depletion of alveolar macrophages ($CD11c^{+}CD11b^{lo}F4/80^{+}$ cells) upon DT injection in CD169-$DTR^{+/-}$ mice. I then infected control and DT-treated CD169-DTR mice with mild dose of mouse-adapted Influenza A strain PR8. Collectively, my results suggest that alveolar macrophages play an essential role in executing antiviral immune responses in the pulmonary environment. Future research will be conducted to understand how the alveolar macrophages control different components of antiviral immunity. Knowledge provided by studying the roles of alveolar macrophage using CD169-DTR mice will further our understanding in influenza immunity and benefit translational research.

ABBREVIATIONS

AE2	alveolar epithelial type II
AEC	3-Amino-9-ethylcarbazole
AM	alveolar macrophage
APC	allophycocyanin (fluorophore)
APC	antigen presenting cell
BAC	bacterial artificial chromosome
BALF	broncho-alveolar lavage fluid
Batf3	basic leucine zipper transcription factor, ATF-like 3
BM	bone marrow
BST	bone marrow stromal antigen
C/EBP	CCAAT enhancer binding protein
CCL	Chemokine (C-C motif) ligand
CCR	C-C chemokine receptor
CD	Cluster of distribution
cDNA	complementary DNA
CTL	cytotoxic T lymphocyte
CX3CR	Chemokine (C-X3-C motif) receptor
DC	dendritic cell
dLN	draining lymph node
DMEM	Dulbecco's modified Eagle medium
DMSO	dimethyl sulfoxide
DNA	deoxyribonucleic acid
DT	diphtheria toxin
DTR	diphtheria toxin receptor
DTSRB	DTR-2A-tomato-synthetic poly A-RecA-blasticidin
E. coli	Escherichia coli
EDTA	ethylenediamineteetraacetic acid
EGF	epidermal growth factor
EGFP	enhanced GFP
ES cell	embryonic stem cell
FACS	fluorescent-activated cell sorter
FCS	fetal calf serum
FITC	fluorescein isothiocyanate
FSC	forward scatter

GFP	green fluorescent protein
GM-CSF	granulocyte macrophage-colony stimulating factor
HA	hemagglutinin (influenza protein)
HA	homology arm
HoxB4	HomeoBox 4
HRP	horseradish peroxidase
i.p.	intraperitoneal
i.t.	intratracheal
IAV	influenza A virus
IFN	interferon
Ig	immunoglobulin
IL	interleukin
iNOS	inducible nitric oxide synthase
IMDM	Iscove's modified Dulbecco's medium
IRES	internal ribosome entry site
ISG	IFN-stimulated genes
LB medium	Luria Bertani medium
LTR	long terminal repeat
mAb	monoclonal antibody
MARCO	macrophage receptor with collagenous structure
MBL	mannan-binding lectin
MCP	monocyte chemotactic protein
M-CSF	mononuclear phagocyte colony-stimulating factor
MDCK cell	Madin-Darby canine kidney cell
MEF	mouse embryonic fibroblast
MEF	mouse embryonic fibroblast
MFG-E8	milk fat globule-EGF factor 8
mGJA5	mouse gap junction channel protein alpha 5
MHC	major histocompatibility complex
moDC	monocyte-derived DC
mRNA	messenger RNA
MZM	marginal zone metallophilic
NA	neuraminidase
NB4	Nup-HoxB4
NDV	Newcastle disease virus
Neo	neomycin
NK	natural killer

NO	nitric oxide
NOD	nucleotide binding oligomerization domain
NOD/SCID	nonobese diabetic severe combined immunodeficiency
OCT	optimal cutting temperature
p.i.	post-infection
PAMPs	pathogen associated molecular patterns
PBS	phosphate buffered saline
PCR	polymerase chain reaction
pDC	plasmacytoid dendritic cell
PE	phycoerythrin
PFA	paraformaldehyde
PFU	plaque forming unit
PRRs	pattern recognition receptors
qPCR	quantitative PCR
RBC	red blood cell
RNA	ribonucleic acid
RNP	ribonucleoprotein
SCF	stem cell factor
SCID	severe combined immunodeficiency
SCS	sub-capsular sinus
SDS	sodium dodecyl sulfate
SIGN	specifi intercellular adhesion molecule 3-grabbing nonintegrin
SIRPα	signal-regulatory protein alpha
SPF	specific pathogen-free
SSC	side scatter
ssRNA	single-stranded RNA
TCR	T cell recognition
TE buffer	Tris-EDTA buffer
Tip DC	TNF-iNOS DC
TLR	Toll-like receptor
TNF	tumor necrosis factor
TPCK	tosyl phenylalanyl chloromethyl ketone
TRAIL	tumor necrosis factor-related apoptosis-inducing ligand
VSV	vesicular stomatitis virus
WT	wild type
YFP	yellow fluorescence protein

CHAPTER 1

INTRODUCTION

1.1. The Influenza A Virus

Influenza A virus (IAV) belongs to *Orthomyxoviridae*, a family of negative sense, single strand RNA viruses. Unlike other groups of influenza virus, (influenza B and C virus) that are associated solely with human disease, influenza A virus infect hosts ranging from mammalian to avian species; causing seasonal, acute, and highly contagious outbreaks. Influenza A subtypes are classified based on the virus' major surface envelope glycoproteins, namely hemagglutinin (HA) and neuraminidase (NA). So far, 19 HA variants and 9 NA variants are known to date [1, 2].

The genome of IAV comprises of 8 gene segments (about 13.6 kb) that encodes 11 proteins; namely HA, NA, NP, M1, M2, NS1, NS2, PA, PB1, PB1-F2 and PB2 [3]. Schematic diagram of the virus is depicted in Fig. 1.1; while summary of the viral proteins' functions is presented in table 1.1. The infection cycle starts when IAV HA protein binds to sialic acid residues on the epithelial cell lining the respiratory tract followed by proteolytic cleavage of HA, triggering endocytosis [4]. In the endosome, M2 ion channel mediates acidification of the viral core, followed by fusion of the viral envelope to the vacuole membrane which is mediated by conformational change of the cleaved hydrophobic HA residues [5, 6]. These series of events lead to disassembly and release of the viral RNA and proteins; which are then transported into the cell nucleus. RNA polymerase then transcribes mRNA from the viral RNA, which is subsequently exported into the cytoplasm for translation. The transcription machinery could eventually switch to viral genomic RNA synthesis, and the product will be packaged with RNA-dependent polymerase and viral core proteins. These components will be exported out to the cytoplasm and packaged into new virions on the plasma membrane. Virions will bud from the host cell, acquiring HA and NA proteins on the host cell phospholipid membrane. Lastly, NA cleaves the sialic acid residues to facilitate virus release from the infected cell surface; thus aiding virus spreading [3, 7].

RNA Segment	Protein	Molecular Weight (KDa)	Function
1	PB2	86	A basic component of viral polymerase subunit, snatches the host 5'cap structure to prime viral mRNA synthesis
2	PB1	87	A basic viral polymerase subunit, interacts with PA
	PB1-F2	11	This protein, which is generated from alternative open reading frame, inhibits host mitochondrial function and induces apoptosis of host immune cell.
3	PA	83	An acid viral polymerase subunit, acts as endonuclease in its interaction with PB1
4	HA	64	Hemagglutinin mediates viral attachment to host cell surface receptors and membrane fusion
5	NP	56	Nucleoprotein is a polymerase complex that mediates cap binding (encapsidation) of RNA
6	NA	50	Neuraminidase is a sialidase which facilitates release of virions from infected cells by cleavage of sialic acid
7	M1	28	This matrix protein has a role in viral assembly, giving structural support to the virion.
	M2	11	This matrix protein is an ion channel with role during viral entry, i.e. by dissociating viral RNP from M1 during uncoating process
8	NS1	26	This non-structural protein has role in RNA splicing and translation, could antagonize the host immune responses such as IFN
	NS2	14	A non-structural protein with role in nuclear export of ribonucleoprotein complex

Table 1.1. Function of proteins encoded by 8 Influenza viral segments.
Adapted from Hale et al., 2010 [7]

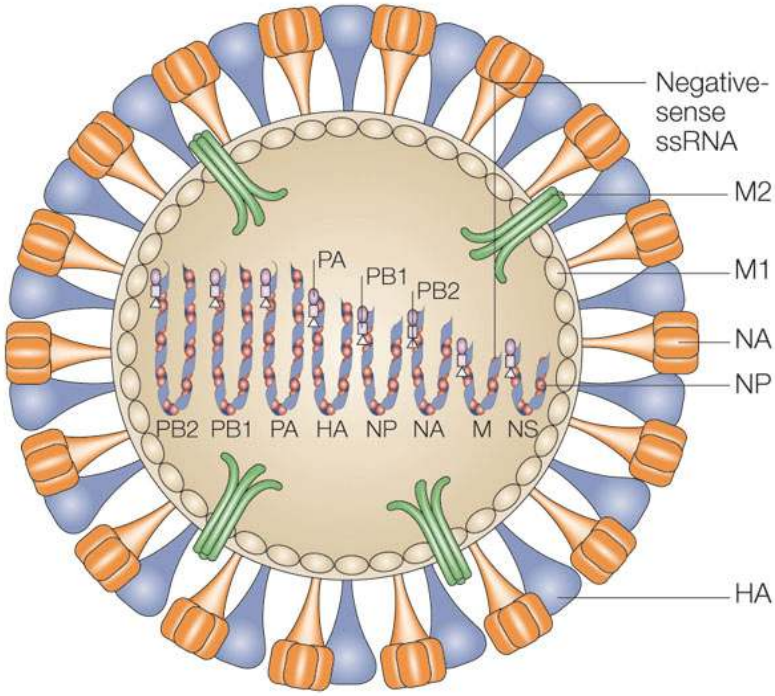

Figure 1.1. Schematic diagram of Influenza A virus. HA and NA are glycoproteins found embedded in the viral envelope. Viral genome comprises of RNA associated with NP, PA, PB1, and PB2 forming ribonucleoprotein (RNP) complexes. M1 protein is associated with both viral envelope and ribonucleoprotein complexes. Adapted from Horimoto and Kawaoka, 2005 [8].

In the past, IAV has caused a number of devastating pandemic outbreaks. The H1N1 Spanish flu alone killed 20-50 million people in 1918, while around one million deaths were caused by 1957 H2N2 Asian flu and 1963 Hong Kong flu [9, 10]. More recently, IAV is responsible for H5N1 avian flu and H1N1 2009 outbreaks. In addition, every year IAV causes seasonal outbreaks, resulting in 3 to 5 million cases of respiratory illness and also 250,000-500,000 deaths worldwide [11]. Infection is typically transmitted via airborne droplets and affects the upper respiratory tract. Common disease manifestations include fever, headache, cough, sore throat, anorexia and malaise. However, young children and elderly are more susceptible to Influenza A disease complications, such as pneumonia, secondary bacterial infections, and even death. [12, 13]

The ability of IAV to evolve rapidly is attributed to a process termed as antigenic drift and antigenic shift. Antigenic drift is the ability of IAV to reassort surface antigens and exchange genomes between different subtypes, which

gives rise to novel progenies. IAV genome also undergoes high mutation rate due to the low fidelity of its RNA dependent RNA polymerase, transcriptional error rate is 1 out of 10^5 bases [14]. This results in antigenic drift – whereby the constantly mutating viral antigens could enhance viral tropism or facilitate evasion from the host immune response.

Emergence of a novel highly infectious IAV strain will be a major public threat, leaving us with little or no protective immunity against new variant. Therefore, to improve on vaccination strategies, we need to understand the specific roles and interplay of immune cells in influenza A immunity.

1.2. Innate and adaptive immunity against influenza A virus infection

1.2.1. Innate immune responses

Innate immune defense mechanisms are non-specific and some components are conserved amongst mammals, lower vertebrates and even invertebrates. However, no memory or long-lasting protection is mediated by innate immune responses. There are several different components of innate immune system, namely: physical barriers, pattern recognition receptors (PRRs), antimicrobial mediators, cytokines, and innate immune cells.

The first line of innate protection is formed by physical barriers consisting of mucus and epithelial layers. The lung epithelium's cilia movement pushes the mucus trapped pathogens out of the airway. The mucus contains PRRs which can block virus binding to epithelial cells [15, 16]. These PRRs recognize microbial antigens that share pathogen associated molecular patterns (PAMPs). Examples of soluble PRRs are Collectins, and mannan-binding lectin (MBL). Other types of PRRs are Toll-like receptors (TLRs), which mediate pathogens' detection on cell surfaces (e.g. TLR 1, 2, 4, 5, 6, 10, and 11) or inside intracellular endosomes (TLRs 3, 7, 8, and 9). Meanwhile, RIG-1 (retinoic acid inducible gene -1), MDA-5 (melanoma differentiation associated gene-5), NOD-1/2 (nucleotide binding oligomerization domain-1/2) and other C-type lectins (e.g. dectin-1) can detect PAMPs in the cytosol [17, 18].

Moreover, there are soluble antimicrobial mediators such as complement, lysozyme, lactoferrin, and defensins. Upon binding and activation,

complement system mediates opsonization, by which phagocytes will clear and lyse complement- bound pathogens.

The most potent innate antiviral cytokine is the type I Interferon (IFN-I). IFNα/β are able to concert initiation of transcription of IFN-stimulated genes (ISG) to limit virus infection [19]. IFN-I is secreted by epithelial cells and innate immune cells like monocytes, macrophages, and plasmacytoid dendritic cells (pDCs). Moreover, IFN is also able to enhance dendritic cell (DC) major histocompatibility complex (MHC) class I expression as well as to promote survival and development of effector functions by activated CD8 T cells; thus promoting cross-priming [20, 21]. The Influenza NS1 protein has evolved to inhibit IFN-I production by infected cells [22-25]. NS1 protein has been shown to inhibit a number of transcription factors essential for the transcription of IFN-β, and also disrupt the nuclear export of host mRNA into the cytosol [22, 26]. Besides, animals devoid of either IFN-I or downstream IFN induced-genes clear virus slower and are more susceptible to IAV-induced lethality [27, 28]

Another cytokine, IFN-γ (type II interferons) functions to activate macrophages, and is mainly produced by T cells and NK cells. Besides, Interleukins (IL) group of cytokines could act locally or systemically to effect innate and adaptive immune response. Interleukins can have pro-inflammatory, e.g. IL-1, IL-6, and IL-12, or anti-inflammatory effects, e.g. IL-10.

Finally, there are innate immune cells that mediate early responses against pathogen invasion, namely dendritic cells, macrophages, neutrophils, and natural killer cells. The last three cell types are the main cell populations in the pulmonary infiltrates. Macrophages and dendritic cells are myeloid cells with roles in innate immune response as well as in initiation or sustenance of adaptive immunity. Further description of the roles of dendritic cells and macrophages in IAV infection are elaborated in section 1.3.

Natural killer (NK) cells are large innate cytotoxic lymphocytes that mediate protection by producing cytokines (IFN-γ and TNF-α) and direct cytotoxicity of virus infected cells [29]. Upon activation by proinflammatory cytokines (e.g. IFN-α) they could lyse target cells by either creating membrane pores through perforins or granzymes; or by activating apoptosis signalling of target cells [30]. Recognition of Influenza A-infected cells is mediated by NCR1, a murine

receptor related to human NKp46 which recognize the influenza HA proteins [31-34]. Mutation or depletion of these NK receptors aggravates the influenza disease [34-36]. In addition, NK cells can mediate killing of infected cells by antibody dependent cell-mediated cytotoxicity (ADCC) [37, 38]. NK cells are able to modify isotype switching, especially associated to IgG2a, an antibody isotype that is known to drive antibody dependent cytotoxicity (ADCC), initiate complement fixation, and bind to Fc receptors on phagocytes. IFN-γ produced by activated NK cells may feed forward this response, for in the absence of IFN-γ, significant reduction of virus-specific IgG2a level was observed [39, 40]. Notably, the role of NK cells in antibody switching was demonstrated in polyoma virus study. The virus display sufficiently repetitive cell surface determinant, thus T cell help is not required for B cell activation. The IgG2a response in the mice lacking both T and NK cells are significantly lower than mice deficient in T cells alone [41].

In addition, neutrophils, which rapidly infiltrate the lung together with NK cells, are crucial because they eat debris and secrete pro-inflammatory cytokines that limit viral replication [42, 43].

1.2.2. Adaptive immune responses

Adaptive immune responses comprise of antigen-specific T and B cells. The adaptive immunity is activated and controlled by innate immunity. It develops in the later stage of infection and can form memory or lasting protection against recurring pathogen.

1.2.2.1. T cells

T lymphocytes, CD4 and CD8 cells, play a major role in adaptive immunity as an important effector arm by eliciting cell-mediated immunity against IAV infection.

CD4 T cells, also known as T helper cells, have no cytolytic activity like CD8 T cells. Antigen-specific signalling via T cell receptor (TCR) recognition of MHC-II presented antigen is required to activate CD4 T cell. Upon IAV infection, $CD4^+$ T cells undergo clonal expansion and differentiation in the draining

lymph nodes. On the peak of this response (at 6-7 days post-infection), CD4 T cells produce Th1 cytokines such as IFN-γ and TNF-α which will stimulate macrophages and cytotoxic T lymphocytes (CTLs) effector functions [44]. This polarization into Th1-type cells is driven by IL-12 cytokines produced by DCs. CD4 T cells could also regulate inflammation through IL-10 secretion [45]. Although CD4 T cells are not required for primary CTL response, secondary CD8 response is attenuated without CD4 T cells during the primary infection [46, 47]. CD4 T cells are also required for optimal CD8 T cells recruitment and CTL viral clearance [47]. More importantly, $CD4^+$ T cells indirectly mediate protection by helping B cells maturation (explained further in section 1.2.2.2.). After clearance of IAV infection, some activated CD4 T cells become memory cells, but these CD4 memory T cells decrease in number faster than CD8 memory T cells [48].

CD8 T cells (or CTLs) mediate clearance of virus by killing the infected cells, mediated by granzyme, perforin exocytosis, or Fas mediated apoptosis [49-52]. In mice model depleted of CD8 T cells, clearance of influenza virus is delayed, leading to higher viral titres and increased mortality [53]. Within the first week or so of IAV infection, naïve CD8 T cells in the lymph node undergo initial priming and expansion [54, 55]. Mature CTLs exit to the lung such that at the peak of primary infection, 30-90% (depending on the experimental model) of the lung-infiltrating lymphocytes are cytotoxic, mostly recognizing epitopes of IAV HA or NP proteins [56-58]. In addition, CTLs also produce pro-inflammatory cytokines IFN-γ and TNF-α in large amounts, thus helping in recruiting leukocytes to the inflamed lung [54]. Moreover, CD8 T cells regulate inflammation by producing IL-10 [45]. After clearance of IAV, some effector CTLs gradually become memory CD8 cells and circulate in both lymphoid and non-lymphoid tissues [59]. Upon re-exposure to the same antigen, memory CTLs are recruited and expand in lymph node, rapidly mediating viral clearance [58, 60].

1.2.2.2. B cells

B cells secrete natural, low-affinity antibodies that function as first line of antibody-mediated defense that restrict virus dissemination [61]. Nevertheless, effective humoral immunity during infection is provided by antibodies secreted from mature B cell lymphocytes (plasma cells) against specific antigen [62].

Protective role elicited by B cells by producing high titer of neutralizing antibodies against HA and NA epitopes is the main vaccination strategy. $CD4^+$ T helper cells promotes B-cell differentiation and class switching; thus $CD4^+$ T cell expansion correlates with vaccine protection [63-65]. Importance of B cells in recovery from IAV infection is demonstrated by the fact that mice deficient of B cells display higher mortality rate than the wild type [66, 67]. Conversely, IAV-specific antibodies mediate protection when passively transferred into severe combined immunodeficiency (SCID) mice [68, 69]. Following infection, B cell memory as well as long lived plasma cells (antibody secreting cells) are established, which further develop in bone marrow, and continuously produce antibodies to mediate protection. Additionally, quiescent memory B cells develop in the lungs or lymph nodes, ready to differentiate into plasma cells upon re-infection [70].

1.3. Roles of dendritic cells and macrophages in influenza A virus infection

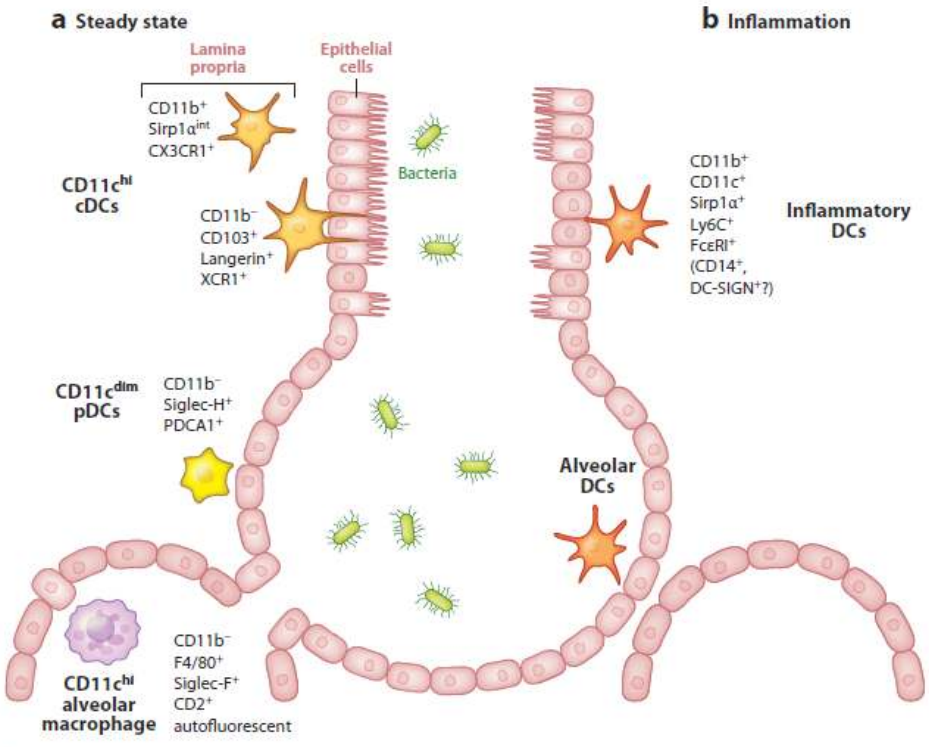

Figure 1.2. Lung myeloid cell subsets during steady state and inflammation in mice. (a) In the steady state, $CD11c^{hi}$ CD11b and CD103 DCs reside in the lamina propria and epithelial layer respectively. Also, pDC can be found in conducting airways, while the alveolar macrophages can be found in the alveolar spaces. (b) In the course of inflammation, additional $CD11b^+$ monocyte-derived DCs are recruited to the lungs. Adapted from Lambrecht et al., 2012 [71].

1.3.1. Dendritic cells

DCs are well known as potent antigen presenting cells (APCs) which bridge innate and adaptive immune responses [72, 73]. Also, distinctive DC morphology and surface markers allow them to be distinguished from macrophages [74, 75]. In our body, DC could be found in lymphoid, such as spleen and lymph nodes, as well as in non-lymphoid tissues, such as lung and skin. Lung DCs are believed to originate from either common myeloid progenitors or common lymphoid progenitors in the bone marrow. Committed precursors then migrate from bone marrow to the blood and enter the lung, giving rise to lung DCs [76, 77].

Study in mice reveals two main subsets, namely $CD11b^{-/lo}CD103^{+}$ (CD103 DC) and $CD11b^{hi}CD103^{-}$ (CD11b DC) respiratory DCs [78, 79]. Both mainly reside in the lung parenchyma in the steady state. CD103 DCs populate also the conducting airway epithelial layers and extend cellular processes between basal epithelial spaces. CD103 DCs are also known to express langerin molecule and to depend on Batf3 transcription factor for their development [80, 81]. Upon infection, they are able to migrate to lung draining lymph nodes (dLNs) and initiate adaptive immune responses [82, 83]. CD11b DCs can be found beneath, in the lamina propria, expressing signal-regulatory protein alpha (SIRPα) and chemokine (C-X3-C motif) receptor 1 (CX3CR1) [80, 84]. Similar with CD103 DCs, CD11b DCs carry antigen, and migrate to dLNs [85, 86]. In the initial stage of influenza infection, CD103 DCs demonstrated significant priming ability, while CD11b DC is suggested to have a role in later phase of infection [78-80]. These lung DCs induce cytotoxic T lymphocyte effector functions that are critical for IAV clearance [87].

Another population characterized as immature monocyte-derived DCs ($MHC\text{-}II^{low}CD11c^{low}$) are poor activators of T cell responses [83]. They reside in lung interstitium and can give rise to mature DC [88]. During inflammation, exudate monocytes can also differentiate into inflammatory DC and CD11b DC [89]. Activated monocytes can upregulate CD11c and MHCII [90, 91] as well as present antigens upon stimulation [92, 93]. Because these populations share similar markers, it is often difficult to distinguish between DC, monocytes and macrophages and dissect their specific contribution *in vivo* [94].

Additionally, a unique dendritic cell population known as pDCs reside in the conducting airways and lung parenchyma [95]. This population expresses Siglec-H, bone marrow stromal antigen-2 (BST2), and is $CD11c^{dim}$ [78, 96]; and also has the capacity to produce large amounts of type I interferon during infection [97]. It has been shown that lung pDCs are able to transport antigens to the drain dLNs but are not potent activators of naïve T cells [98].

1.3.2. Macrophages

Macrophages are white blood cells that function as the first line defense in innate immune system as well as initiating adaptive immunity. Macrophages were first discovered by Metchnikoff and Ehrlich with regards to their role as phagocytes, which are important for removal of dying cells and microbes [99]. Studies of macrophage development revealed monocytes as macrophage precursors in steady state or inflammation (Fig. 1.3). Monocytes circulate in blood and are ready to elicit rapid response to infection or tissue damage. They are heterogeneous and able to differentiate into long-lived resident tissue macrophages such as Kupffer cells, splenic and alveolar macrophages (Fig. 1.4). Tissue-resident macrophages make up 10-15% of numerous tissues; and they maintain the tissue homeostasis by monitoring tissue's state and provide growth factors according tissue needs [100, 101]. Macrophages recognize different pathogens with their diverse surface receptors and subsequently engulf them for killing. Besides, macrophages secrete chemokines and cytokines to induce inflammation, helping to orchestrate the adaptive immune response. Later, macrophages were also discovered to present antigen for activated T-cells. Hence, macrophage is an important cell linking the innate and adaptive responses of the immune system.

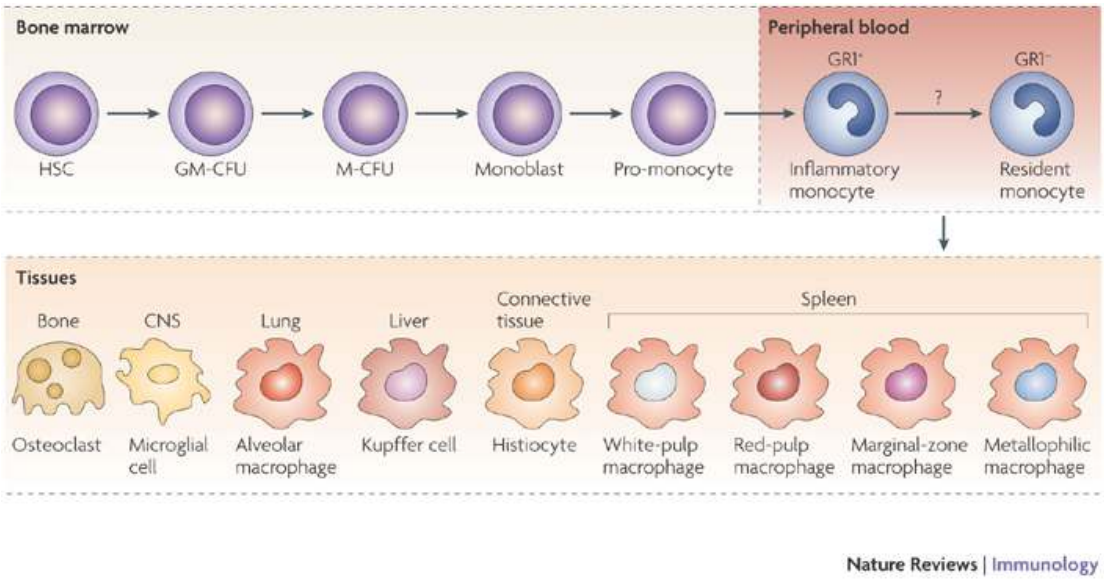

Figure 1.3. Development and heterogenerity of monocyte and macrophages. Adapted from Mosser et al., 2008 [102].

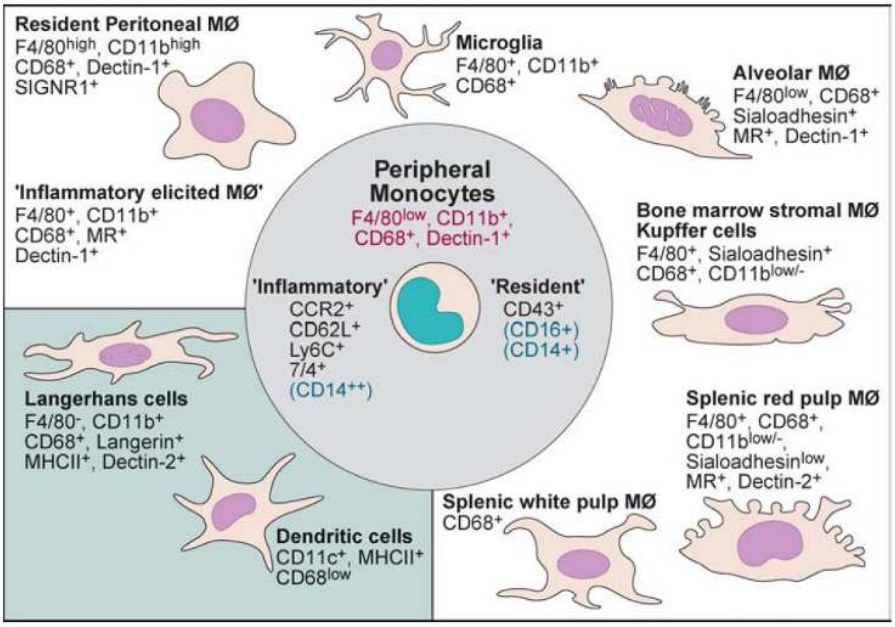

Figure 1.4. Heterogeneity of macrophages phenotype.
Adapted from Taylor et al., 2005 [103].

There are at least two populations of macrophages present in the airways and lung parenchyma during normal homeostasis: the ‘alveolar macrophages’ (AMs) which are found in the alveolar spaces and ‘interstitial macrophages’ which reside in the pulmonary interstitium. Upon inflammation such as in IAV infection, lung will be infiltrated by ‘exudate macrophages’ derived from blood-borne precursors. However, a number of previous studies did not differentiate between these populations, and often the terms ‘alveolar macrophages’ or

'lung macrophages' were used loosely to refer to lung macrophages in general. Hence, we should exercise caution when interpreting previous data.

The AMs are found in the alveolar spaces and conducting airways as the predominant APC population during physiological conditions [104].This cell type is one of the first pulmonary immune cells studied *in vitro* and is thought to have a role in regulation of homeostasis [105]. In resting state, AM produces low level of inflammatory cytokines and exhibit less phagocytosis activity than macrophages in other tissues [105]. AM is also shown to suppress the initiation of adaptive immune response, for in vivo depletion of AM via clodronate liposomes cause excessive inflammatory response towards harmless antigens [106-109]. Others reported that upon appropriate stimulation, AM overcome its inhibitory phenotype, become highly phagocytic, and release pro-inflammatory cytokines and chemokines [109-112].
During homeostasis, another type of macrophages resides in the pulmonary interstitium with $CD11b^{+}$ $CD11c^{-}$ phenotype. This population is termed interstitial macrophage and is derived from blood $CCR2^{+}$ monocytes [86, 113, 114]. However, not much is known about the specific role of this population in IAV infection.

Macrophages are prone to IAV infection, but they undergo quick apoptosis before virus progenies are released from the cell [115, 116]. Increase of anti-viral cytokines (IL-1β, IL-6, TNF-α, IFNα/s) and chemokines (Chemokine C-C motif ligand 5/CCL5, monocyte chemotactic protein-1/MCP-1) expression was observed in the influenza-infected macrophages [115]. Previous studies have described that lung macrophages suppresses DC maturation by producing nitric oxide (NO) [106, 108].

There is some evidence that upon IAV infection, these cells could transport antigens from lungs to the draining lymph nodes [83], although it is still unclear about their importance in initiation of adaptive response. This population is shown to expand in response to IAV infection, and is suggested to play a role as APC for activated T cells in the lungs [86, 113]. Both influx of blood monocyte precursors or local macrophage proliferation may contribute to the observed increase of macrophages during IAV infection [117]. The inflammatory monocytes are recruited via C-C chemokine receptor type 2/CCR2 (receptor for MCP-1/CCL2 ligand produced largely by alveolar

epithelial cells) [118, 119] and are capable of differentiating into monocyte-derived DC (moDC/inflammatory DC) and inflammatory exudate macrophages [86, 119-122]. These exudate macrophages may eventually become the precursors of lung resident AMs with suppressor phenotype, and they contribute in restoring homeostasis [123, 124].

Different modes of activation can lead to two types of functionally characterized macrophages (M1 and M2) [125, 126]. Stimulation by IFN-y and TLR ligands lead to M1 cells that upregulate MHC class II, CD86 co-stimulatory molecules, and secrete cytokine IL-12; hence M1 cells support Th1 driven immune responses [125-128]. The production of inducible nitric oxide synthase (iNOS) is another hallmark of M1 macrophages [126]. This type of activation is essential for cell-mediated immunity to intracellular pathogens. On the other hand, the alternative M2 activation is induced by different set of signals which includes IL-4, IL-13, and TGF-β [125, 126]. M2 macrophages are associated with promotion of anti-inflammatory responses, tissue repair, and chronic inflammation.

The exudate macrophages that are recruited upon influenza infection are likely to conform with M1 phenotype for they respond to lung injury and secrete pro-inflammatory cytokines. On the other hand, alveolar macrophages are likely skewed into M2 phenotype because of their known role in reducing inflammation and restoring the damaged lungs [129]. Nevertheless, not many studies categorize the lung macrophages subpopulations into M1 or M2 macrophages. These subpopulations express markers that do not associate with either M1 or M2 polarization profile exclusively [130].

Some groups attempted to study the effect of AM depletion in influenza A infection. Tumpey et al. treated BALB/c mice with clodronate liposomes to deplete macrophages prior to sublethal infection with 1918HA/NA:Tx91 recombinant virus; resulting in significant increase of virus titre and mortality [42]. The authors conclude that macrophages and neutrophils act primarily to control viral replication at the early stages of infection [42]. Most likely, it is the phagocytosis capacity of macrophages that contributes to the control of virus growth [131]. Another study by Kim et al. described the importance of AM in swine model of IAV infection [132]. Depletion of AM did not cause mortality, but did induce respiratory stress, increase of IL-10, and decrease of TNFα.

Moreover, reduced antibody and CD8 T cell responses were observed [132]. Others observed that inhibition of phagocytosis promoted viral growth and mortality [133], thus again suggesting phagocytosis as the key mechanism to clear apoptotic cells and further limit virus spread.

In addition, macrophages express Fc receptor that can mediate opsonophagocytosis and ADCC. Huber et al. assess the importance of these processes in influenza virus infection. In this study they first utilized an Fc receptor knockout mouse life, the $FcR\gamma^{-/-}$ mice, and observed that these mice were more susceptible to influenza infection even though similar Ig titers were observed [134]. They further exclude the NK and T cells for mice lacking both NK and T cells and inferred from *in vitro* data that the Fc receptor-mediated phagocytosis of opsonized virus particles by macrophages is necessary for an effective clearance of influenza virus infections [134]. Further in vivo study is needed to support this notion.

1.4. Quest for a better mouse model to study alveolar macrophages in influenza A virus infection

In order to study more specifically the roles of certain cell subsets, I believe that deleting the targeted subpopulation in vivo is the best approach. For achieving conditional and selective ablation of macrophage subpopulations, I employ human diphtheria toxin receptor-diphtheria toxin (DTR-DT) technology because this approach has several advantages that surpass other *in vivo* ablation techniques.

Several experimental approaches have been used to understand roles of AMs in vivo. One of the most popular method is *in vivo* administration of clodronate (chloromethylene diphosphonate), which have been widely utilized since 1980s to deplete macrophages [109, 135]. This compound is delivered by liposomes, which upon release, will induce cell suicide [136]. However, intravenous administration of this compound affects both macrophages and DC in spleen and liver because uptake is dependent on phagocytic activity of a cell [137]. Yet, this is one of the most effective methods to deplete mononuclear phagocytes in rodents [138]. Many studies to date have shown that up to 85% of AMs in broncho-alveolar lavage are depleted within 3 days

of clodronate administration [139-141]. However, there is a risk that it might as well affect monocytes, macrophages, and DCs [142].

Others attempted to transgenically express Fas under c-fms (colony stimulating factor-1 receptor), which depletes 70-95% of macrophages and DCs [143]. Also, antibodies against some macrophage markers, for example anti-Gr-1 monoclonal antibody (mAb), have been developed to target selected population [144]. However, these methods have limited selectivity and inducibility and also cause inflammation or side effects. Another potential mouse model to study AMs is the granulocyte-macrophage colony-stimulating factor knockout (GM-CSF$^{-/-}$). These mice lack of AM and suffer from alveolar proteinosis (unpublished observation and [145]).

Recently, inducible ablation by using the human diphtheria toxin receptor-diphtheria toxin system (DTR-DT system) is recognized as the gold standard to deplete cell subsets *in vivo*. DT is produced by *Corynebacterium diphtheriae* and consists of A and B subunit. DTR itself is a membrane-anchored form of heparin-binding epidermal growth factor-like growth factor. Upon binding of DTR to the B subunit, internalization of A subunit will occur via receptor-mediated endocytosis [146]. Subsequently, protein translation in the cytosol will be inhibited and cell will die by apoptosis [147-149]. The toxin is very potent so that a single DT-A entry into the cell is enough to induce cell death [150]. Depletion strategy by using DT technology is based on difference in DT-DTR affinity between murine cells and human cells (Fig 1.5). The three amino acid differences of rodent DTR prevents effective binding of the DT-B subunit; causing mice to be 10^3–10^5 times more resistant to DT than human [149]. Therefore, transgenic expression of the human or simian DTR under specific cell or tissue promoter can mediate targeted depletion *in vivo*.

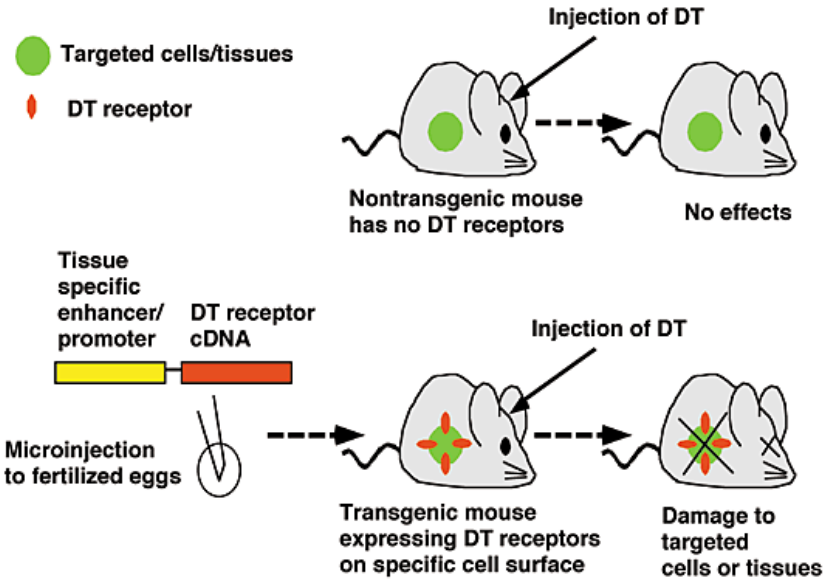

Figure 1.5. Schematic illustration of DTR-DT system.
Adapted from Saito et al. 2001 [149]

The first advantage of using this model is its inducibility. Depletion could be done by simply injecting the toxin to mice at the desired time point. Thus, it does not affect the development like the other methods that deplete cells constitutively. In addition, this system causes cell death by apoptosis, which does not induce proinflammatory immune responses [151]; and it could target even nondividing/differentiated cells [152, 153]. The expression of DTR at any time point in the murine cell is neither toxic nor causing significant adverse effect. Moreover, we can achieve specificity of depletion upon careful choice of cell-specific promoters to express DTR. One possible weakness of this system is the generation of neutralizing antibodies against DT which might reduce the efficiency of ablation [144].

Some of the popular DT mouse models that have been generated for immunological studies include CD11c-DTR, CD11b-DTR, and Foxp3-DTR mice. CD11c-DTR mice were the first mice generated for the study of DC biology [144, 146]. In addition, CD11b-DTR line has been generated, targeting depletion of monocytes and macrophages in various settings [154-157]. However, this mice model depletes broad myeloid cell populations such as neutrophils, monocytes, eosinophils, macrophages and DCs; but AMs are spared in CD11b-DTR mice. Study of regulatory T cells (Treg) using Foxp3-DTR mouse was published recently. The authors inserted IRES-DTR-GFP fusion cassette at the 3' untranslated region of *foxp3* gene by homologous

recombination [158, 159]. However, to have a thorough depletion, perhaps to reach Tregs in the thymus, they injected 40-50 ng/gr DT per day for 7 days [158, 159]. Another application includes Langerin-DTR mice [151] and NK-DTR transgenic mouse [160]. Hence, inducible DTR transgenic mouse models are being favored as a powerful tool to study the roles of specific immune cells in different settings.

In addition, DTR-DT system has also been proven to be effective in targeting cells residing in different peripheral tissue [161]. One study has demonstrated the ability of DT to cross blood brain barrier and target ganglion cells upon intraperitoneal DT administration [162]. Similarly, the skin Langerhans cells have been successfully targeted by Langerin-DTR mice [163]. Depletion of dendritic cells in mucosal organs such as lungs and gut has also been published [78, 164, 165]. Therefore, DT seems to be accessible to most if not all of the bodily tissue, rendering most of the target cells sensitive to DT. Additionally, the dose and route of DT administration have to be considered to optimize different experimental settings.

CD11c-DTR line is known to induce AM depletion *in vivo* [165] and thus is an alternative mouse model to study the population *in vivo.* However, as this widely used mice model expresses DTR on all $CD11c^{+}$ cells, other cell types beside DCs such as splenic marginal zone metallophilic macrophages, lymph nodes subcapsular sinus macrophages, activated T cells, NK cells, plasmablast, and pDC are also depleted upon DT treatment [144, 166]. In addition, repeated DT injection cause lethality in CD11c-DTR mice [167]. Therefore, an extra step to generate bone-marrow chimeras with CD11c-DTR mice as the bone marrow donor is needed, so that DTR expression could be restricted to haematopoietic compartment [144]. In previous Influenza A study utilizing CD11c-DTR mice, assumption that DC is responsible for the observed immunopathology could be misleading. To study this hypothesis, Meredith et al. inserted DTR into the 3'UTR of a zinc finger transcription factor and generated zDC-DTR line that target DC more specifically [168]. They conclude that only a portion of the immune defects observed in parasite and tumor studies using CD11c DTR mice is contributed by DC [168].

Another attempt to target AM for depletion was described by Miyake et al. by generating the Lyzozyme M-DTR mice [152]. However, besides macrophages, administration of DT also killed the alveolar epithelial type II (AE2) cells of the lung. Unfortunately, the mice suffered acute respiratory failure and died in approximately one week [152].

Collectively, depletion of specific cell subset *in vivo* by DTR-DT system has been proven as a powerful tool to study the role of specific subpopulation in homeostasis and infection. In particular, different groups have made CD11c and CD11b DTR mice that could ablate DC and macrophages *in vivo*. However, administration of DT in these mice will ablate a wide range of immune cells sharing the surface marker. Therefore, we need to narrow down the marker that could be directed towards specific depletion of AMs *in vivo*. The proposed candidates for specific tissue macrophages ablation include F4/80 and CD169. In this thesis, I explore whether CD169-DTR mice could be utilized for studying roles of AM in IAV infection.

1.5. CD169 as a candidate marker for DT-DTR system targeting alveolar macrophage

CD169 (Siglec1, Sialoadhesin or Sn) is an adhesion molecule expressed on cell surface that binds sialic acids and glycoproteins for interaction with other cells or microbes [169]. This molecule was first characterized as non-phagocytic sheep erythrocyte receptor in bone marrow macrophages [170]. It has unusual 17 Immunoglobulin (Ig)-like domains which recognize sialylated glycoconjugates although with low affinity. However, its cytoplasmic tail is short and lacks signaling motifs [170-174]. Human CD169 also comprises of 17 Ig domains with 72% similarity with the mouse counterpart, and both species have similar tissue distribution of $CD169^+$ cells [175].

While identified best in the spleen and lymph nodes, $CD169^+$ macrophages are also found in bone marrow, liver, gut, and lungs (summarized in table 1.2). In the spleen, a population of macrophages expressing CD169 is residing at the marginal zone, and known as ‘marginal zone metallophilic macrophages’ (MZM macrophages) [175]. This population has primary access to the blood-borne antigens entering the marginal zone of the spleen. On the other hand, such population of $CD169^+$ macrophages resides at the sub-capsular sinus

(SCS) of the lymph nodes, uniquely exposed to sample the lymph [176]. Another CD169$^+$ subset is found in the medullary cords of the lymph nodes, where lymph exit through the efferent lymphatics [176]. Unlike MZM and SCS macrophages, medullary macrophages bear mannose receptors, thus are distinct in their ability to process antigens [177-179]. CD169 expression is also absent from monocytes and peripheral blood leukocytes on steady state, but some studies observed CD169 expression on inflammatory macrophages [175].

Organ	CD169+ Macrophage population	Other macrophage population
Spleen	Marginal zone metallophilic macrophages F4/80$^-$CD169$^+$ Red pulp macrophages F4/80^{hi}CD11b^{lo}CD169^{lo}MHCII^{lo} CD163$^+$CD68$^+$CD115$^+$CD172a$^+$	Outer marginal zone macrophages F4/80$^-$SIGN-R1$^+$MARCO$^+$ White pulp macrophages/tingible body macrophages F4/80$^-$CD11b$^-$CD68$^+$MFG$^-$E8$^+$
Lymph nodes	Subcapsular sinus macrophages F4/80^{lo}CD11b$^+$CD169$^+$CD11c^{lo} MARCO$^+$ Medullar macrophages F4/80^{hi}CD11b$^+$CD169$^+$SIGN-R1$^+$CD11c^{lo} CD11c^{hi}CD169$^+$ macrophages MHCII$^+$F4/80$^+$CD169$^+$CD11c^{hi}CD8	Macrophages found at lymph nodes cortex CD68$^+$ Tingible body macrophages F4/80$^-$CD11b$^-$CD68$^+$MFG-E8$^+$
Bone marrow	Bone marrow CD169$^+$ macrophages F4/80$^+$CD11b^{lo}CD169$^+$CD11c^{lo} CD68$^+$CX3CR1$^-$CD115$^+$	
Liver	Kupffer cell F4/80^{hi}CD11b^{lo}CD169$^+$CD68$^+$Mac-2$^+$	
Gut	Serosal DC or macrophages MHCII^{hi}F4/80$^+$CD11b$^+$CD169$^+$CD11c^{lo} CX3CR1$^+$CD103$^-$CD115$^+$	Lamina propria macrophages MHCII$^+$F4/80$^+$CD11b$^+$CD11c$^+$C D103$^-$CD115$^+$CX3CR1$^+$CD172a$^+$
Lung	Alveolar macrophages F4/80$^+$CD11b^{lo}CD169$^+$CD11c^{hi}CD68$^+$ SiglecF$^+$MARCO$^+$Mac-2$^+$	Interstitial macrophages CD11c$^-$F4/80$^+$CD68$^+$MHCII$^+$

Table 1.2. Summary of known CD169$^+$ macrophage populations in various organs. Adapted from [94, 142, 180].

Recently, several studies highlight the importance of CD169+ macrophages in infection and tumor immunity. Mice devoid of CD169 still have SCS and MZM macrophages, with slight differences in B and T cell populations [173]. MZM macrophages have been shown to cross-present antigen to CD8α$^+$ DCs [181]. Also, lymph nodes CD169$^+$CD11c$^+$ macrophages demonstrated their ability to

cross-present cell-associated antigens from dead tumour cells [182]. In the bone marrow compartment, CD169 is likely to be involved in the interactions between macrophage and haematopoietic cells. $CD169^+$ cells reside in human bone marrow are proposed to have scavenging function and maintaining microenvironment for haematopoiesis [175]. In mouse study, CD 169^+ bone marrow resident macrophages were shown to promote retention of haematopoietic cells [161].

CD169 is reported to aid the interaction of inflammatory macrophages with mature neutrophils and T cells, or to other activated macrophages; which express the CD169 ligands. In a breast cancer study, $CD169^+$ tumor-infiltrating macrophages were shown to interact closely with carcinoma cells expressing Mucin-1, which is a glycoprotein that can be specifically bound by CD169. Moreover, CD169 was also found to mediate interaction with T cells, with CD43 identified as the potential interaction partner [183], to generate cytotoxic T cells in a graft vs leukemia model [184]. In addition, CD169 is reported to be highly expressed by macrophages present in AIDS-related Kaposi's sarcoma lesions [185]. Two elegant studies described that the SCS macrophages capture and contain vesicular stomatitis virus (VSV), preventing the virus in invading the nervous system [186, 187].

Another study by Barral et al. described the role of the subcapsular sinus $CD169^+$ macrophages in early activation of invariant natural killer T cells (iNKT cells) upon administration of particulate lipid antigen [188]. The event was triggered by a sustained interaction between $CD169^+$ macrophages and iNKT cells that is CD1d-dependent; leading to activation and proliferation of iNKT cells as well as secretion of cytokines such as IFNγ [188]. It would not be surprising to unveil a similar role of the SCS macrophages of the lymph nodes in viral infection such as influenza A infection.

A recent study by Honke et al. reveals a unique control of IFN-I in the spleen marginal zone CD169+ macrophages to permit amplification of adaptive immune response [189]. Upon VSV infection, the authors found that upregulation of ubiquitin-specific protease Usp18 was mediated in $CD169^+$ splenic macrophages to downregulate IFN-I response. Therefore, viral replication was enforced in these cells; ensuring the availability of antigens needed to prime and maintain virus-specific T and B cells. Furthermore, B

cells are recently shown to maintain SCS macrophages upon viral infection through production of lymphotoxin a1b2 [190]. All these data reveal the unique roles of CD169+ macrophages in the bone marrow, spleen, and lymph nodes.

Miyake et al. have generated CD169-DTR mice that demonstrated depletion of MZM and marginal zone macrophages in the spleen [191], medullary and SCS macrophages of the lymph nodes [182], and bone marrow macrophages [161]. The depletion pattern induced in this mice model is specific, such that cell populations not expressing CD169 like monocytes, DCs, neutrophils, microglia, dermal and peritoneal macrophages are not affected in DT treatment [142]. Although this mice line has been around for few years, very few research communities have the access to use the transgenic mice. I believe that much more can be learnt by creating another CD169-DTR line.

There are several reasons behind the rationale to adopt the CD169 marker for the DTR-DT system. First of all, previous studies have shown that AMs stain for CD169 [94, 152]. Hence, I argue that CD169 is a good marker to be targeted for DT-DTR strategy due to its specificity of expression. Moreover, although CD169-DTR mice have been generated independently by other research group [191], whether or not AMs depletion can be induced in CD169-DTR mice has not been addressed. Besides, CD169-DTR mice have not been utilized as a model to study influenza A infection. Furthemore, to date, CD169 is known to be solely expressed by tissue macrophage subsets, and not by non-immune cells. Hence, CD169-DTR mouse is an attractive tool to study role of AM, specifically in influenza setting. CD169-DTR mice could also be harnessed to study the roles of macrophages in numerous settings including infection, tumor and transplantation immunology.

1.6. Aims of this study

Taking the above rationales into account, I decided to generate CD169-DTR mice by using bacterial artificial chromosome (BAC) transgenesis and subsequently study the profile of macrophage *in vivo* ablation induced in the transgenic mice. After confirming the depletion of macrophages in the respiratory system, I proceeded to investigate the role of macrophages in Influenza A infection.

CHAPTER 2
MATERIALS AND METHODS

2.1. Materials

2.1.1. Mice

Wild-type C57BL/6 and BALB/c mice were obtained from Comparative Medicine Centre, National University of Singapore. Transgenic mice (CD169-DTR) were generated in-house at the animal facility of Nanyang Technological University (NTU), Singapore. Experiments were performed under the approval of the Institutional Animal Care and use Committee in compliance with the Law and Guidelines for Animal Experiments. Transgenic animals were bred and maintained under specific pathogen-free (SPF) conditions at the animal facility, NTU, Singapore.

2.1.2. Chemicals and supplements

Name	**Manufacturer**
2-Propanol	Merck
3-Amino-9-ethylcarbazole (AEC)	Sigma
Acetone	Fischer Scientific
Agarose	1st Base Biochemicals, Singapore
Dimethyl Sulfoxide (DMSO)	Sigma Aldrich
DPX mountant for histology	Sigma
Ethylenediamineteetraacetic acid (EDTA)	Affymetrix
Eosin	Sigma
Ethanol	Merck
Ethidium bromide	Bio-rad, Singapore
Ficoll-Paque Plus	Amersham biosciences
Giemsa	Sigma
Haematoxylin	Vector laboratories
Methanol	Merck
Methylcellulose	Sigma
NaCl	Merck
Paraformaldehyde (PFA)	Sigma

Polybrene	Sigma
Sodium dodecyl sulfate (SDS)	Hoefer
Tissue-Tek O.C.T. Compound	Sakura Finetek
Triton X-100	Bio-Rad
Tris	USB
Trizol reagent	Invitrogen
Trypan blue	Sigma
Tryptone	Bacto
Yeast extract	Bacto
Xylenes	Sigma Aldrich

2.1.3. Buffers, media, and additives

Name	**Manufacturer/composition**
0.05%Trypsin -EDTA	GIBCO® Invitrogen
2.5%Trypsin - EDTA	GIBCO® Invitrogen
2-mercaptoethanol	Sigma Aldrich
Ampicilin	Merck
Blasticidin	A.G. Scientific
Chloramphenicol	Boehringer Mannheim, dose: 15 µg/ml
Diphtheria Toxin	Sigma
Dulbecco's modified Eagle medium (DMEM)	DMEM/GlutaMax™, GIBCO® Invitrogen
ES medium	DMEM, 15% FCS, 100 U/ml penicillin/streptomycin, 1mM sodium pyruvate, 0.1mM nonessential amino acids, 0.05 mM 2-mercaptoethanol, and 2 mM L-glutamine, 1 µg/l LIF
FACS buffer	2% FCS in PBS
FACS fixation buffer	1% Paraformaldehyde in PBS
Fetal Calf Serum (FCS)	Biowest
Freezing medium	FCS with 10% DMSO
G418 Sulphate Solution	PAA Laboratories
Iscove's Modified Dulbecco's Medium (IMDM)	IMDM Powder (Hyclone), 3.02 gr/l NaHCO3, 1%(v/v) Penicillin/ Streptomycin 100x, 50µM β-Mercaptoethanol, 1%(v/v) MEM non-essential amino acid (100x), Primatone
IMDM 2% FCS	IMDM medium, 2% FCS
Insulin-Transferrin-Selenium-G supplement	GIBCO® Invitrogen
LB medium	dH20, 1% (w/v) tryptone, 0.5% (w/v) yeast extract, 1% (w/v) NaCl, pH 7.5

LB plates	LB medium with 1.6% Bacto-agar
L-glutamine	GIBCO® Invitrogen
MDCK medium	DMEM, 0.5% FCS, Primatone, 0.1% (v/v) 100xInsulin-Transferrin-Selenium, 0.05 mM 2-mercaptoethanol, 100U/ml penicillin/streptomycin
MEF medium	DMEM, 10% FBS, 100 U/ml penicillin/streptomycin, 0.05 mM 2-mercaptoethanol, and 2 mM L-glutamine
MEM-non-essential amino acids solution (100x)	GIBCO® Invitrogen
PBS pH 7.2,	GIBCO® Invitrogen
Penicillin/Streptomycin	GIBCO® Invitrogen
Primatone	Sigma
Red blood cell (RBC) lysis buffer	0.89% Ammonium Chloride (NH_4Cl)
RPMI 1640 without L-Glutamine	PAA Laboratories
SNET buffer	2 0mM Tris-Cl pH 8.00, 5 mM EDTA, 400 mM NaCl, 1%(w/v) SDS
TAE (1x)	40 mM Tris (pH 8.0), 1 mM EDTA
TE buffer	Invitrogen
Tetracycline	Sigma
TPCK Trypsin	Thermo Scientific

2.1.4. Antibodies and conjugates

Cognate antigen	**Label**	**Clone**	**Source**
Anti-mouse CD11c	FITC	N418	BD Pharmigen
Anti-mouse CD4	FITC	H129.19	BD Pharmigen
Anti-mouse CD8	PE	53-6.7	BD Pharmigen
Anti-mouse B220	PE	RA3-6B2	Biolegend
Anti-mouse CD11b	FITC	M1/70	Biolegend
Anti-mouse CD4	PE	H129.19	Biolegend
Anti-mouse GR-1	PE	RB6-8C5	Biolegend
Anti-mouse I-A/I-E	FITC	M5/114.15.2	Biolegend
Anti-mouse Ly6C	PE/Cy7	HK1.4	Biolegend
Anti-mouse Ly6G	APC	1A8	Biolegend
Anti-mouse SiglecH	PE	551	Biolegend
Anti-mouse CD103	APC	2E7	eBioscience
Anti-mouse CD11b	perCP-Cy5.5	M1/70	eBioscience

Anti-mouse CD11c	APC	N418	eBioscience
Anti-mouse CD11c	PE	N418	eBioscience
Anti-mouse CD4	APC	GK1.5	eBioscience
Anti-mouse CD8	FITC	53-6.7	eBioscience
Anti-mouse CD8	APC	53-6.7	eBioscience
Anti-mouse F4/80	PE	BM8	eBioscience
Anti-mouse F4/80	APC	BM8	eBioscience
Anti-mouse MOMA-1	FITC	MOMA-1	Serotec
Anti-rat IgG	FITC	Poly4054	Biolegend
Anti-goat IgG	HRP		Southern Biotech
AntI-IAV IgG	biotin		Virostat

2.1.5. Oligonucleotides

No	Name	Sequence
1	5'HA PCR forward	5'-TGAGCTGCCAAGTTGAGAAC-3'
2	5'HA PCR reverse	5'-ttagctcttcTTCATcccagtgcccaggtgcattc 3'
3	3'HA PCR forward	5'-ggagctcttcATTAAatgtgtgtcctgttctccct-3'
4	3'HA PCR reverse	5'-AGAGAAAAGGGTGATGCAAG-3'
5	5'check forward	5'-TGAGCTGCCAAGTTGAGAAC-3'
6	5'check reverse	5'-ATTGGATCCGTGGGAATTAGTCATGCCCAAC-3'
7	3'check forward	5'- TGTGTGACGCGTGTTGACAATTAATCATCG-3'
8	3'check reverse	5'-AGAGAAAAGGGTGATGCAAG-3'
9	Neo forward	5'-CAGATGCGCGCTTTCTCTGT-3'
10	Neo reverse	5'-TATACGAAGTTATTATCTATGTCG-3'
11	5'check Neo forward	5'-AACAGAGAACGTCACACCGT-3'
12	5'check Neo reverse	5'-ACCAAAGAACGGAGCCGGTT-3'
13	3'check Neo forward	5'-ATTCGCAGCGCATCGCCTTC-3'
14	3'check Neo reverse	5'-TCAACCCAGTCAGCTCCTTC-3'
15	Tomato forward	5'-TCCGAGGACAACAACATGGC-3'
16	Tomato reverse	5'-TACAGCTGGTCCATGCCGTA-3'
17	Bb R check forward	5'-GGCTGCATGCACAGACCATC-3'
18	Bb R check reverse	5'-CTCCCGAATTGACTAGTGGGTAG-3'
19	Bb F check forward	5'-GGATCGATCCGGCGCGCCAATAG-3'
20	Bb F check reverse	5'-CATTGGGTGCATTGGGGTCC-3'
21	DTR forward	5'-CATCTGTCTGTCTGGTCA-3'

22	DTR reverse	5'-TCATGCCCAACTTCACTTTCT-3'
23	mGJA5 forward	5'-ACCATGGAGGTGGCCTTCA-3'
24	mGJA5 reverse	5'-CATGCAGGGTATCCAGGAAGA-3'
25	Inf-M-protein forward	5'-GGACTGCAGCGTTAGACGCTT-3'
26	Inf-M-protein reverse	5'-CATCCTGTTTATATGAGGCCCAT-3'
27	Beta-actin forward	5'-AGAGGGAAATCGTGCGTGAC-3'
28	Beta-actin reverse	5'-CAATAGTGACCTGGCCGT-3'

2.2. Molecular methods

2.2.1. Polymerase chain reaction

Polymerase chain reaction (PCR) for screening purposes was performed using GoTaq Flexi DNA Polymerase (Promega). To achieve high fidelity in construct generation, Phusion high-fidelity DNA Polymerase (Finnzymes), Expand Long Range, dNTPack (Roche), and Pfu DNA Polymerase (Promega) were used accordingly. All primers used for this study are listed in section 2.1.5. All primers were ordered from 1st BASE, Singapore. PCR reactions were run on T3000 Thermocycler (Biometra).

2.2.2. Gel electrophoresis and gel extraction of DNA

To visualize the results of PCR or restriction digest, gel electrophoresis was performed with 1% agarose gel containing Ethidium Bromide (0.1 µg/ml) in 1x TAE buffer. Gene Ruler 1kb DNA ladder (Fermentas, Canada) was used for size comparison. For cloning purpose, appropriate DNA fragments were cut with a scalpel from the agarose gel, and purified using Invitrogen PureLink Quick Gel Extraction Kit (Invitrogen) according to manufacturer's instruction. DNA was eluted in appropriate amount of elution buffer and stored at -20˚C.

2.2.3. Preparation of BAC DNA

BAC DNA was extracted for mini-preparation according to Counter-Selection (Advanced) BAC Modification Kit protocol version 3.0 (Gene Bridges, USA). For mini-preparation, BAC clone was inoculated into 2 ml of LB with appropriate antibiotic and incubated for 12-16 hours at 37˚C. The extracted DNA was then solubilized in 30 µl TE buffer. For BAC maxi-preparation, clone

was cultured in 500 ml of LB with appropriate antibiotic added, was used. Maxi-preparation of BAC DNA was conducted with PureLink® HiPure Plasmid Filter Maxiprep Kit (Invitrogen) according to manufacturer's protocol. The extracted BAC DNA was solubilized in appropriate amount of ddH_2O.

2.2.4. Restriction enzyme digestion

Digestions with restriction enzymes were performed in recommended buffer and temperature. SapI was used for cloning the targeting construct, SmaI was used for BAC digestion analysis, and PI-SceI was used for BAC linearization. All restriction enzymes and buffers were purchased from New England Biolabs, USA. Restriction digest reactions with SmaI were conducted for 2 hours; while digestion with SapI and PI-SceI required 4 hours and 6 hours respectively.

2.2.5. Ligation

Ligations were performed in a total volume of 20µl at 16℃ for at least 12 hours (or overnight) with T4-DNA ligase (Fermentas) as per manufacturer's instruction.

2.2.6. BAC recombineering

Counter-Selection BAC Modification Kit was purchased from Genebridges, Germany. Counter-selection step was omitted, and instead, two steps recombineering was done. The first recombineering was meant to incorporate the targeting fragment right at the start codon of CD169 gene. Moreover, in the second recombineering step, Chloramphenicol resistance cassette was replaced with Neomycin resistance to facilitate ES cell screening. In this system, homologous recombination was mediated by proteins encoded by pRed/ET plasmid [192], which is explained further in section 3.1 of this thesis. Steps of the recombineering strategy are illustrated in Fig. 2.1.

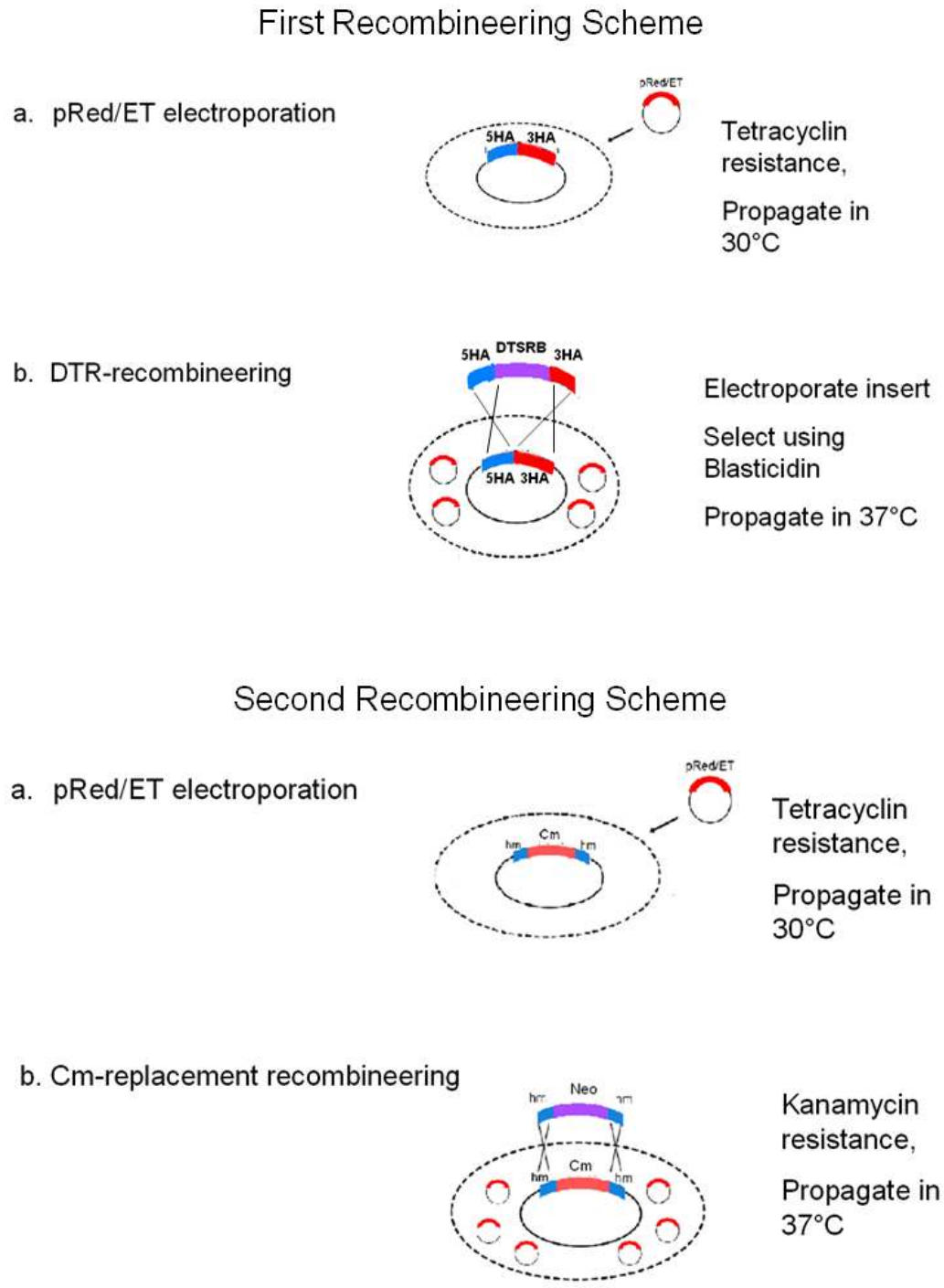

Figure 2.1. Simplified BAC recombineering scheme. For both recombineering steps pRed/ET plasmid is first electroporated into the E. coli harboring the BAC. Homologous recombinations are then initiated to incorporate targeting insert in the first recombineering place and to replace the antibiotic resistance in the second recombineering step respectively. Antibiotic selection strategies are indicated in each step. Cm: Chloramphenicol; Neo: Neomycin; HA: homology arms flanking CD169 start codon; hm: homology arms flanking Chloramphenicol cassette.

Antibiotic	Chloramphenicol	Blasticidin	Tetracycline	Kanamycin/ Neomycin
Concentration of stock	15 mg/ml in ddH_2O	100 mg/ml in ddH_2O	10 mg/ml in Ethanol	15 mg/ml in ddH_2O
Dilution towards working concentration	1:1000	1:100	1:1000	1:1000
Component responsible for the corresponding antibiotic resistance	Harbored by the BAC	Blasticidin cassette in intron	pRed/ET plasmid	Neo casette

Table 2.1. Description of antibiotic stock concentrations and components that are responsible for the resistance in the BAC recombineering.

2.2.6.1. BAC clone containing CD169 locus

BAC clone harboring CD169 locus of C57BL/6 (RP23-32L15) was purchased from BACPAC Resources Center at Children's Hospital Oakland Research Institute (CHORI, USA). The BAC has Chloramphenicol resistance incorporated the pBAC3.6 backbone and was propagated in DH10B *E. coli* strain. BAC sequence was obtained from UCSC genome browser and aligned (using BLAT tools) with mRNA sequences to view the exon-intron structure.

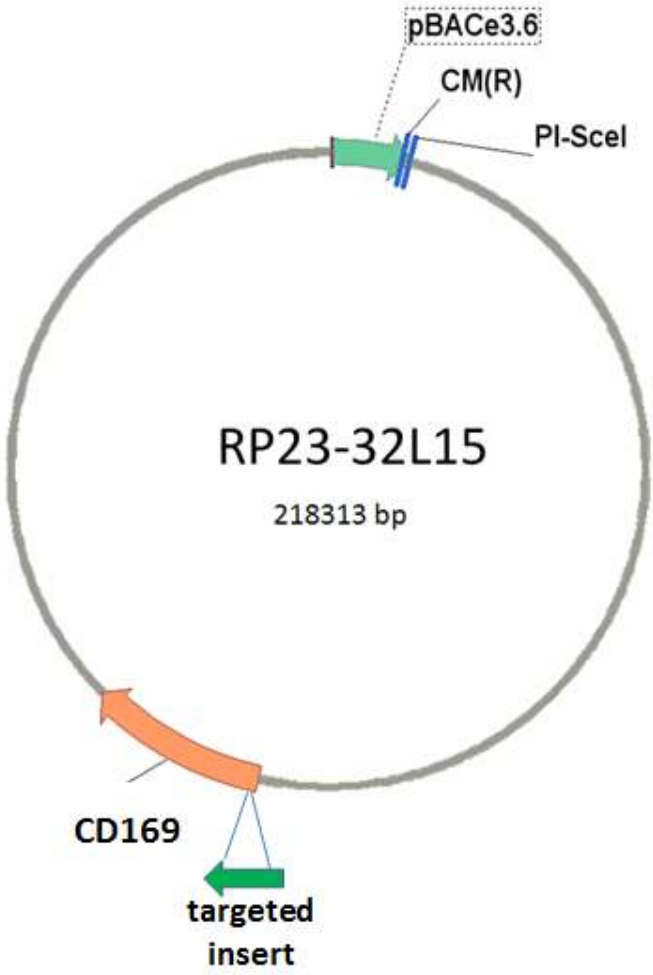

Figure 2.2. Schematic illustration of unmodified RP23-32L15 BAC harboring the CD169 locus. The targeting insert containing the human DTR sequence will be integrated into the start codon of CD169 gene by homologous recombination. Backbone containing chloramphenicol antibiotic resistance/CM(R) and linearization site (PI-SceI) are also illustrated.

2.2.6.2. Generation of the targeting construct

The main components of the targeting construct are the human DTR sequence followed by the tandem dimer Tomato sequence; both are separated by the coding sequence for 2A, a self-cleaving peptide. The DTR-2A-Tomato construct is followed by synthetic poly-A sequence, RecA bacterial promoter, and Blasticidin (BSD) antibiotic resistance gene (designated as 'DTSRB', Fig. 2.3). The 2A sequence [193] replaces the role of internal ribosome entry site (IRES) in the construct. Cloning of DTSRB was done in pMYc vector [194], where expression is regulated by viral long terminal repeat (LTR) promoter. This plasmid containing the targeting construct is designated as pDTSRB, which cloning and preparation was done by Mr. Wu Zhihao.

Figure 2.3. Schematic diagram of DTSRB.

2.2.6.3. Primer design and amplification of homology arm

Insert of the first recombineering was assembled from 3 fragments: 5' homology arm (5'HA) PCR product, DTSRB fragment, and 3' homology arm (3'HA) PCR product (Fig. 2.4). SapI recognition sequences were cloned to flank the DTSRB region in the pDTSRB vector. Homology arms were designed such that they contained SapI site at the appropriate ends; thus enabling ligation with the DTSRB fragment (Fig. 2.4). By using this unique enzyme, the end product would be free of extra nucleotides. SapI enzyme cuts the sequence that is downstream of its recognition sites as below.

SapI site 5'.. G C T C T T C N N N N ..3'
3'.. C G A G A A G N N N N ..5'

DTSRB construct was inserted at the start codon of the CD169 locus. Hence, homology arms were generated from ~500 bp of nucleotides upstream of the start codon (5'homology arm/5'HA), ~300 bp of nucleotides downstream of the start codon (3'homology arm/3'HA). There was a SapI site present within 500 bp of the 3' homology arm, hence only ~300 bp downstream sequence was amplified as the 3' homology arm. Primer pairs used for this purpose were 5'HA PCR (forward and reverse) and 3'HA PCR (forward and reverse).

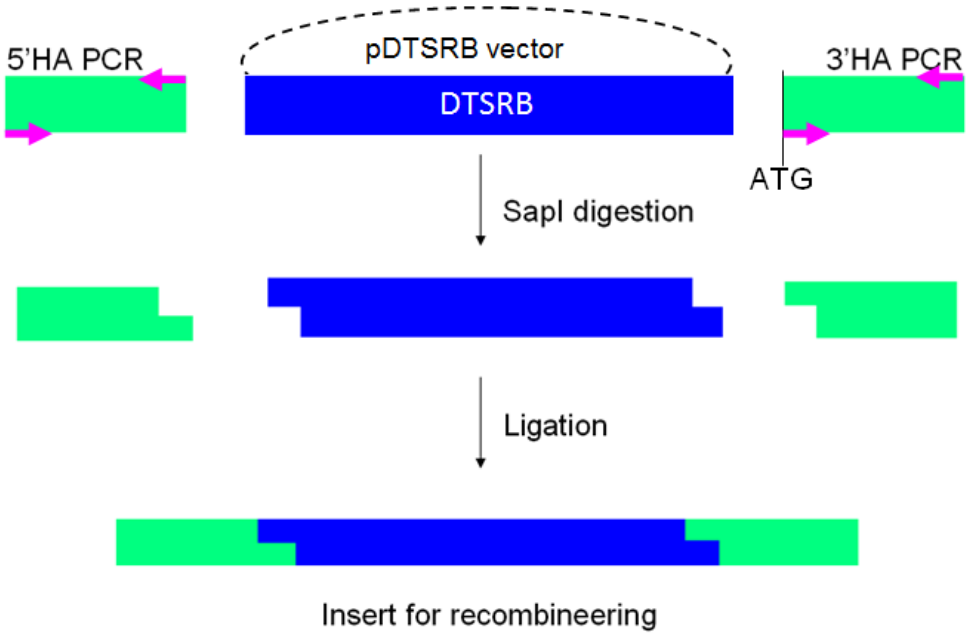

Figure 2.4. Generation of the insert for first recombineering purpose.

2.2.6.4. First recombineering step

Transformation of bacteria with pRed/ET plasmid and recombineering step was performed according to Counter-Selection BAC Modification Kit protocol (page 12-16, Genebridges). Successful clones were selected with blasticidin. PCR flanking the insert and external right and left arms were done to identify successful clones. Primer sequences used were 5'check (forward and reverse, 1135 bp) and 3'check (forward and reverse, 755 bp). Moreover, restriction digestions with selected enzymes were performed to ensure the integrity of the BAC. Figure 2.1. illustrates the recombineering steps schematically.

2.2.6.5. Second recombineering step

The next recombineering step was done to replace chloramphenicol resistance harbored in the pBACe3.6 backbone with neomycin resistance sequence (neo insert). The replacement cassette is composed of neomycin resistance cassette flanked by homology arms and cloned by Miss Loh Shuzk Cheng. The neomycin resistant gene was placed downstream of PGK eukaryotic promoter and EM7 prokaryotic promoter; thus enabling selection in both bacteria and ES cell. Neo insert was prepared by PCR using neo forward and reverse primer sequences.

Again, bacteria were first transformed with pRed/ET plasmid, and recombineering was conducted accordingly, with adjustment of the antibiotic used. Selection of successful clones were mediated by kanamycin selection and verified by PCR. Primer sequences for checking second recombineering were 5'check neo forward and reverse. Sequencing was performed to confirm fidelity of the recombineering inserts.

2.2.6.6. BAC linearization

The pBACe3.6 backbone contains sequence that is recognized by PI-SceI endonuclease. Selected BAC clones were then amplified by maxipreparation and then linearized with PI-SceI enzyme (37℃, 6 hours), followed by heat inactivation of the enzyme (65℃, 20 mins). Linearized BAC was either precipitated with isopropanol or electroporated directly into the ES cells.

PI-SceI recognition sequence:

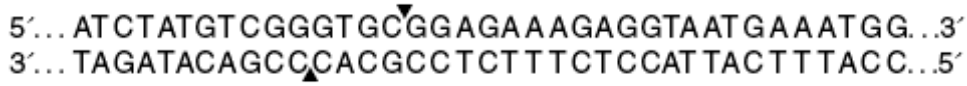

2.2.7. Preparation of genomic DNA from embryonic stem cells

Genomic DNA was extracted from individual embryonic stem (ES) cell clones using Blood & Tissue Kit (Qiagen) according to the protocol: purification of total DNA from Animal blood or cells (spin-column protocol). The extracted DNA was then used as a template for PCR reactions in order to identify successful ES clones.

2.2.8. Preparation of tail DNA and genotyping

DNA extraction from mouse tail was done for genotyping purpose. Mouse tails were cut and digested in SNET buffer containing Proteinase K (Promega), then incubated in 55℃ for 2-3 hours. Centrifugation was performed to remove the debris. Supernatant was then harvested and mixed with cold Isopropanol to precipitate the DNA. Precipitate was then washed with 70% Ethanol and DNA was dissolved in TE buffer with incubation at 65℃ for 10 minutes. PCR to detect the presence of transgene was carried out against Tomato sequence

using Tomato forward and reverse primers. PCR was performed with annealing temperature of 61℃.

2.2.9. Real-time PCR

To confirm on zygosity, quantitative PCR (qPCR) was performed against DTR gene with reference to mGJA5 (mouse gap junction channel protein alpha 5). Primer sequences used were DTR forward and reverse, as well as mGJA5 forward and reverse.

Quantitative reverse-transcription PCR (qRT-PCR) was conducted to analyse lung viral load in IAV infection. RNA from lung tissues were isolated using PureLink RNA Mini Kit (Invitrogen) and synthesis of complementary DNA (cDNA) were obtained using M-MLV Reverse Transcriptase (Promega) according to manufacturer's instructions. The following primer sequences against Influenza M protein and beta-actin as endogenous control were used: Inf-M-protein forward and reverse, as well as beta-actin forward and reverse

Reactions were prepared using KAPA Sybr fast Universal qPCR kit (KAPA Biosystems) according to manufacturer's instruction. All reactions were performed in triplicate, carried out in the 7500 real time PCR System (Applied Biosystem), and analysed using 7500 system software instrument.

2.3. Tissue culture

2.3.1. Maintenance of immortalized bone marrow cell culture

Nup98-HoxB4 (NB4) bone marrow (BM) line was cultured in with IMDM 2%FCS medium supplemented with IL-6 (10ng/ml) and Stem Cell Factor/SCF (50ng/ml).

2.3.2. Transfection of Platinum-E cells

For testing DTR-2A-Tomato expression, Platinum-E (Plat-E) cells, a packaging line for retroviral viruses [195], were transfected with 80ng of pDTSRB. To increase the transduction efficiency, 5 µg/ml polybrene was added to the supernatant.

2.3.3. Viral transduction of immortalized bone marrow cells

The viral-containing soup was added onto fibronectin-coated dish and spun down at 4000rpm, 4℃, for 45 minutes. Then, NB4 BM cells were added onto the plate and incubated at 37℃ to establish the culture. Afterwards, the culture was expanded and cell sorting was done to enrich the top 5% of the cells that highly expressing Tomato.

2.3.4. In vitro differentiation of Nup98-HoxB4 cells into macrophages

To differentiate NB4 BM line into macrophages, NB4 cells were cultured in IMDM 2% FCS medium added with 20% of L-929-conditioned media for >7days. L929 is a fibroblast cell line that produces factors that are required for macrophage differentiation, such as mononuclear phagocyte colony-stimulating factor (M-CSF). For analysis, cells were detached with 2.5% Trypsin, stained for macrophage markers, and analyzed by flow cytometry.

2.3.5. Maintenance of mouse embryonic fibroblasts

DR-4 mouse strain was selected as the mouse embryonic fibroblast (MEF) donor because of its resistance to multiple drugs, namely G418, 6-thioguanine, puromycin, and hygromycin; and thus is suitable for the selection of drug-resistant ES cell. DR-4 fibroblasts were extracted from mouse embryo, and maintained in MEF medium. For maintenance purpose, a confluent plate of MEF was passaged in 1:4 ratios using 0.5% Trypsin EDTA. Freezing was done in freezing medium into cryovials at ~10^7 cells per vial.

2.3.6. Maintenance of embryonic stem cells

BALB/c ES cell line was maintained in ES medium supplemented with leukemia inhibitory factor (LIF), and ~70% confluent culture was passaged in at least 1:10 ratio onto the plate containing MEF as feeder cells. Prior to seeding, MEF was irradiated with 30 Gray of gamma irradiation (Bio-beam 8000).

2.3.7. BAC electroporation and selection of ES cell clones

ES cells (from frozen stock) were passaged at least one time before electroporation. For electroporation, 1 plate of ~70% confluence ES cells was

harvested with trypsin, and then washed twice with PBS. Then, the cells were mixed with 30µg of linearized BAC DNA and resuspended in 600-80 µl final volume of PBS. Cell suspension was then placed in sterile 0.4 cm gap cuvette and electroporation was conditioned at 500 µFD/250 volts with Bio-Rad Gene Pulser. After 10 min incubation at 37℃, 2 x 10^6 cells were put in new MEF feeder plates (2-4 MEFs in 10cm plate). After 24 hour post-electroporation, G418 (300 µg/mL) antibiotic was added to allow selection. Round-shaped ES colonies (after 4 days) were handpicked and expanded in 96-well plate with replica. The main wells were used for ES cell expansion, while the replica wells were subjected to genomic DNA extraction and verification by PCR.

PCR against Tomato sequence (using Tomato reverse and forward primers) was conducted to detect the presence of the transgene. In addition, PCR against both ends of the linearized BAC was performed to ensure that the whole BAC was intact while being inserted into the genome. Primer sequences used were Bb F check (forward and reverse) and Bb R check (forward and reverse). After checking, individual positive colonies were expanded or frozen for further use.

2.4. Immunological methods

2.4.1. Flow cytometry and cell sorting

For flow cytometry, cell suspensions were stained in FACS buffer at 4℃. Cells were blocked with anti-Fc receptor mAb (2.4G2) antibodies in FACS buffer for 15 min at 4℃ to reduce non-antigen-specific binding of antibodies to Fc receptors-expressing cells such as B cells, monocytes, and macrophages. Flow cytometry analysis were performed on FACSCalibur (BD Biosciences) or LSR II (BD Biosciences) and analyzed with FlowJo software (Treestar, USA). All cell sortings were performed by FACSAria (BD Biosciences).

2.4.2. Detection of virus specific CD8 T cells by MHC Dextramer™ staining

Single cell suspensions were prepared from the lung samples and the lymphocytes were enriched using Ficoll gradient. Briefly, lung cells were resuspended in 3 ml of FACS buffer and 3 ml of Ficoll were carefully layered to the bottom of cell suspensions. After centrifugation at 2500 g for 20 mins

(acceleration/deceleration was set to 4-6), cloudy ring of lymphocytes were recovered and washed once with FACS buffer. Enriched lymphocytes were counted and stained for APC-labeled anti-CD8 antibody together with PE labeled H-2Kd MHC Dextramer^{TM} of Influenza A hemagglutinin epitope IYSTVASSL (Immudex) for 20min. Cells were washed once with FACS and then fixed with FACS fixation buffer. The reagent is composed by a dextran polymer carrying fluorescent-labelled MHC-peptide molecules in optimized number. Multimeric nature of this reagent mediates increased avidity and affinity, and thus enables us to distinguish a distinct population of T cells specific for the MHC-peptide complex.

2.4.3. Influenza plague assay

Lungs were homogenized with handheld homogenizer (Wiggen Hauser) in 1ml RPMI and then pelleted. The supernatants were serially diluted to determine virus titers by performing plague assay on confluent Madin-Darby canine kidney (MDCK) cells in 48-well plates. Briefly, cells were incubated with 100 µl of lung homogenates for 5 hour in 37℃ and then overlaid with 1% methylcellulose media containing 2 ug/ml TPCK trypsin. After 48 hours, cells were permeabilized and fixed with 4% PFA/1% Triton X-100, and subsequently incubated with biotynilated primary goat-anti-IAV IgG and secondary HRP-conjugated anti-goat IgG for 45 min each. Finally, the cells were stained with AEC for 20 min and visible foci were counted using a light microscope (Nikon Eclipse TS100).

2.5. Animal work

2.5.1. Microinjection and generation of transgenic mice

Microinjections of ES cells into mouse blastocysts were conducted by Dr. Piotr Tetlak and Mr. Arun Kumar in animal facility, NTU. Our strategy for generation of germline chimeras is illustrated in Fig. 2.5. For each injection, 10 female C57BL6 aged 4-5 weeks were used as blastocysts donor. As pseudo-pregnant recipients, ICR strain females were mated with vasectomised males. ES clones (passaged at least once) in one confluent 6-well plate were used for injection. After microinjection, 12-16 injected blastocysts were transferred into one foster female (6-8 embryos per uterus side). Male pups born with ~40%

and ~70% chimerism were mated with BALB/c females. White-colored progenies were then screened for transgenes by PCR specific for Tomato gene and positive ones were deemed heterozygous. In order to obtain homozygous mice, heterozygous mice were mated with each other. F1 pups were screened by quantitative PCR with primer against DTR gene and backcrossed to confirm the genotype. Mice were then maintained on BALB/c background.

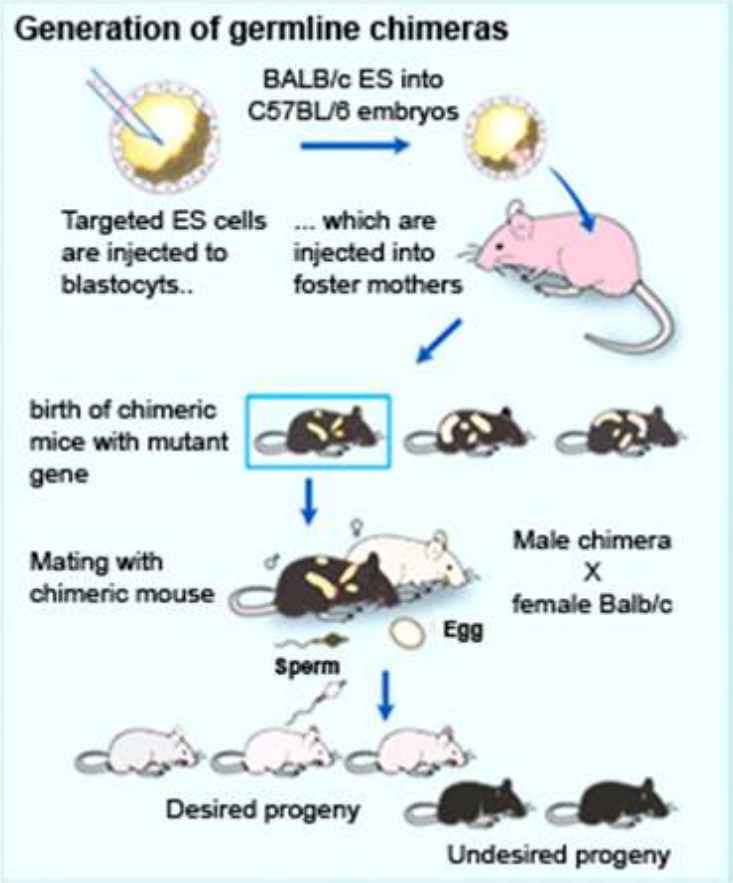

Figure 2.5. Strategy for gene targeting in mice. Adapted with modifications from Hansson et al., 2007 [196].

2.5.2. Administration of Diphtheria Toxin

$CD169^+$ cells were ablated by intraperitoneal administration of DT (Sigma) in 200 µl PBS containing 1:100 mouse serum 48 and 24 hour before infection or analysis. General Working dose was 10 ng/gr body weight, such that a mice weighing 20 gr would receive 200ng DT in 200 µl of PBS. For intratracheal administration, 50ng DT in 50µl of PBS (25% of usual dose) was given to the lightly anesthetized mice.

2.5.3. Influenza A Virus infection and monitoring

Influenza virus strain A/PR/8/34 (H1N1) was a gift from Dr. Sivasankar Balasubramanian (Singapore Institute for Clinical Sciences/SICS, Singapore). Mice were anesthetized mice with 2,2,2-tribromoethanal in tert-amyl alcohol (Avertin, Sigma) before intranasal challenge with 1, 3, or 6 plaque forming units (PFU) of PR8 in 25 µl of PBS. Female mice of 6-8 weeks age were routinely used for Influenza infections. Measurements of weight were conducted daily throughout the infection course.

2.5.4. Tissue collection and processing

Blood was collected by bleeding the mice through retro-orbital plexus while under anaesthetics. Serum was collected in BD Microcontainer, serum separator tubes (BD, USA), centrifuged for separation, and kept in -20℃ for further use.

For spleen and bone marrow collection, mice were euthanized by CO_2 and organs were dissected out. Spleens were dissected out and digested with 1 mg/ml Collagenase D (Roche Diagnostics) with agitation at 37℃ for 45 minutes. Digested spleen was then passed through a 70µm cell strainer to obtain single cell suspension. Tibia and femurs bone cavities were flushed with FACS buffer to obtain bone marrow. Red blood cells of spleen and bone marrow suspensions were lysed by 0.89% Ammonium chloride solution.

For pulmonary tissue harvesting, mice were culled by cervical dislocation. Broncho-alveolar lavage fluid (BALF) was obtained by performing lung lavage with 3 x 1 ml of PBS. Lung parenchyma were excised, cut into small pieces, and digested in 2mg/ml Collagenase D (Roche Diagnostics) for 45 min with agitation. Digested lung tissue was then passed through a 70 µm cell strainer to obtain single cell suspension. Red blood cells were lysed with RBC lysis buffer solution for 10 min at room temperature, and pellets were resuspended with FACS buffer.

2.5.5. Generation of bone marrow chimeric mice

Bone marrow cells were isolated from tibias and femurs of wild type BALB/c or from CD169 DTR$^{+/+}$ donor mice. The bone ends were cut and cells were flushed out of marrow cavity with sterile IMDM 2% FCS. Erythrocytes were lysed and single cell suspensions were prepared in PBS.

Recipient BALB/c or CD169 DTR$^{+/-}$ mice were lethally irradiated with 2 doses of 4.25 Gray of gamma irradiation given in 4 hours interval. Injection of 2x10^{6} cells in 200 µl PBS was given via retro-orbital route within 24 hours after irradiation. Mice were analysed or infected with influenza 8 weeks afterwards.

2.6. Microscopy

Cytospin (Thermo Scientific) of broncho-alveolar lavage was fixed and stained with giemsa. For pathology, fixed sections of paraffin-embedded lungs were stained with haematoxylin and eosin. Slides were then mounted with DPX mountant for histology (Sigma) and subjected to microscopy.

For frozen section, lungs were slowly inflated with 1.5 ml of 1:1 mixture of OCT and PBS. Lung or other tissue were then snap frozen in OCT compound, cut with cryosection machine (Leica CM 1850) and mounted on glass slides and fixed with Acetone. Slides were blocked with PBS containing 10% FCS for 30 min and stained with indicated antibody each for 1 hour. Before microscopy, slides were mounted with fluorescent mounting medium (Dako). All pictures were taken with Nikon Eclipse 80i fluorescence microscope and analysed with Adobe Photoshop software.

2.7. Statistical analysis

All data were analyzed with Prism software (Graph Pad). Statistical significance was determined by unpaired Student's t-test. *, $p<0.05$; **, $p<0.01$; ***, $p<0.001$.

CHAPTER 3: RESULTS I

GENERATION AND CHARACTERIZATION OF CD169-DTR MICE

3.1. Background

To generate CD169-DTR ablation model, I exploited the bacterial artificial chromosome (BAC) transgenesis approach. BAC was chosen because of its large insert size and good insert stability [197]. BAC for recombineering allows targeting of any DNA almost without size and positional constraint. One significant advantage of using BAC is that all required promoter/enhancer elements of the gene of interest are usually present; thus, prior characterization is not necessary.

The classical approaches in molecular cloning utilize mainly restriction endonucleases. This method is associated with difficulties in finding convenient restriction sites and size constraints of the inserted DNA fragments [198]. Then, recombineering technology was established, overcoming those limitations of the classical molecular cloning. Red/ET recombineering, developed in Francis Stewart's lab at EMBL, mediates homologous recombination in *Escherichia coli (E. coli)*. It was marked with the discoveries of proteins encoded by phage that are able to facilitate homologous recombination. Those proteins are Rac prophage proteins RecE/RecT or Redα/Redβ proteins of λ phage as well as some other helper proteins [192]. A plasmid (named the pRed/ET) harboring all of the necessary proteins was constructed; and its electroporation into bacteria will mediate homologous recombination.

Aside from encoding the phage λ recombination machinery, the pRed/ET plasmid (Fig. 3.1.A) has features that benefit the recombineering event. This plasmid replicates on certain range of temperature due to the temperature-sensitive origin of replication ori pSC101[199]. Incubation in 30˚C allows pRed/ET to stay within the cells, whereas it will be lost upon propagation in 37˚C. The presence of the plasmid inside the cell can be maintained by Tetracycline selection. Upon the presence of inducer (L-arabinose), the pBAD

promoter will drive the expression of the relevant genes, and only transient recombineering events will occur. This will keep the unwanted recombination events at minimum [200].

The pRed/ET plasmid also directs the expression of a number of other proteins necessary for recombineering. RecA facilitates two homologous DNA to find each other in order to recombine. It increases the number of obtained transformants after electroporation. Redα is a 5'- 3' exonuclease while Redβ is a DNA annealing protein (Fig. 3.1.B) [192, 198]. Gam protein inhibits RedBCD-dependent destruction of linear DNA in the cell [201, 202].

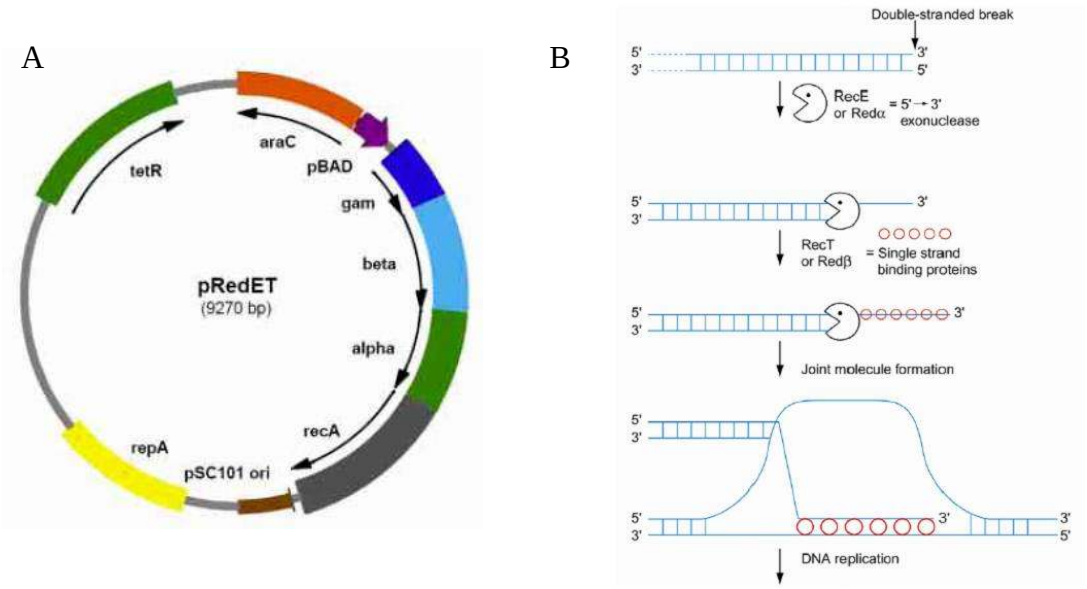

Figure 3.1. Illustration of the pRed/ET plasmid which encodes the components responsible for Red/ET recombineering. (A) Schematic diagram of pRed/ET plasmid construct. (B) Illustration of the role of Redα and Redβ proteins in homologous recombination. Adapted from Red-ET recombineering protocol (Gene Bridges).

Along the recombineering steps, the bacteria will change antibiotic resistance upon introduction of different components. Thus, proper antibiotic selection pressure was utilized to select for the desired recombinants.

In this section I describe the steps involved in generation of CD169-DTR line. First, I performed retroviral transduction of immortalized mouse bone marrow (BM) line in order to test the function of the DTR construct. Subsequently, BAC recombineering was performed to clone the targeting insert into the start codon of CD169 locus. Afterward, the final BAC construct was introduced into ES cells, which were then injected into blastocysts to give rise to chimeric

mice. Chimeric mice were then bred to obtain CD169-DTR transgenic line. Lastly, the ablation profiles of $CD169^{+}$ macrophages were assessed in these mice.

3.2 Testing the functionality of the targeted insert

3.2.1. Transduction of immortalized bone marrow line with DTR construct

Nup-HoxB4 (NB4) BM cells were first transduced with pDTSRB in order to check the functionality of the DTR construct. This immortalized bone marrow line can be expanded and directed into macrophage differentiation [194]. Upon transduction with the transgene, NB4 BM cells were expected to express both DTR and Tomato fluorescence. After one round of transduction, a small fraction of the BMs expressed Tomato; as detected with FL-2 BD FACSCalibur channel. The transduced NB4 cells were sorted for Tomato expression (Fig. 3.2.A) and expanded. Fig. 3.2.B. shows the profile of sorted cells ('red cells') mixed with non-transduced NB4 cells ('white cells') in 1:1 ratio.

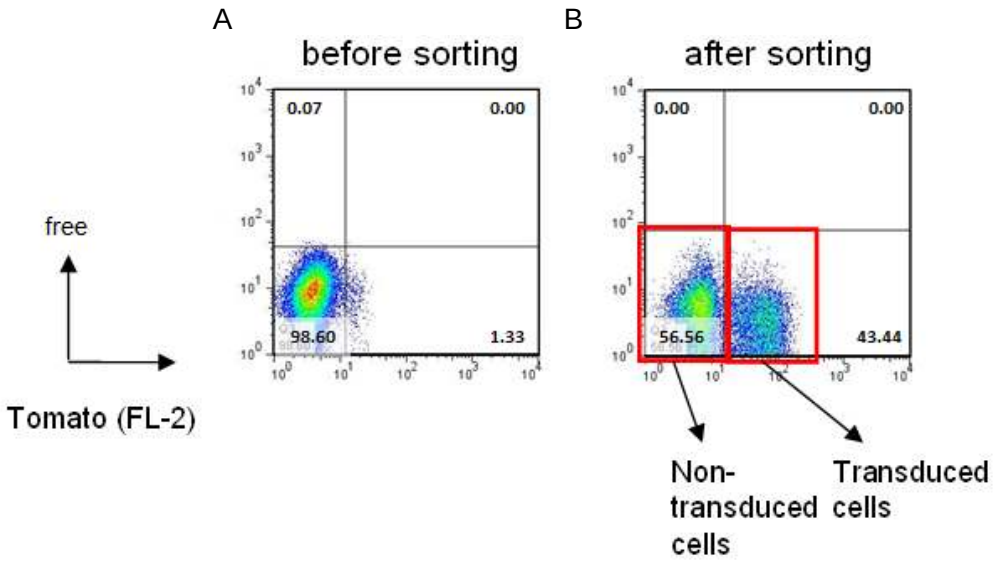

Figure 3.2. Flow cytometry analysis of pDTSRB-transduced NB4 BM cells. (A) Transduced NB4 BM cells before sorting. The transduced NB4 cells were sorted for Tomato expression. (B) Non-transduced and transduced NB4 BM cells were mixed in 1:1 ratio and analyzed as indicated.

3.2.2. DT sensitivity of the transduced NB4 cells

In order to test the DTR function, 2 x 10^5 white cells alone or 1:1 mixture of white and red cells were added per well of 24-well plate. DT was added in different concentrations. Flow cytometry analysis performed 48 hours after DT treatment showed that the red cells were ablated in concentration-dependent manner (Fig. 3.3). Titration showed that 100 ng/ml DT was the minimum concentration needed to obtain almost complete red cell depletion *in vitro* (Fig. 3.3). However, ~0.3% of Tomato-positive cells remained upon treatment with 100, 300, or 1000 ng/ml DT; and they could represent cells that do not express DTR.

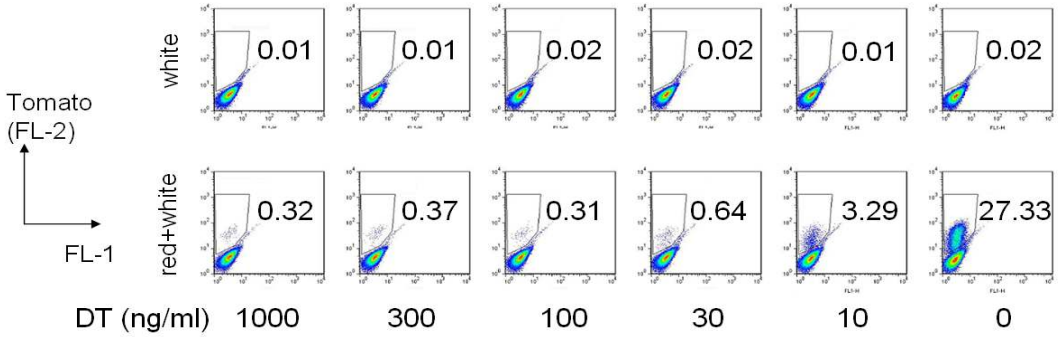

Figure 3.3. Flow cytometry profiles of NB4 cells 48 hours after indicated amount of DT addition. Upper row represents white (non-transduced) NB4 cells. Lower row represents mixture of white (non-transduced) and red (transduced) NB4 cells in 1:1 ratio.

3.2.3. NB4-derived macrophages

To assay the tomato expression and DTR function in macrophages, 10^6 of white or mixed NB4 cells were plated per 10 cm cell culture plate. Culture was maintained for >10days in IMDM 2% FCS supplemented with 30% of L-929-conditioned media. Using this method, NB4 cells were successfully differentiated into macrophages as evident by their typical shape and surface expression of F4/80 (Fig. 3.4 and 3.5). However, Tomato expression ceased in intensity as bone marrow cells differentiated into macrophages (Fig. 3.4 and 3.5). It seems likely that macrophages did not support the expression of the viral Long Terminal Repeat (LTR) promoter and subsequently reduced the Tomato fluorescent intensity. Nevertheless, I observed by microscopy that red NB4-derived macrophages were ablated in the presence of 10 ng/ml DT (not shown).

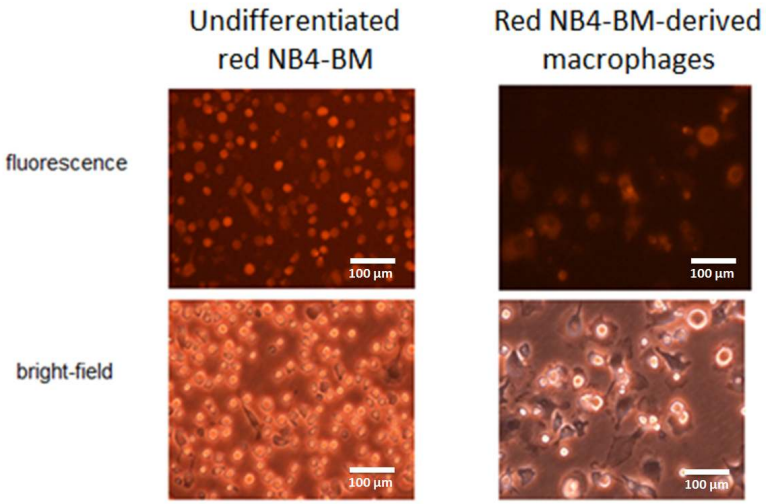

Figure 3.4. Microscopy of undifferentiated and differentiated NB4 BM transduced with DTSRB construct. The left panel shows undifferentiated red NB4 BM. The right panel shows the NB4 BM-derived macrophages at day 11 of culture in 30% L-929-conditioned media.

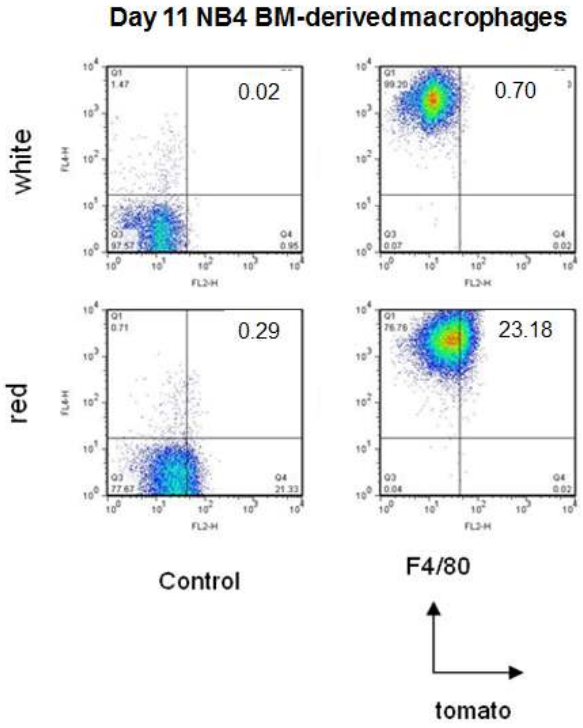

Figure 3.5. Flow cytometry analysis of NB4-derived macrophages. NB4 cells were cultured in 30% L-929-conditioned media for 11 days; after which macrophages are trypsinized and subjected to analysis with indicated markers. The upper panel shows white (untransduced) cells, while the lower panel displays the red (transduced) cells analyzed with indicated markers.

3.3. BAC recombineering

Prior to recombineering, the unmodified RP23-32L15 BAC was digested with SmaI to ensure BAC integrity (fig 3.6.A). The resulting fragments

corresponded with the predicted digestion patterns and thus BAC was intact. DTSRB Insertion fragment containing the transgene was prepared and cut from pDTSRB vector (Fig. 3.6.B). Homology arms spanning 500 bp upstream and 300 bp downstream of the targeted region were generated by PCR (Fig. 3.6.C) and ligated to the DTSRB fragment. After the first recombineering, Blasticidin resistant colonies were picked and screened by 5' and 3' check PCR; which flank DTSRB and the homology arms upstream and downstream of the transgene (Fig. 3.6.D). One positive clone was selected for second recombineering.

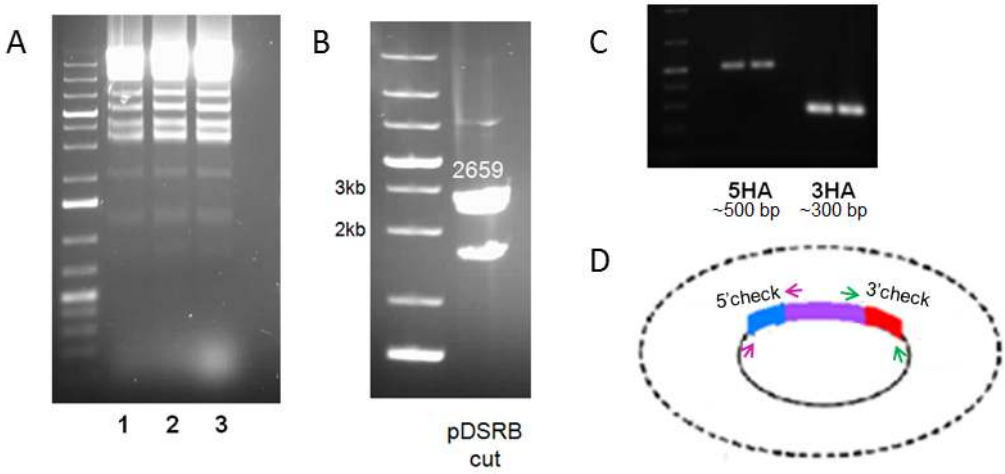

Figure 3.6. Agarose analysis for BAC and construct preparation for the first recombineering. (A) RP23-32L15 BAC containing the CD169 locus was digested with SmaI to check BAC integrity. (B) pDTSRB vector was cut with SapI enzyme, and 2659 bp band containing the transgene was purified. (C) PCR product of the homology arms upstream (5HA) and downstream (3HA) of the CD169 start codon. Both fragments were then digested with SapI enzymes and ligated with DTSRB construct. (C) Schematic diagram of PCR checking strategy for first recombineering. Blue and red regions represent homology arms, and purple region represents DTSRB. PCR was performed with 5' check primer pairs (purple) and 3'check primer pairs (green) to verify the resulting clones of the first recombineering step.

Second recombineering step was subsequently conducted to replace cloramphenicol with neomycin/kanamycin resistance sequence, thus aiding G418 selection in the ES cell stage. Colonies surviving the Kanamycin antibiotic selection were picked and analyzed for 5' and 3' Neo PCR (Fig. 3.7). Clone no. 1 was selected for sequence verification. Sequencing results confirmed the fidelity of the recombined sites, especially homology arms surrounding the DTSRB insertion site as well as the FRT sequence, which is the eukaryotic promoter of the Neomycin antibiotic marker.

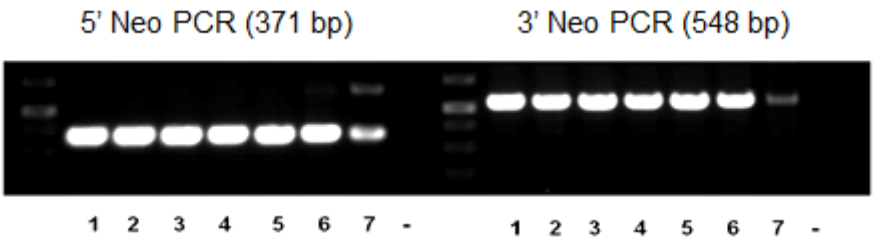

Figure 3.7. Agarose gel analysis of the second recombineering step. All clones gave the predictale agarose bands. No. 1 to 7 are the clones picked for second recombineering analysis, (-) is the PCR mix without template as negative control.

3.4. ES cell electroporation and selection

BAC maxiprep of the clone from second recombineering step (clone 1) was prepared, and the resulting BAC DNA was subsequently linearized using PI-SceI enzyme. Linearized BAC DNA was electroporated into BALB/c ES cell line, and positive clones surviving G418 selection were identified. There were 4 clones that survived the selection, and all are positive for the presence of transgene (Fig. 3.9). To ensure that the BAC molecule was intact upon integration into ES cell genome, additional BbR and BbF PCRs were performed (Fig. 3.8 and 3.9). Clone no. 4 was selected for injections into blastocysts. The low number of ES colonies might result from low amount of DNA electroporated (~30µg).

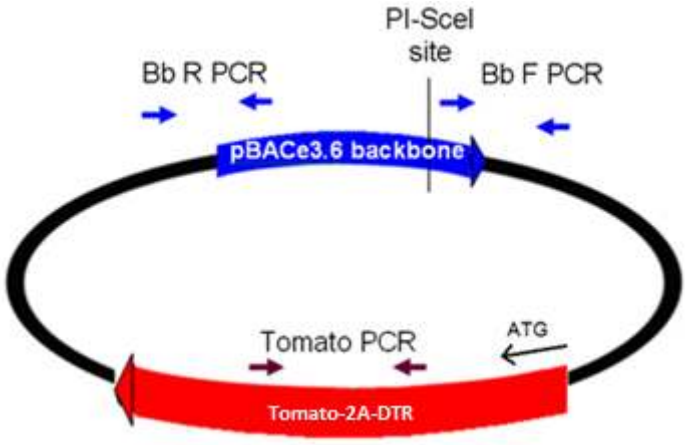

Fig. 3.8. Schematic structure of modified BAC and PCR strategy to screen positive ES clones. PI-SceI linearization site at the BAC backbone is shown. PCR primers that were used for ES clones screening are indicated in the diagram.

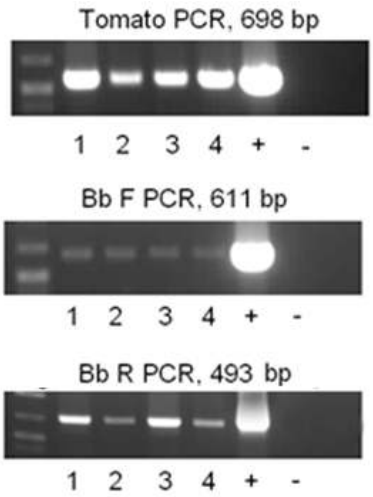

Figure 3.9. Agarose gel analysis for ES cell clones. All clones gave the predictale agarose bands. No. 1 to 4 are the ES clones surviving G418 selection, (+) is the BAC DNA as positive control, and (-) is the PCR mix without template as negative control.

3.5. Generation of CD169-DTR transgenic mice

CD169 clone 4 was injected into C57BL6/J blastocysts. Sixteen embryos were planted into two pseudopregnant mothers. The foster females gave birth to 4 pups, two of which were males with good chimerism (Fig. 3.10). Both males were mated with BALB/c females. One male gave rise to pups carrying germline transgene transmission as confirmed by tail DNA PCR. Heterozygous F1 progenies were mated to each other into homozygosity in order to maintain the CD169-DTR line. Homozygous candidates were first screened by qPCR (Fig 3.11) and confirmed by backcrossing with BALB/c mice. The underlying assumption of this qPCR method is that homozygous mice possess two copies of transgenes, while the heterozygous only have one copy [203]. However, due to the close fold differences, this method was not very accurate and resulting values from qPCR reactions often accompanied with big standard deviations. Thus, backcrossing is still necessary to confirm the genotype. Heterozygous mice were used for experiments.

Figure 3.10. Chimeric pups born from pseudopregnant mothers. Two out of four pups are chimeric. Both chimeric mice were males and subsequently mated with BALB/c females. One male was competent for germline transgene transmission to the progenies.

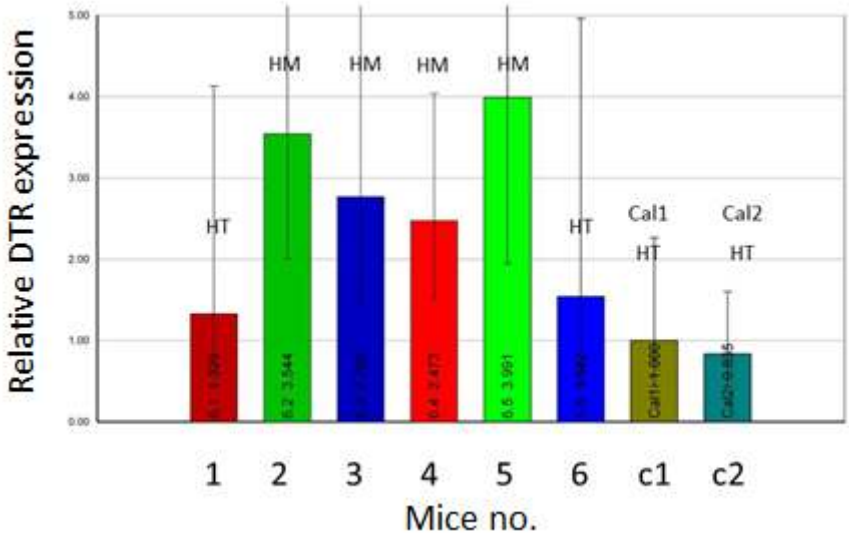

Figure 3.11. Representative qPCR graph for determining zygosity. Mice no. 1 and 6 were deemed heterozygous (HT), and mice no. 2, 3, 4, and 5 were homozygous (HM) candidates. Cal1 and Cal2 are known heterozygous controls which were used as calibrators.

3.6. Phenotype of CD169-DTR mice

3.6.1. Ablation of tissue macrophages in CD169-DTR mice

CD169 is well known to be strongly expressed on Marginal Zone Metallophilic (MZM) macrophages of the spleen and sub-capsular sinus (SCS) macrophages of the lymph nodes. Hence, these myeloid cell subsets are expected to be depleted upon DT administration to the CD169-DTR mice.

CD169-DTR$^{+/-}$ mice were injected with two-doses of DT intraperitoneally. Spleen and peripheral lymph nodes were harvested and subjected to cryosection. Stainings were performed with rat-anti-mouse CD169 antibody clone MOMA-1, which had been extensively used to study CD169^{+} macrophages in the past [171, 204]. However, this antibody gave weak signal, and thus subsequently secondary goat-anti-rat FITC antibody was used in order to amplify the signal in all immunohistochemistry studies performed. Indeed, MZM macrophages that formed ring-like structure surrounding B-cell follicles in spleen were depleted in DT-treated transgenic mice (Fig 3.12 upper panel). Likewise, SCS macrophages of the peripheral lymph nodes were also efficiently ablated in the CD169-DTR$^{+/-}$ mice (Fig. 3.12 lower panel).

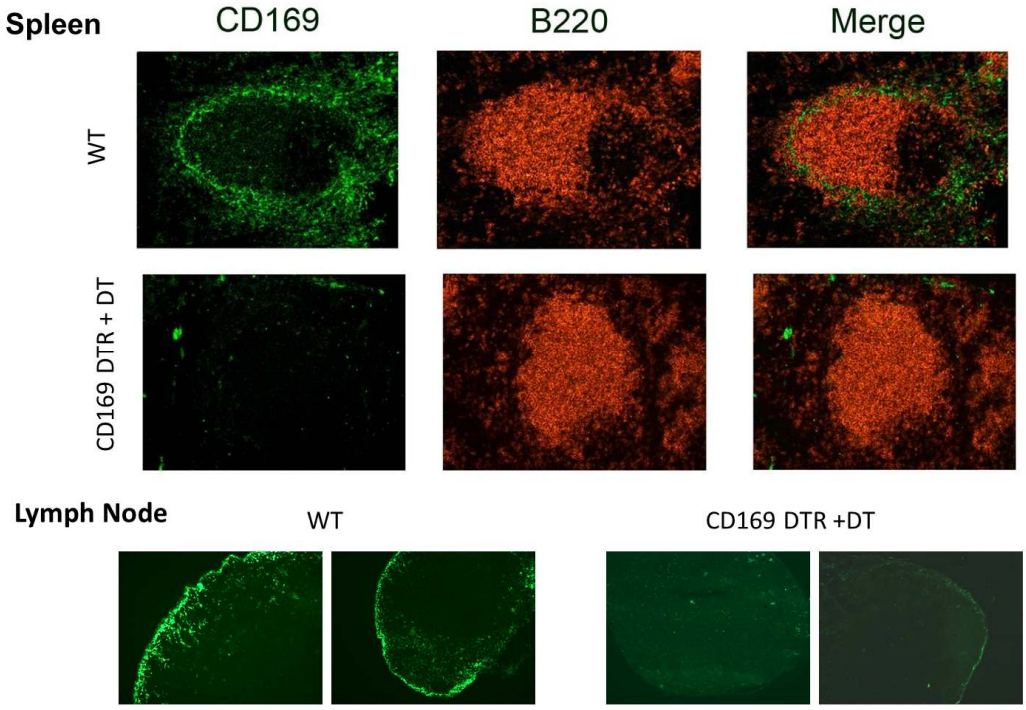

Figure 3.12. Depletion of CD169^{+} macrophages in a spleen and a peripheral lymph nodes. CD169-DTR$^{+/-}$ mice were injected with two doses of 20ng DT per gr body weight by intraperitoneal (i.p.) injections in one-day interval. Twenty-four hours after the second injection, mice were sacrificed and spleens and peripheral lymph nodes were harvested and frozen for cryosection. Staining was performed with anti-B220 PE antibody to visualize B-cell follicles in spleen. Rat-anti-mouse MOMA-1 FITC antibody against CD169 was conjugated with goat-anti-rat FITC antibody to amplify the signal. Data is representative of two experiments (n=2).

Spleens from wild type (WT) and DT-treated mice were further stained with different markers for myeloid cells (Fig. 3.13). Aside from the clear ablation of CD169^{+} cells, F4/80^{+} and CD11c^{+} splenic cells were partially depleted.

Previously, red pulp macrophages were also described to express CD169 in minute amount during their development [94]. Hence, this population was expected to be depleted as well in the treated spleen. However, aside from depletion of $CD169^+$ macrophages on the subcapsular region (Fig. 3.14), depletion of $F4/80^+$, $CD11b^+$, and $CD11c^+$ cells in the lymph nodes were hard to judge. I expected medullar macrophages, which are defined as $F4/80^{hi}CD11b^+$ $CD169^+CD11c^{lo}$ cells [94], to be ablated as well. However, it was difficult to ensure the depletion of medullary macrophages by microscopy as other myeloid cells such as DCs express similar markers. Stainings against additional markers which could discriminate red pulp macrophages and medullar macrophages are needed to confirm their depletion.

To further analyse macrophage depletion in flow cytometry, single-celled suspension of spleen and bone marrow from untreated and DT-treated mice were prepared. It would be ideal to perform flow cytometry analysis with antibody against CD169 molecule; however, MOMA-1 antibody gave weak signal and could not be visualized clearly in flow cytometry (data not shown). Hence, stainings were performed with antibodies against CD11b and F4/80. As expected, flow cytometry analysis revealed depletion of $F4/80^+CD11b^{+/lo}$ cells which corresponded to splenic red pulp and bone marrow $CD169^+$ macrophages (Fig. 3.15). The nondepleted $CD11b^+$ cells are neutrophils ($F4/80^-CD11b^+$ cells), monocytes ($F4/80^+CD11b^+$ cells), and other $CD11b^+$ macrophages.

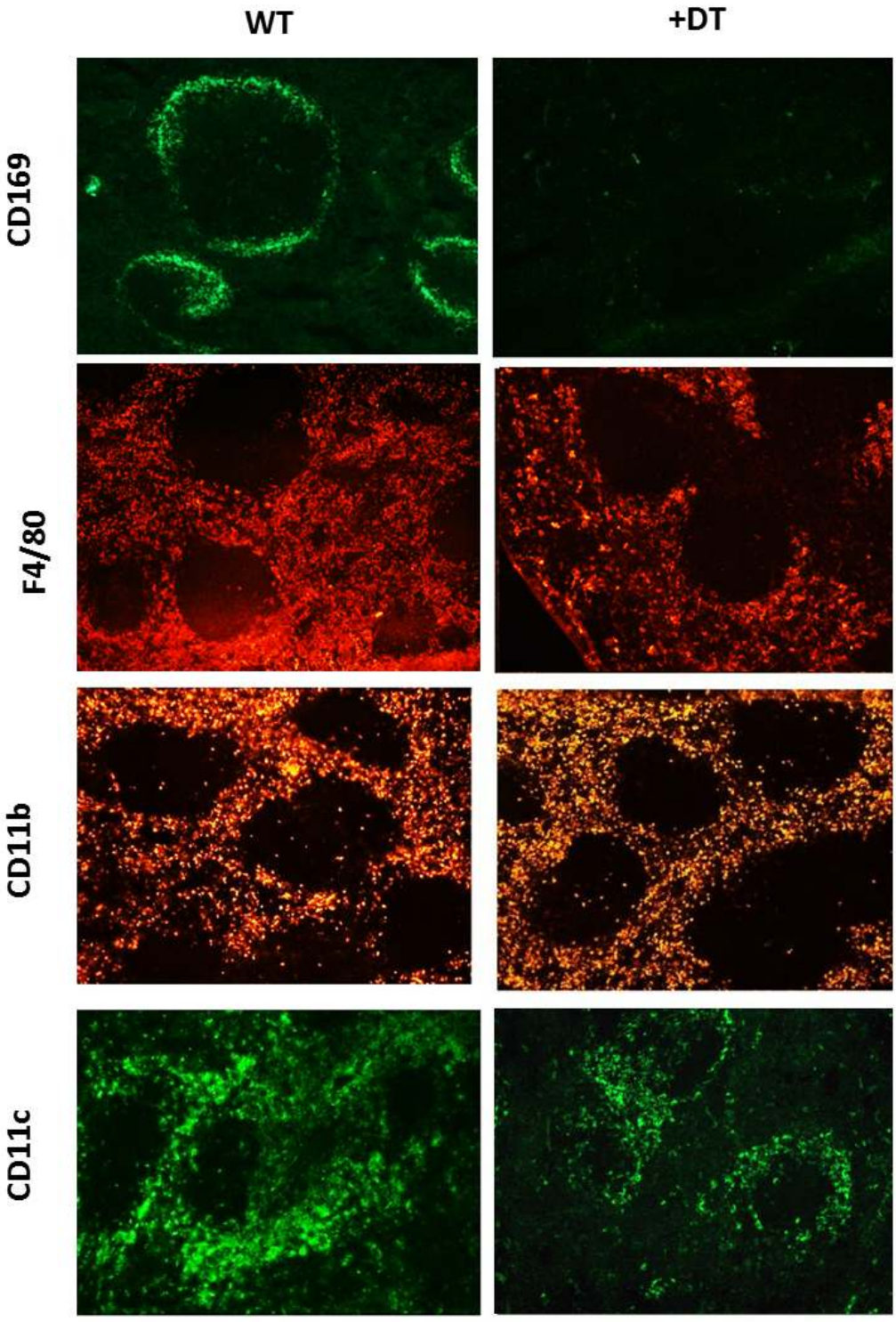

Figure 3.13. Ablation specificity of splenic CD169^{+} cells in CD169-DTR mice. CD169-DTR$^{+/-}$ mice were injected intraperitoneally with two doses of 20 ng/gr body weight DT in one-day interval. Twenty-four hours after the second injection, mice were sacrificed and spleens were harvested and snap-frozen for cryosection. Spleen sections were analysed with antibodies as indicated. Results are representative of two experiments (n=2).

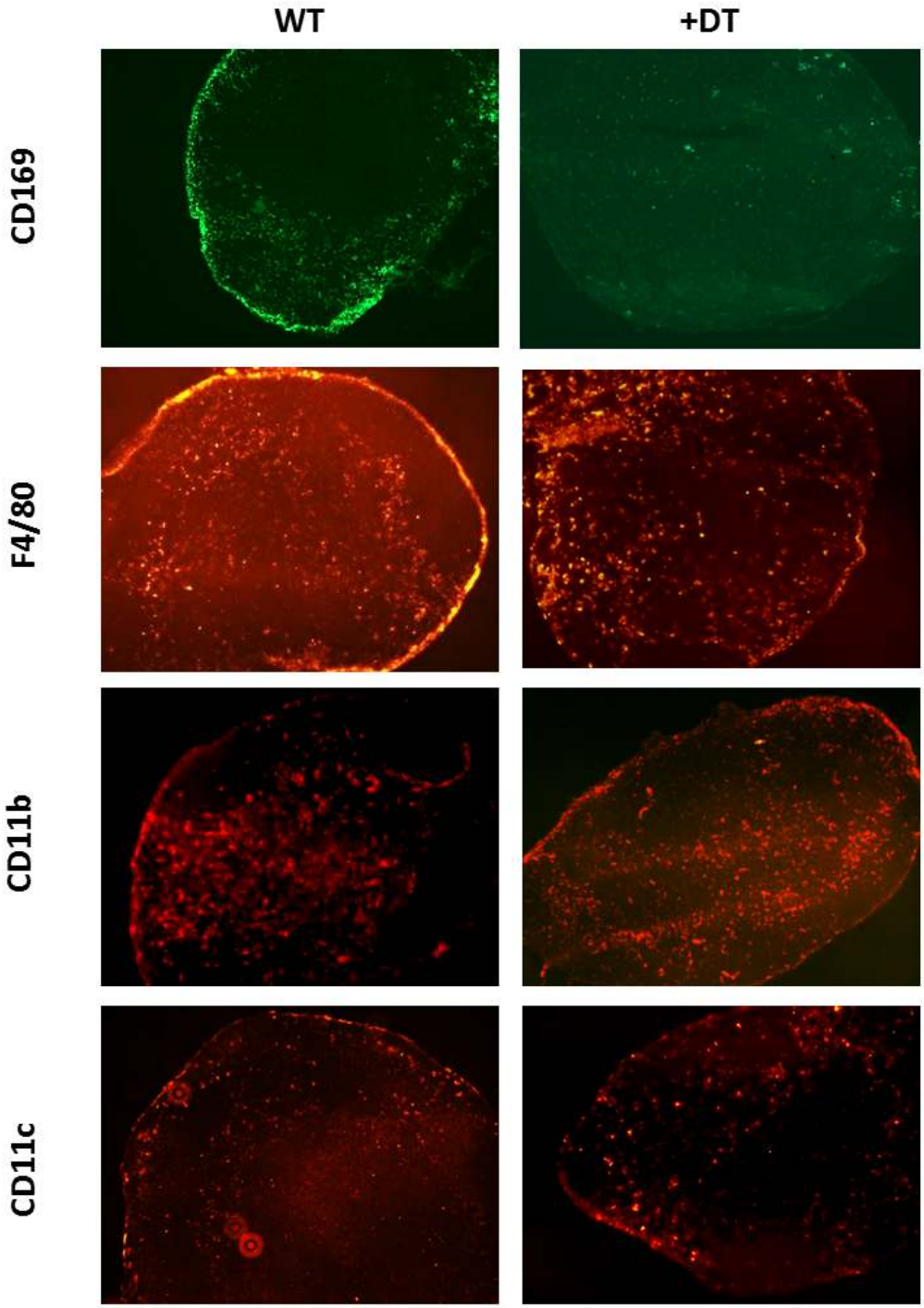

Figure 3.14. Ablation specificity of CD169^{+} cells in the lymph nodes of CD169-DTR mice. CD169-DTR$^{+/-}$ mice were injected intraperitoneally with two doses of 20 ng/gr body weight DT in one-day interval. Twenty-four hours after the second injection, mice were sacrificed, lymph nodes were harvested and snap-frozen for cryosection. Lymph node sections were analysed with indicated antibodies. Results are representative of two experiments (n=2).

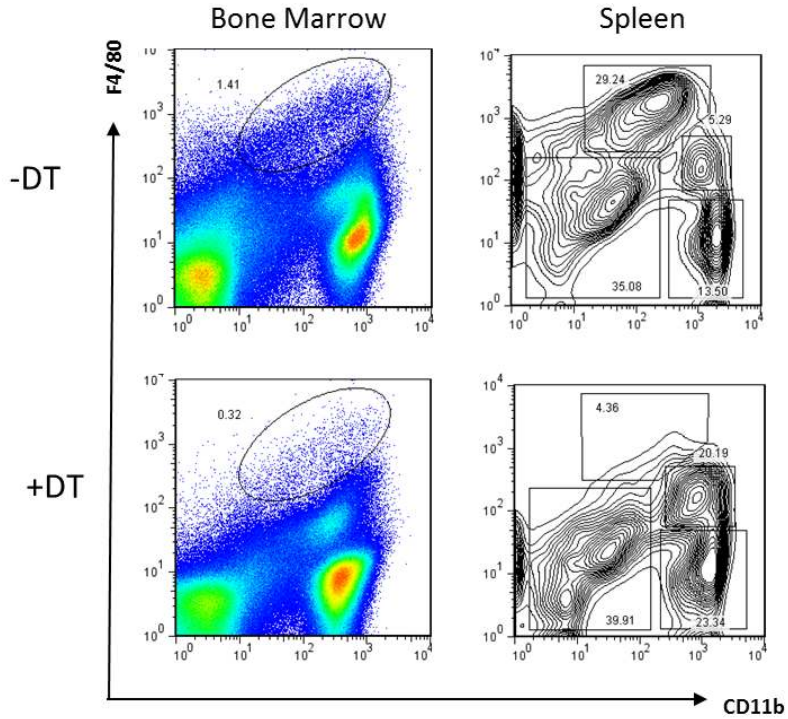

Figure 3.15. Ablation specificity of macrophages in spleen and bone marrow of CD169-DTR mice. CD169-DTR$^{+/-}$ mice were injected intraperitoneally with two doses of 20 ng/gr body weight DT in one-day interval. Twenty-four hours after the second injection, spleens and bone marrows were harvested, processed, and stained with antibodies against CD11b and F4/80. The above plots were gated on SSC-FSC high cells. Results are representative of two experiments (n=2).

Therefore, I have confirmed that the CD169-DTR mice mediate *in vivo* ablation of CD169^{+} macrophages in spleen, lymph nodes, and bone marrow. Assessment of depletion profiles in other lymphoid and peripheral tissues requires further study.

3.6.2. Determination of optimal dose of DT for CD169-DTR mice

To determine the minimum effective DT dosage for CD169 transgenic mice, 4, 8, 16, and 32 ng/gr of mice body weight DT were injected in 48 and 24 hours before analysis. Cryosection were performed to assess the depletion efficiency of spleen MZM macrophages. Few traces of cells remained in spleen of mice injected with 4 ng/gr DT as viewed by fluorescence microscopy (Fig. 3.16, top panel). Meanwhile, mice injected with 8, 16, and 32 ng/gr DT displayed complete depletion. Hence, 8ng/gr is the minimum working

concentration. For the rest of the depletion or influenza experiments, 10 ng/gr body weight DT dose were used.

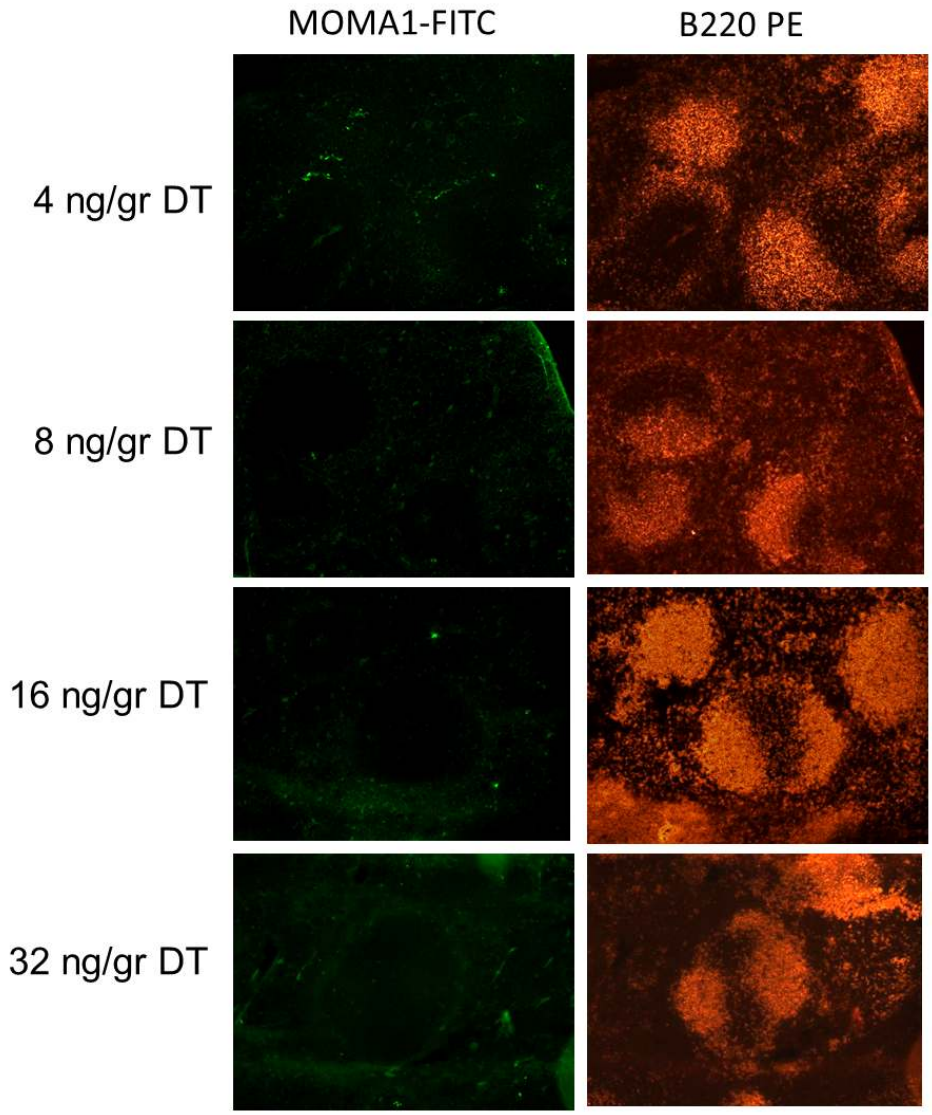

Fig 3.16. Titration of optimal DT dose for depleting spleen CD169^{+} macrophages. CD169-DTR$^{+/-}$ mice were injected intraperitoneally with indicated doses of DT in one-day interval. Twenty-four hours after the second injection, spleens were harvested and snap-frozen for cryosection. Stainings were performed with MOMA1-FITC conjugated with anti-rat FITC antibody and subsequently with anti-B220 PE antibody. Results are representative of two mice per group.

3.6.3. Turnover kinetics of splenic CD169^{+} macrophages

I then explored on how frequently DT need to be injected to maintain depletion. Cryosections of spleens harvested at different time-points after DT treatments were examined (Fig. 3.17). I observed that macrophages were fully ablated up to day 2 after DT injection, and began to repopulate as early as day 3 post-

treatment. To maintain 100% depletion, one would need to inject DT every 2-3 days.

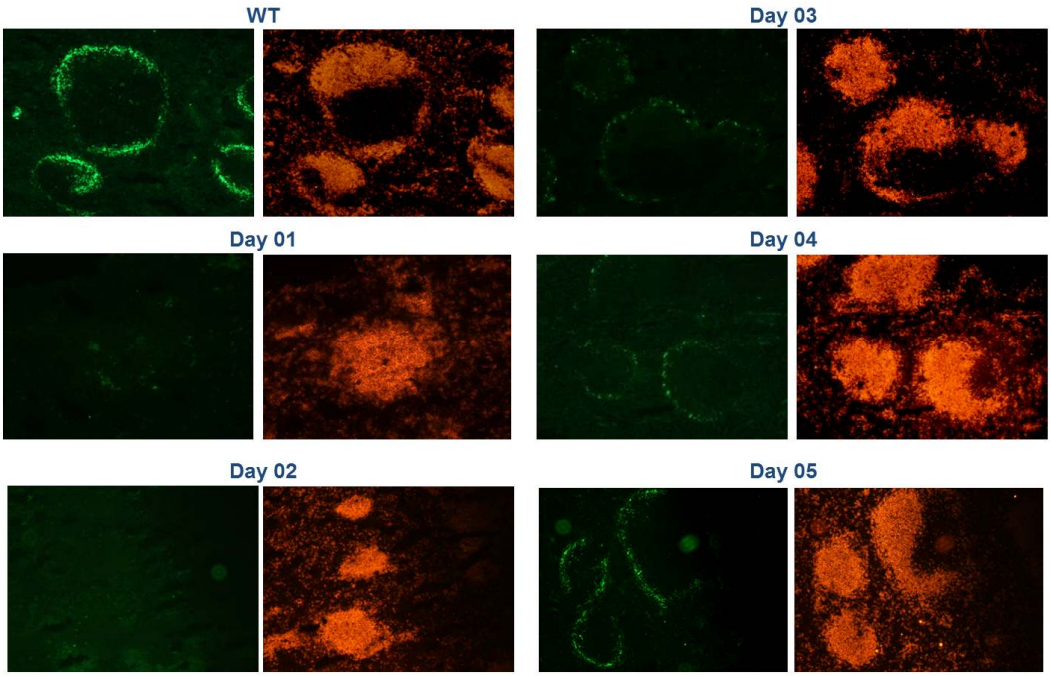

Figure 3.17. Splenic CD169^{+} macrophages turnover kinetic upon DT treatment. CD169-DTR$^{+/-}$ mice were injected intraperitoneally with two doses of 10 ng/gr body weight of DT in one-day interval. For 5 consecutive days after the last DT injection, spleens were harvested daily and snap-frozen for cryosection. Stainings were performed with MOMA1-FITC conjugated with anti-rat FITC antibody and subsequently with anti-B220 PE antibody. Results are representative of two mice per group.

3.6.4. Maintaining depletion in experimental time window

Repeated injection of DT may induce the production of neutralizing antibody [144] that dampen the depletion efficiency. Therefore, I injected DT daily from day 0 till day 14 and monitored the effectiveness of spleen CD169^{+} MZM macrophage depletion. As depicted in Figure 3.18, some CD169^{+} cell traces were detected on day 14 after infection. At this point, mice had been injected 14 times with DT consecutively; thus the return of CD169^{+} cells may result from DT neutralization by antibodies. This factor may need to be considered for future study; especially if longer experimental time window is required.

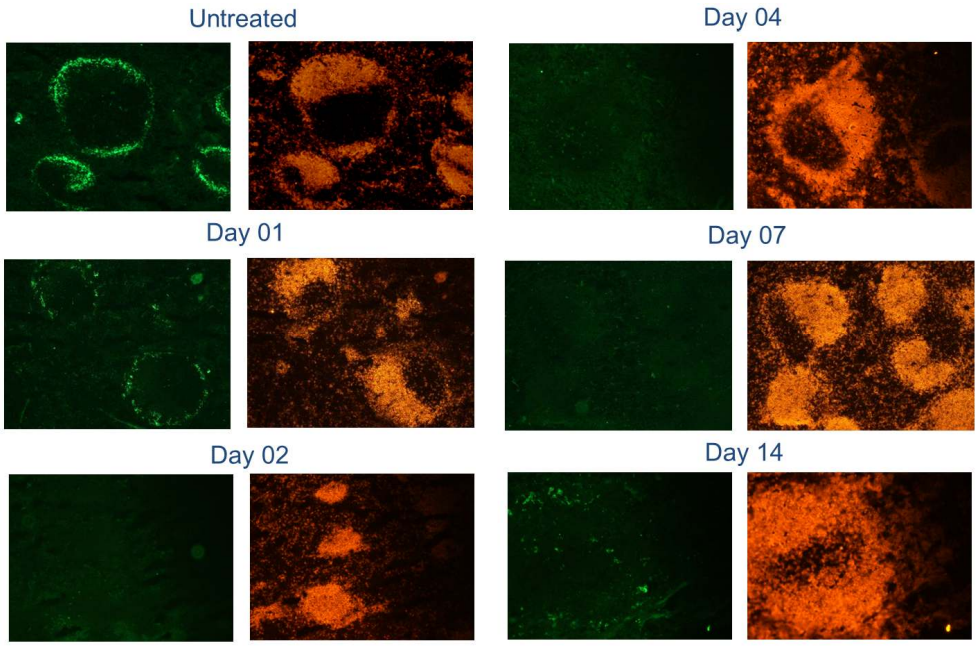

Figure 3.18. Spleen CD169^{+} macrophage depletion upon repeated injections of DT. CD169-DTR$^{+/-}$ mice were injected intraperitoneally with daily dosage of 10 ng/gr body weight of DT. On day 1, 2, 4, 7, and 14, spleens were harvested and snap-frozen for cryosection. Stainings were performed with MOMA1-FITC conjugated with α-rat FITC antibody and subsequently with B220 PE antibody. Results are representative of two mice per group.

3.7. Discussion

To generate CD169-DTR mice, I utilized BAC transgenesis and inserted the DTR construct into CD169 locus. The usage of 2A peptide separating the DTR and Tomato coding sequences was meant to replace IRES (internal ribosomal entry site). Two disadvantages of IRES are the large size and discrepancy in translation levels between coding sequences upstream and downstream of IRES; with the genes downstream often being expressed in much lower level [205]. On the other hand, 2A sequence mediates co-translational cleavage of multiple proteins flanking the peptide; ensuring protein expression at equimolar levels [206]. The 2A sequence is relatively short (20 amino acids) and contains consensus motif Asp-Val/Ile-Glu-X-Asn-Pro-Gly-Pro. This peptide mediates self-cleaving because the ribosomes skip the peptide bond formation between Glycine and the last Proline [207]. Also, 2A was proven to be non-cytotoxic, inherited through the germ-line and able to mediate co-translational cleavage efficiently in transgenic mice [208].

Moreover, I chose to utilize tandem dimer Tomato which was developed to achieve extra brightness while preventing aggregation [209, 210]. I have verified the function of the DTR-2A-Tomato construct by using mouse BM cell line engineered to over-express NB4 fusion protein. The line was shown to provide robust support of HSC and MPP expansion, without causing leukemia in mice [194]. The DTR-mediated ablation worked nicely, but Tomato signal was rather weak. Moreover, BM-derived macrophages *in vitro* seemed to downregulate the Tomato signal. One reason was possible expression of C/EBPβ (CCAAT enhancer binding protein beta) transcription factors by macrophages, which may downregulate the HIV-1 LTR – the promoter of pDTSRB in this experiment. Three C/EBP binding sites were present in the negative regulatory element of the HIV-1 LTR, and hence may mediated repression of the activity [211]. In addition, integration of BAC in low copy number to ES genome might as well result in inadequate level of Tomato expression. Premature 2A-mediated-cleaving that occurred before Tomato was fully translated may be another reason. Nevertheless, other studies were also unable to detect fluorescence reporters for gene expressions in transgenic mice; as in the case of CD11b-DTR-EGFP and zDC-DTR-mCherry mice [157, 168]. Efforts to detect DTR/Tomato expression can be done in the future. One method is by developing good antibodies against DTR; thus enabling detection of cells expressing the respective molecules on their surfaces.

I chose to electroporate linearized BAC into ES cell in order to avoid random breaks during recombination into the ES genome; which may occur in the case of circular BAC. Nonetheless, circular BACs have been proven to generate functional transgenic mice as well [212]. However, in our lab, we observed that linear BACs were taken up and incorporated into the ES cell genome more effectively than circular ones (unpublished observation).

The ES cell screening strategy used in this study did not discriminate between random integration and targeted integration (knocked in via homologous recombination) of the BAC DNA into the ES cell genome. Copy numbers and the position of the BAC DNA integration were not assessed as well. Nonetheless, the CD169-DTR mice have healthy progenies, with no observed congenital defects in heterozygous or homozygous mice. Moreover, the tissue distribution of CD169 macrophages and the ablation profiles were consistent

with previous studies [94, 191]. Thus, the targeting strategy, whereby the DTR construct (DTTSRB) was engineered into the start codon of the CD169 locus by BAC transgenesis, did not disrupt the structure of the endogenous locus; hence allowing physiological expression of CD169 and DTR. Unlike some published DTR line, the CD169-DTR mice did not suffer from repeated DT injection. This was the case with CD11c-DTR mice which died after multiple DT injections due to depletion of an essential radioresistant population causing mortality [167, 168]. Since DT treatment is non-toxic to the CD169-DTR mice, further experiment in this line can be performed without the need of generating bone marrow chimeras.

BALB/c mice that were used to generate CD169-DTR line are a typical Th2 strain, while C57BL/6 mice are a Th1 strain. Th1 and Th2 strains will have different preference in type of cytokines produced in response to infection, with Th1 strain skewed into Th1 responses (high IFNγ and low IL-4) and Th2 strains to Th2 responses (low IFNγ and high IL-4) respectively. There may be differences in immune responses against IAV infections; such as in lymphocyte proliferation, cytokine profiles, and even macrophage responses between the two mice strains [213]. To resolve this matter, crossing of the existing BALB/c CD169-DTR mice with WT C57BL/6 mice can be done; and study can be conducted to assess any differences in the outcome of IAV infections.

To detect $CD169^+$ population *in vivo*, I mainly performed immunostaining on organs prepared by cryosection. Flow cytometry with the MOMA-1 FITC antibody was attempted but this antibody gave very weak signal, even after amplification with secondary antibody (results not shown). Improvement can be done by generation of new monoclonal antibody with better affinity against CD169 molecule.

I have shown by immunohistochemistry and/or flow cytometry the depletion profiles of spleen, lymph nodes, and bone marrow macrophages upon DT treatment (Fig. 3.13-3.15). Further characterization with additional markers is needed to confirm the phenotypes of these depleted macrophages. One can also look into other organs such as liver and gut to see if depletion of $CD169^+$ macrophages can be mediated in those organs.

Furthermore, I have determined the DT working dosage and spleen MZM repopulation kinetic (Fig. 3.16 and 3.17). Minimum DT working dosage is determined as 8 ng/gr body weight, which is accepted as safe range [144]. In the future, I will use 10 ng/gr body weight DT for Influenza experiment, which is also rendered non-toxic to mice. Observation by immunohistochemistry on frozen spleen section demonstrated that MZM macrophages were beginning to repopulate as early as day 3, and approximately half of the population were back on day 5 (Fig. 3.17). Likely, these macrophages have half-life of 7 days and would fully repopulate on day 10-14 post-DT treatment; consistent with observation from the other group [191]. Additionally, I had given the mice daily i.p. DT treatments up to 14 days. From the results, I estimated that DT began to lose its effectiveness after 10-14 consecutive injections; arguably because the mice immune system produced neutralizing antibodies. In real experiment, I will inject DT every 3-5 days, thus I estimate that the experimental time window will be effective for one-two months, depending on the frequency of DT injection. To address this matter more closely, experiments whereby the DTR mice are DT-treated on fixed interval and monitored over longer period are required.

There are much to be learnt about roles of $CD169^{+}$ macrophages in the tissues they reside in; both in homeostasis and inflammation. Therefore, I believe that this CD169-DTR mice model can be utilized to study of various pathological/physiological processes that involve macrophages.

CHAPTER 4: RESULTS II

THE ROLE OF ALVEOLAR MACROPHAGES IN INFLUENZA A INFECTION

4.1. Background

In influenza research, mice have been favored as the animal model because of their small size, availability, low maintenance cost, as well as the diversity of genetic backgrounds, genetic tools, and immunology reagents available [214]. The current animal model to study human influenza viruses is ferrets, since their symptoms, pathogenesis, and immunity upon influenza infection closely resemble human influenza diseases [215]. However, ferrets are bigger and bring extra cost for maintenance; and generally they are inaccessible to most researchers.

BALB/c or C57BL/6 mouse strains have been commonly used in influenza studies. The two most common influenza A virus (IAV) adapted strains used are Puerto Rico/8/1934 (H1N1) [PR8] and A/WSN/1933 (H1N1) [WSN] [215]. Unlike non-laboratory wild type mice, most laboratory mice lack the functional Mx1 protein, and thus are highly susceptible to IAV including PR8 and WSN [216, 217]. Human virus isolates require adaptation to the mice, due to the preference of human IAV to bind α2,6 linked sialic acids which are abundant in human, but not in mice airways [218, 219]. Unlike the occurrences of contact transmission in human, mice do not transmit the IAV infection to other mice [220], Mice also do not develop fever, although they might suffer from hypothermia [221]. Influenza A infection in mice damages mainly the lower respiratory tract rather than the upper tract; with clinical manifestation of weight loss and lethargy.

As mentioned in chapter 1, Influenza immunity is a complex interplay between different innate and adaptive components, taking place in different stages during the course of infection. Figure 4.1 illustrates the course of innate and adaptive immune responses during primary influenza infection [222, 223]. Upon acute infection, influenza virus rapidly replicates in the host. The virus

titer peaks approximately at day 3 post infection, usually correlating with fever and symptoms of upper respiratory infection in human [222]. The innate immunity such as NK cells and interferon responses are activated early to restrain the virus growth while adaptive immunity undergoes priming [223]. At day 3-6, when the first wave of innate immune responses goes down, the adaptive immunity starts to develop. T cell mediated-immunity peaks on approximately 6-10 days p.i. and then diminishes to memory or resting state; while the antibody responses come through on later stage. Due to the sustenance of the antibody in the host serum and mucosa, reinfection with similar strain will result in lower viral titers and alleviation in symptoms [222].

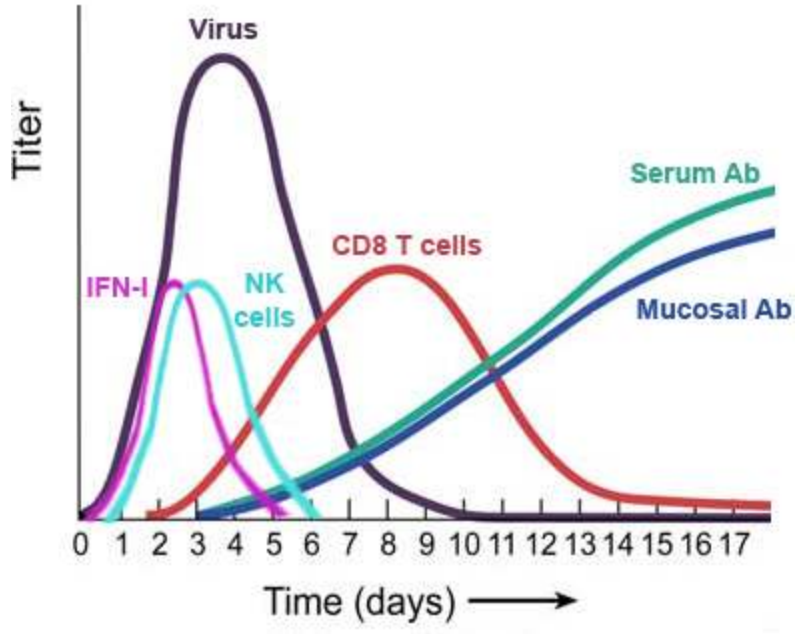

Figure 4.1. The course of innate and adaptive immune responses during primary Influenza virus Infection. Adapted from Subbarao et al., 2006 [222] and Janeway's Immunobiology sixth edition, 2005 [223].

In this section, I first demonstrate that alveolar macrophage (AM) depletion could be induced in CD169-DTR mice. Preliminary experiments were then conducted to assess the working dose of PR8, the route of DT administration, and the turnover of lung AMs. I proceeded to infect CD169-DTR mice with PR8 IAV strain and monitored a number parameters that are regularly used to monitor IAV infection in mice [224]; namely the changes in body weight, mean time to death, pathology, and lung viral titer. Bone marrow chimeric mice were also generated to confirm the observation made in CD169-DTR mice. In addition, I also studied the kinetics of myeloid cell subsets during the early phase of IAV infection, as well as examined the flu-specific CD8 T cell

responses in both WT and CD169-DTR mice. Lastly, I assessed the effects of AM ablation initiated at different time points post infection. Findings are discussed at the last part of this chapter.

4.2. Depletion of alveolar macrophages in CD169-DTR mice

4.2.1. Lung sections from DT-treated CD169-DTR mice

To visualize depletion in lung myeloid cells, CD169-DTR$^{+/-}$ mice were injected with two-doses of DT intraperitoneally. Mice were sacrificed by cervical dislocation 24 hours after the last DT treatment, and lungs were harvested for cryosection. In untreated mice, CD169^{+} and F4/80^{+} cells are distributed in the alveolar spaces and also near the mucosa of bronchioles/respiratory ducts (Fig. 4.2). Note that expression of both markers is overlapping. As expected, most of the CD169^{+}F4/80^{+} cells were depleted upon DT treatment (Fig. 4.2). CD11b^{+} cells were located throughout the lung parenchyma and mostly remained after depletion. These cells are presumably dendritic cells, other macrophages (interstitial macrophages), and granulocytes. CD11c^{+} cells were found in alveolar air spaces, lung interstitium, and in the subepithelial regions of the airway mucosa. Upon DT treatment, CD11c^{+} AMs were ablated, while the other CD11c^{+} cells remained. In addition, CD103^{+} DCs were also not affected by DT treatment (Fig. 4.2).

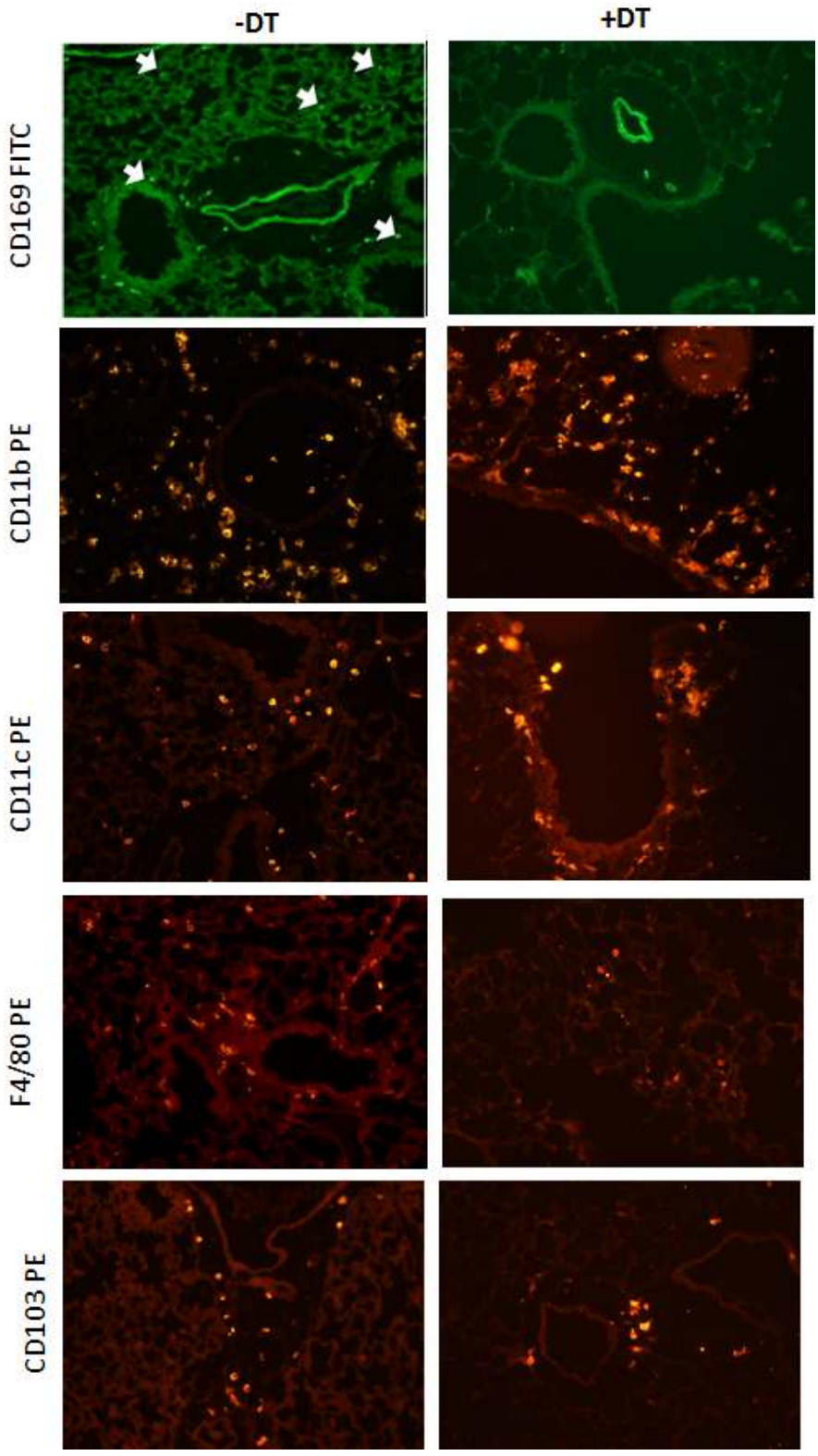

Figure 4.2. Ablation specificity of lung macrophages in CD169-DTR mice. CD169-DTR$^{+/-}$ mice were injected intraperitoneally with two doses of 10 ng/gr body weight DT in one-day interval. Mice were 24 hours after the last DT treatment by cervical dislocation. Lungs were inflated with PBS/OCT (1:1) and were snap-frozen en bloc. Cryosections were performed and 6µm thick sections were fixed in acetone and then stained with antibodies against indicated markers. Results are representative of two experiments (n=2).

4.2.2. Flow cytometric analysis of DT-treated CD169-DTR mice

The depletion profile in the bronco-alveolar lavage fluid (BALF) and lungs of control and DT-treated mice were further examined by flow cytometry. The gating strategies to analyze lung immune cells are depicted in Fig. 4.4.

BALF analysis of naïve mice revealed major depletion of $FSC^{high}SSC^{high}$ cells (Fig. 4.3.A). These cells were characterized as $F4/80^{+}CD11b^{lo}CD11c^{hi}$ $MHC\text{-}II^{low}$ cells (Fig. 4.3.B), fitting the description of AM in previous studies [94, 225]. In addition, some infiltrations of neutrophils and even dendritic cells into the alveolar spaces were observed upon DT treatments (Fig. 4.3.C-D).

Similarly, efficient (>90%) depletion was observed in lung tissue (Fig 4.5). Some literature display AMs in CD11c against F4/80 plot [225] where $F4/80^{+}CD11c^{+}$ cells are described as AMs, and $F4/80^{+}CD11c^{-}$ cells as interstitial macrophages. However, $F4/80^{+}CD11c^{+}$ cells include also monocytes and DC, and thus this combination of markers is not reliable to monitor depletion efficiency (Fig. 4.5.A). Instead, I decided to monitor AMs by using $CD11b^{-}F4/80^{+}$ combination of antibodies (Fig. 4.5.B). No major differences in DC, pDC, or lymphocyte counts were observed (Fig 4.5.C-F). Minute reduction in B cells number, however, was observed. Hence, I concluded that CD169-DTR mice facilitate specific depletion of AMs in both lung parenchyma and alveolar airspaces.

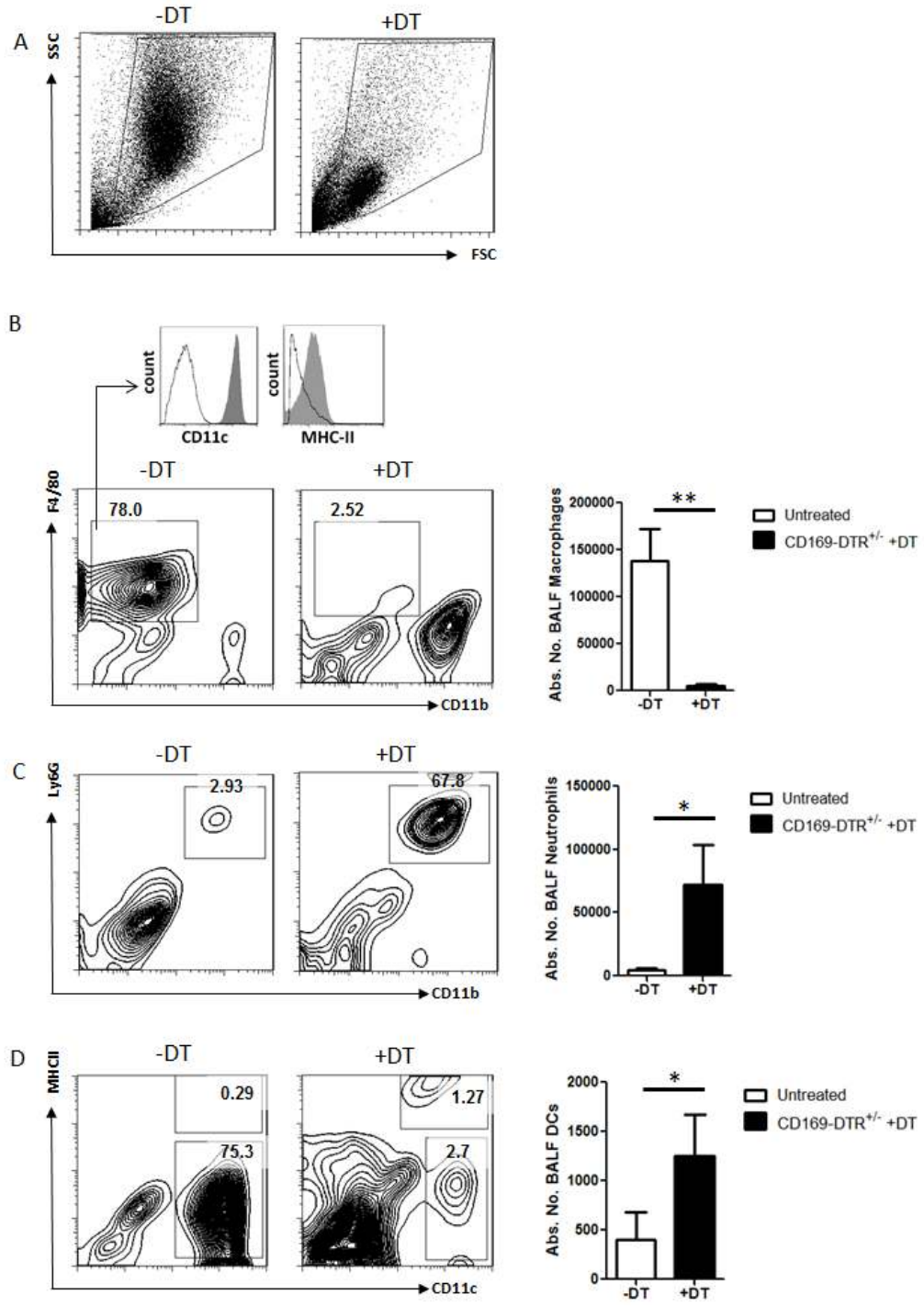

Figure 4.3. Depletion of AMs in BALF of DT-treated CD169-DTR mice. CD169-DTR$^{+/-}$ mice were injected intraperitoneally with two doses of 10 ng/gr body weight DT in one-day interval. Twenty-four hours after the second injection, broncho-alveolar lavage was harvested, processed, and stained with combination of myeloid markers as indicated. (A) FSC/SSC plot and gating strategy of BALF cells. Flow cytometry analysis (left panel) and absolute number (right panel) of (B) AMs, (C) Neutrophils, and (D) MHCII^{hi}CD11c^{hi} DCs. Error bars represent the mean ± SD. Results are representative of two experiments (n=3).

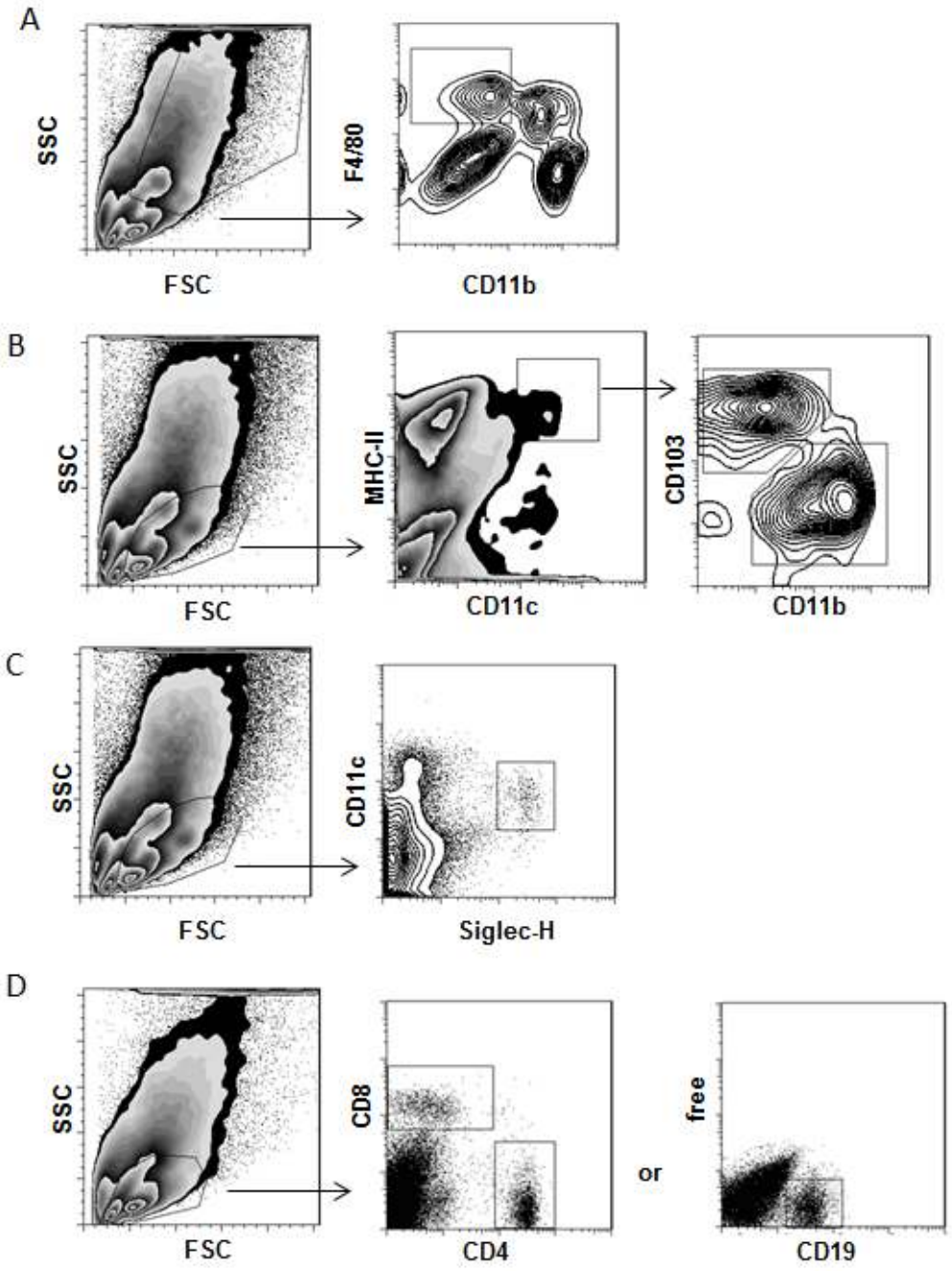

Figure 4.4. Gating strategies to visualize lung immune cells. (A) To analyse lung macrophages, SSC^{low}/FSC^{low} cells were excluded. (B) Dendritic cells were gated on SSC^{low}/FSC^{low} cells and MHC-$II^{hi}CD11c^{hi}$ cells. (C) pDCs were gated on SSC^{low}/FSC^{low} cells. (D) Lymphocytes were gated on SSC^{low}/FSC^{low} cells. The gated cells were then analyzed with antibodies against indicated markers.

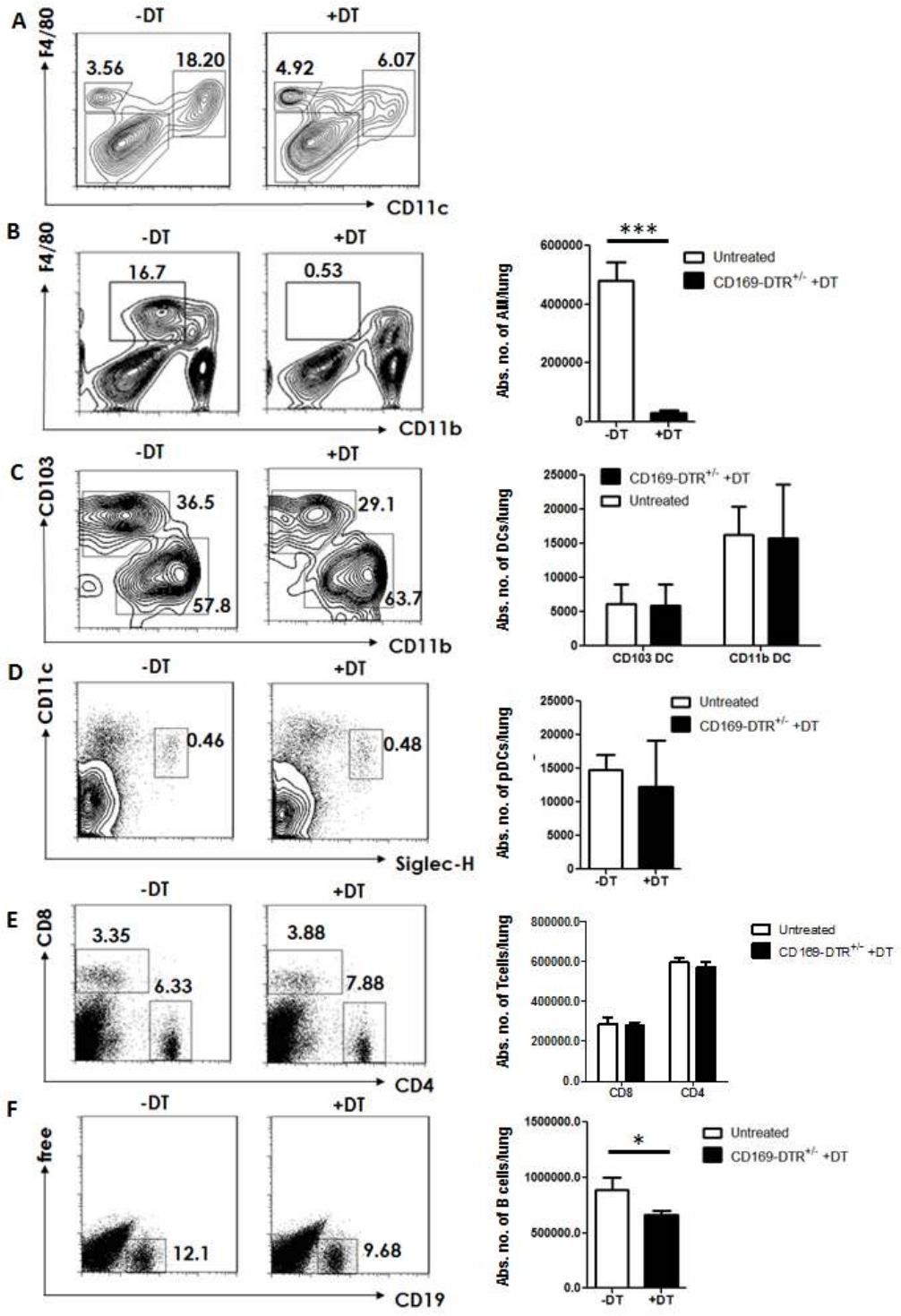

Figure 4.5. Specific depletion of lung AMs CD169-DTR mice. CD169-DTR$^{+/-}$ mice were injected intraperitoneally with two doses of 10 ng/gr body weight DT in one-day interval. Twenty-four hours after the second injection, lungs were lavaged and perfused with PBS before they were processed and stained with antibodies against indicated markers. Flow cytometry analysis (left panel) and absolute number (right panel) of lung (A) (B) macrophages, (C) DCs, (D) pDCs, (E) T cells, and (F) B cells. White bars represent WT mice, while black bars represent CD169-DTR mice. Gating strategies for flow cytometric analysis are shown in Fig. 4.4. Results are representative of two experiments (n=3).

4.3. Alveolar macrophages are critical for protection against influenza A virus infection

To evaluate whether depletion of AM affected disease prognosis or survival during influenza infection, I infected the mice with mice-adapted flu strain of A/PR/8/34 (PR8). WT or DT-treated CD169-DTR$^{+/-}$ mice were infected with different dose of PR8 as indicated. Intraperitoneal injections of 10 ng/gr body weight DT were given on day -2, -1, 2, 5, 8, 11, and 14 post-infection.

Mild infection with 1 PFU of PR8 caused ~10% weight loss of the WT mice, while the DT-treated CD169-DTR mice suffered ~30% weight loss (Fig. 4.6.A). Strikingly, DT-treated mice infected with 3 and 6 PFU of PR8 loss >30% of their weight and all died within 12 and 14 days respectively (Fig. 4.6.A and B). I also noted that unlike the control group which started to lose weight approximately on day 5 post-infection, the DT-treated groups displayed weight loss starting on day 1 post-infection. From this experiment, infection of the BALB/c strain with 3 or 6 PFU of PR8 suffice when sublethal infection is desired; while 1 PFU may be used whenever mild infection study is necessary. In contrast, no weight loss or signs of clinical illness was observed in CD169-DTR mice treated with DT but were not infected with flu (Fig. 4.6.A); implying that DT was nontoxic to the mice. Hence, the severe disease outcome observed in CD169-DTR mice was mediated by both influenza virus infection and the absence of AMs.

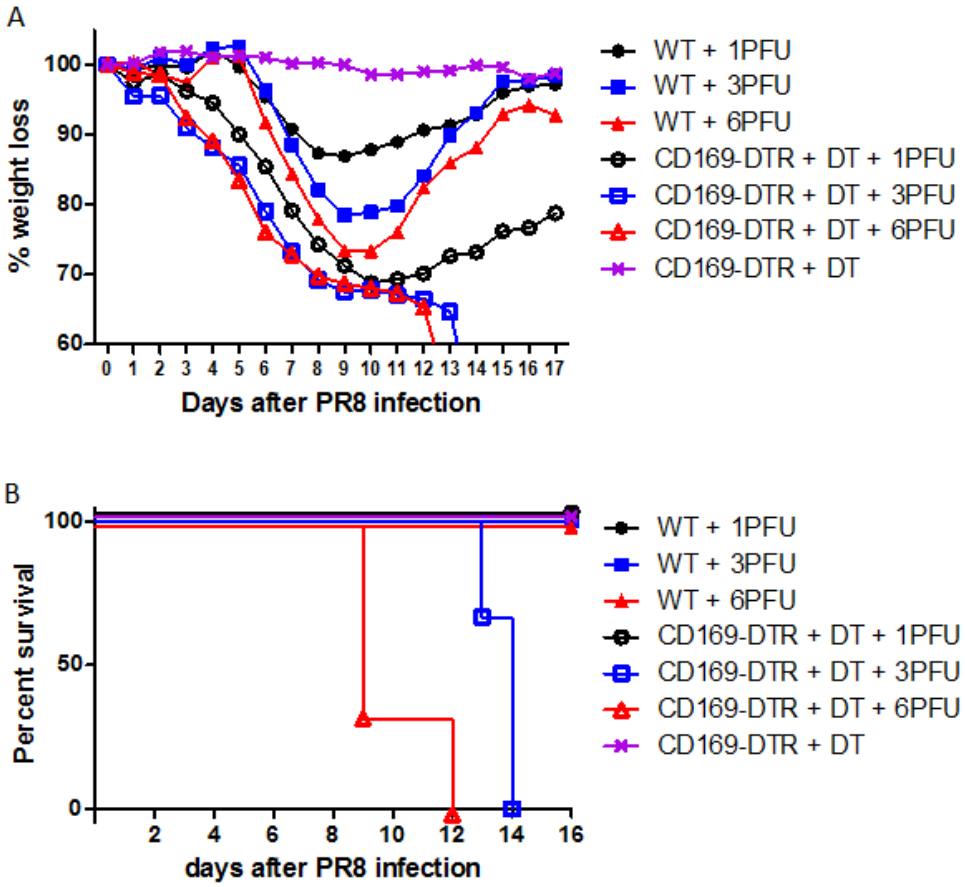

Figure 4.6. Increased mortality and morbidity of DT-treated CD169-DTR mice in IAV infection. (A) Weight loss curve of wild WT or DT-treated CD169-DTR mice with 1, 3, or 6 PFU of PR8 Influenza strain. The values are expressed as mean. (B) Survival curve of control and DT-treated mice infected with different dose of PR8. Results are representative of two experiments (n=3).

4.4. Comparison of the routes to deliver DT

The effects of local and systemic administration of DT were then examined. GeurtsvanKessel et al. preferred intratracheal (i.t.) DT injection to deplete airway immune cells [78]. They argue that depletion is more effective and does not affect distant organs in comparison to i.p. injection. To evaluate this, I administered two doses of DT either by i.p. injections (200 ng/mice) or i.t. injections (50 ng/mice), and sacrificed the mice 24 hours after the last DT treatment. I observed that i.p. and i.t. DT injection resulted in comparable depletion of lung macrophages (Fig. 4.7). Intriguingly, CD103 DC percentage was decreased upon i.t DT administration (Fig. 4.7.B). Moreover, cytospin of BALF revealed increased infiltration of neutrophils and mononuclear cells into

the lung airspace of the mice receiving i.t. DT administration (Fig 4.8). However, macrophages from distant tissue, i.e. spleen, were not affected by i.t. DT administration (Fig 4.7.D).

I then proceeded to evaluate the disease progression and survival of i.t. or i.p. DT-treated mice infected with 6 PFU of PR8. I found that weight loss and survival curve of the two groups behave similarly (Fig 4.9). Since there were no differences in mortality or morbidity between mice treated with DT via i.p. or i.t. route, I chose to adopt i.p. DT injection route for forthcoming experiments.

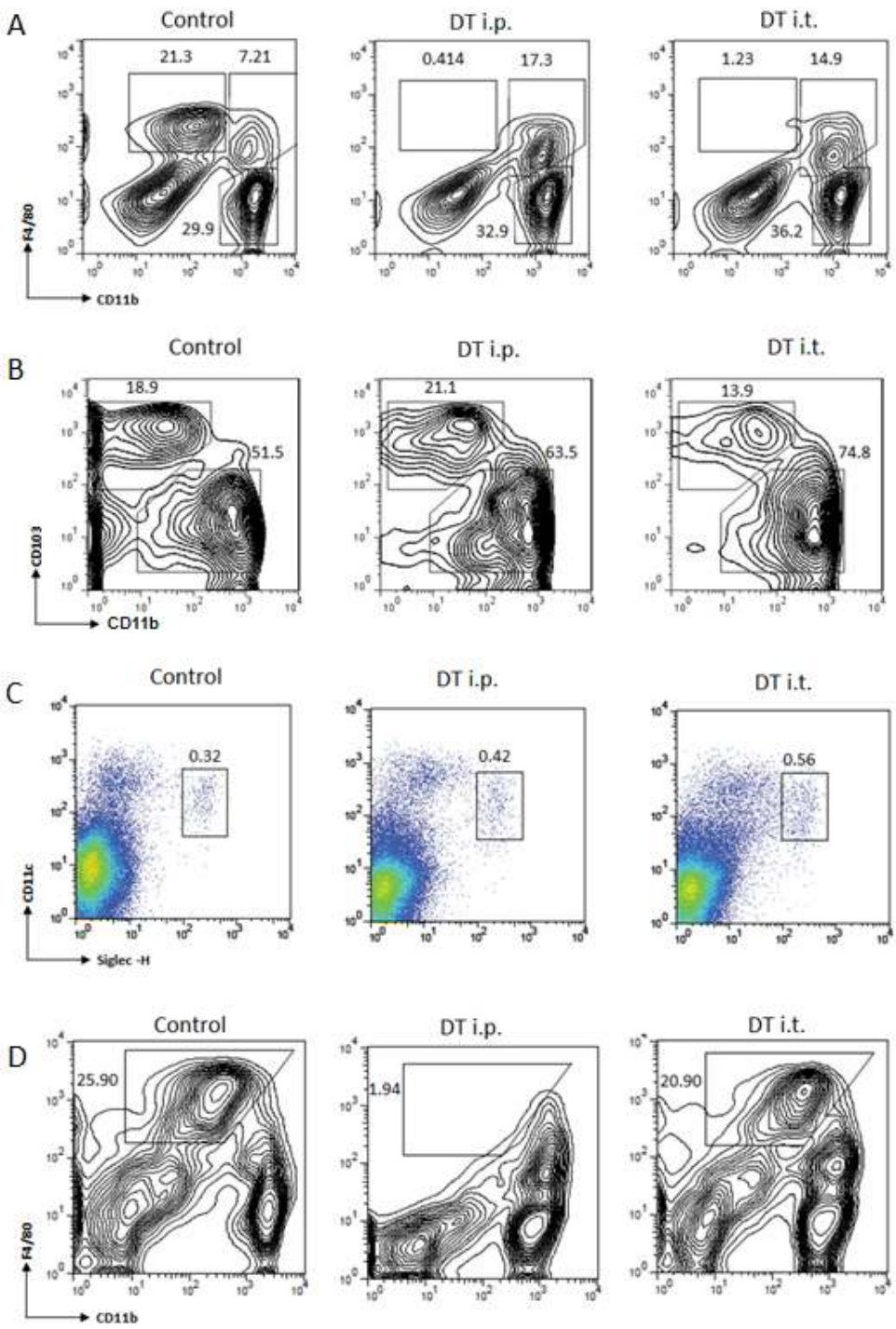

Fig 4.7. Flow cytometric profile of CD169-DTR mice treated with DT via i.p. or i.t. route. CD169-DTR$^{+/-}$ mice were injected with two doses of either 200ng/mice DT by i.p. injection; or 50 ng/mice DT by i.t. injection, given in one-day interval. Twenty-four hours after the second injection, lungs and spleens were harvested, processed, and stained with antibodies as indicated. Flow cytometry analysis of lung (A) AMs, (B) DCs, (C) pDCs, and (D) splenic macrophages. Gating strategies for flow cytometric analysis are shown in Fig. 4.4. Results are representative of two mice per group.

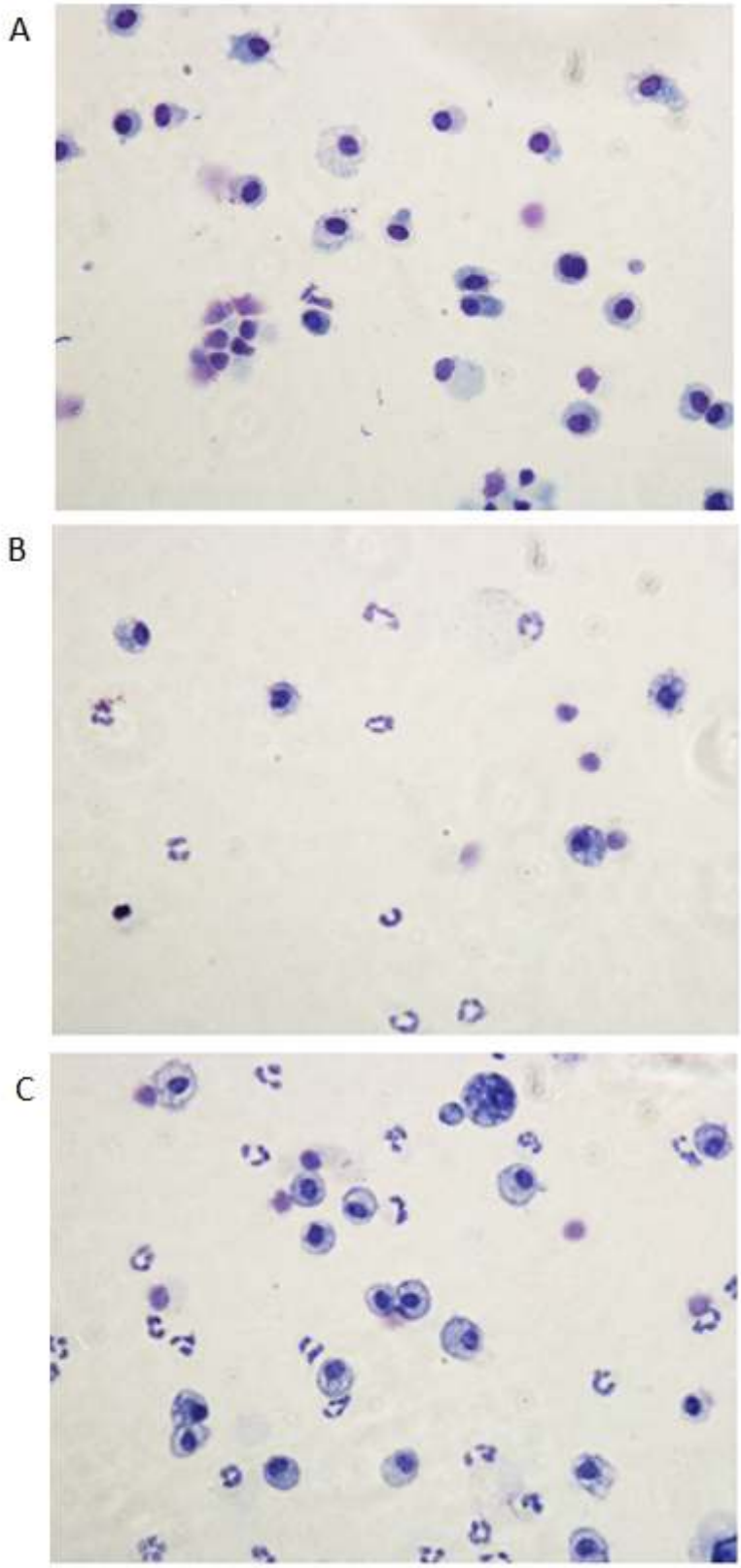

Figure 4.8. Intratracheal administration of DT caused increased infiltration of cells to the alveolar airspaces. Cytospin of BALF lavaged from (A) untreated WT mice (B) CD169-DTR$^{+/-}$ mice treated with DT by i.p. injection, (C) CD169-DTR$^{+/-}$ mice treated with DT by i.t. injection. Results are representative of two mice per group.

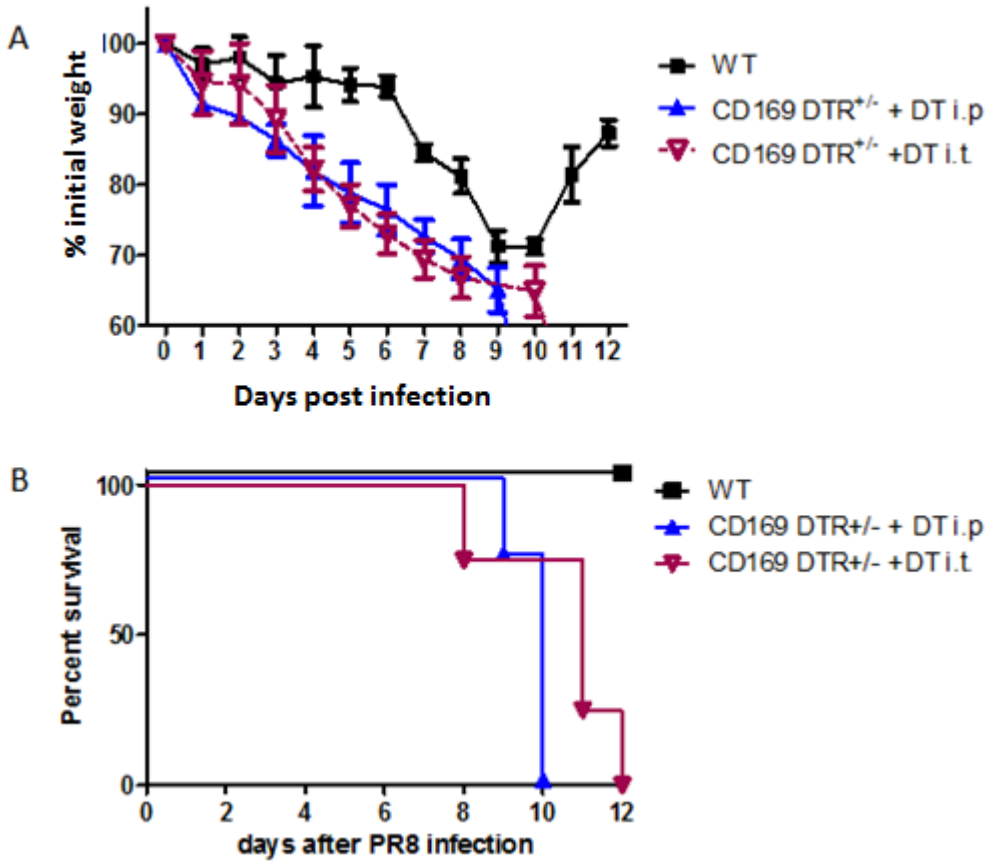

Figure 4.9. Similar weight loss and survival between i.p. and i.t. DT-treated CD169-DTR mice. (A) Weight loss curve of WT or CD169-DTR$^{+/-}$ mice infected with 6 PFU of PR8. The values are expressed as mean and standard deviation. (B) Comparison of survival of WT and i.p./i.t. DT-treated mice. Results are representative of two experiments (n=4).

4.5. Lung alveolar macrophages turnover

I then examined the turnover kinetics of lung AM upon DT treatment. CD169-DTR$^{+/-}$ mice were given two dose of DT via i.p. injections, and lungs were harvested on different time-points. Flow cytometry analysis showed that lung AMs remained depleted for 7 days and then slowly repopulated until the percentage was back to normal in 14 days (Fig. 4.10). Hence, the estimated half-life of lung AMs is ~7 days.

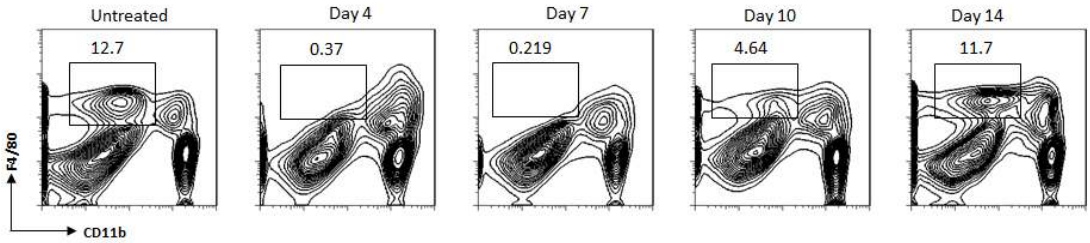

Fig. 4.10. Lung AMs turnover kinetic upon DT treatment. CD169-DTR$^{+/-}$ mice were injected intraperitoneally with two doses of 10 ng/gr body weight of DT in one-day. Mice were sacrificed and lungs were harvested for flow cytometry analysis with indicated antibodies on day 4, 7, 10, and 14. Gating strategy lung AM is shown in Fig. 4.4.A. Results are representative of two mice per group.

4.6. Maintaining alveolar macrophage depletion in experimental time window

Next, I wanted to evaluate whether lung AMs depletion could be maintained throughout the influenza experimental time window of 10-14 days. DT was injected every 3 days and lung macrophages depletion was monitored. Lung AMs remained efficiently depleted on day 14 (Fig 4.11). Taking into account results from section 4.5 and 4.6, I concluded that depletion can be maintained throughout the experimental time window of the influenza experiments.

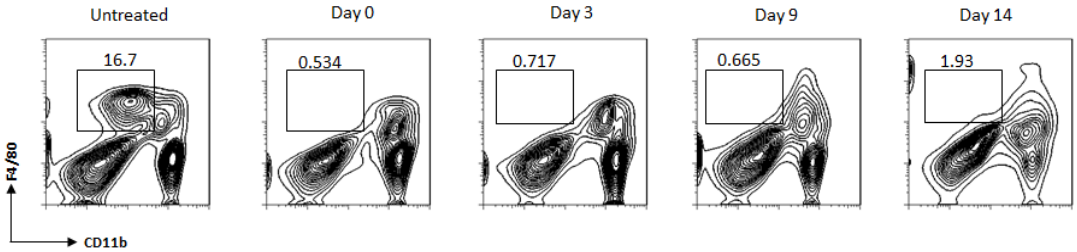

Figure 4.11. Lung CD169^{+} macrophage remained depleted for 14 days upon repeated DT treatments. CD169-DTR$^{+/-}$ mice were injected intraperitoneally with 10 ng/gr body weight of DT on day -2, -1, 2, 5, 8, and 11. Mice were sacrificed and lungs were harvested for flow cytometry analysis with indicated antibodies on day 3, 9, and 14. Gating strategy lung AM is shown in Fig. 4.4.A. Results are representative of two mice per group.

4.7. Bone marrow chimeric mice confirm the requirement of alveolar macrophages in protection against influenza A

DT can cause unintended ablation of non-haematopoietic cells. To rule out the contribution of the depletion of non-haematopoietic cells in this study, I generated two types of bone marrow chimeric mice: (1) CD169$^{+/-}$ mice

receiving BM cells from WT mice (‘group 1’), and (2) WT mice receiving BM cells from CD169 $DTR^{+/+}$ donor mice (‘group 2’). Recipient mice were lethally irradiated 24 hours before injected with $2x10^6$ of BM cells. Eight weeks later, mice were subjected to IAV challenge.

Two mice were sacrificed from each group to assess the efficiency of AM depletion upon DT injection. As expected, mice receiving CD169-DTR (group 2) had both BALF and lung AMs depleted after DT injection (Fig. 4.12.A).

Because these mice were much older than those that were routinely used for 3 PFU of PR8 infection, 6 PFU was used for IAV infection. Mice from the first group displayed ~20% weight loss, and recovered (Fig. 4.12.B). However, one mouse from this group died (Fig.4.12.C). This mouse may have incomplete reconstitution of lung AMs, or suffered from the increased dose of PR8 administered. On the other hand, mice from the second group lost >30% of their weight and all succumbed by day 11 p.i (Fig. 4.12.B and C). Hence, I have confirmed that the disease severity observed in CD169-DTR mice was mediated by DT-induced ablation of cells originated from haematopoietic compartment, i.e. the AMs.

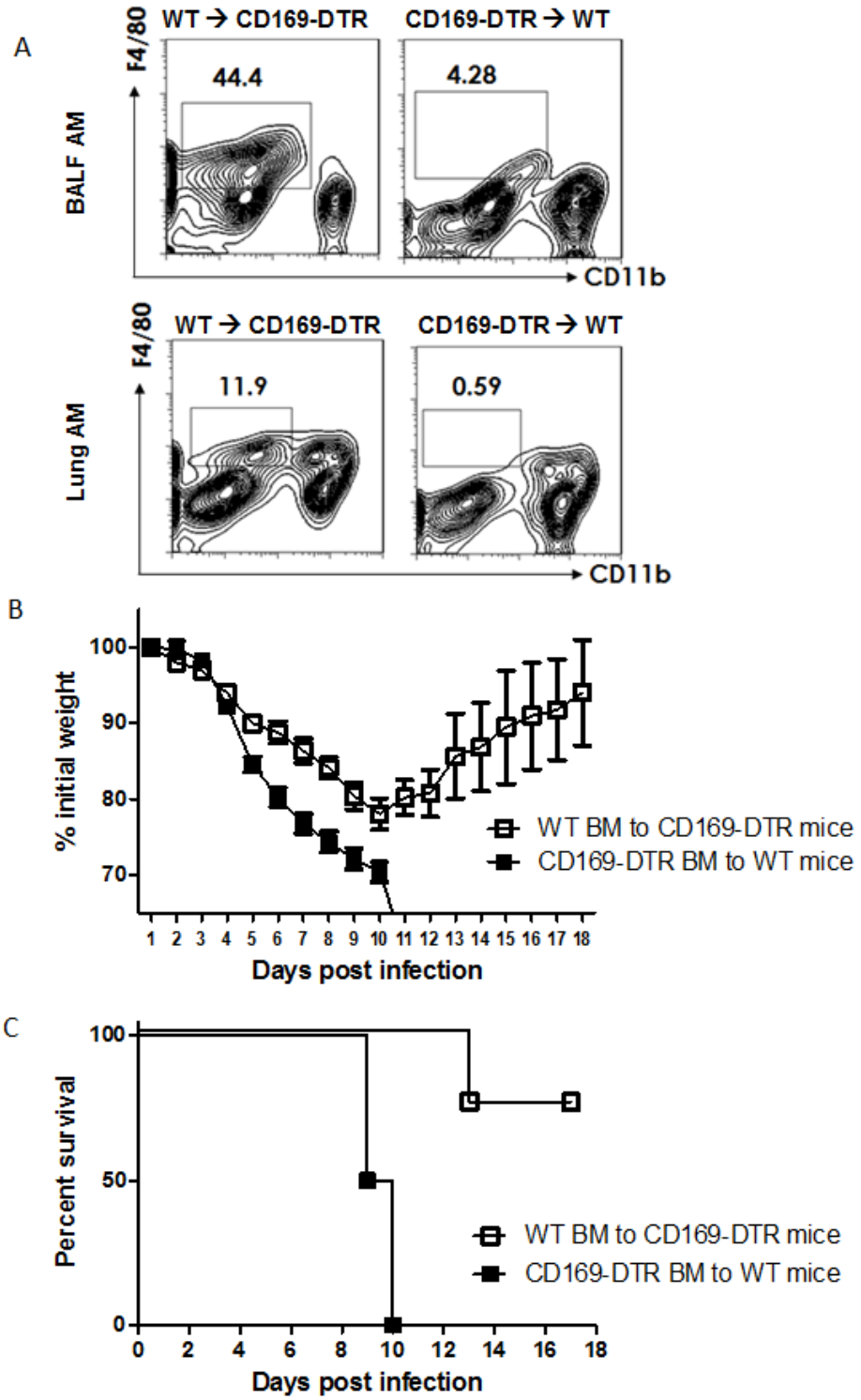

Figure 4.12. Infection of BM-chimeric mice with 6 PFU of PR8. DT injections were given to all mice on day -2, -1, 2, 5, 8, 11, and 14 p.i. (A) Flow cytometry profile of BALF (upper panel) and lung (lower panel) AMs in WT mice receiving CD169-DTR BM (WT → CD169-DTR) and CD169-DTR mice receiving WT BM (CD169-DTR → WT). Gating strategies were shown in Fig. 4.3 for BALF AMs and Fig. 4.4.A for lung AMs. Mice were analyzed 24 hour after 10ng/gr body weight DT administration. (B) Comparison of weight loss, and (C) survival curves between indicated groups. The values in (B) are expressed as mean and standard deviation (n= 4-5).

4.8. Flow cytometric analysis of immune cell subsets in the course of influenza A virus infection

To obtain a deeper understanding of the kinetic of immune cell subsets during the course of Influenza infection, I analyzed flow cytometry profile of WT and DT-treated CD169-DTR mice in day 2, 4, and 8 after infection with 3 PFU of PR8. DT was injected to CD169-DTR mice intraperitoneally on day -2 and day -1, and re-administered every 3 days afterwards. Lungs and pooled draining lymph nodes (dLNs) were harvested and stained with antibodies against markers for myeloid cell subsets as indicated. In addition, counting of total cells recovered from BALF was conducted.

The number of BALF cells recovered from CD169-DTR mice was around twice to that of the WT on day 6 p.i (Fig. 4.13.C). This increased accumulation of cells in the airways could be detrimental to the lung, obstruct breathing, and cause mortality. These cells are yet to be identified, but are suspected to mainly composed of neutrophils and monocytes. On the other hand, lung cell counts showed comparable number of cells between both groups (Fig. 4.13.A). However, there were some differences in the cell count of pooled draining lymph nodes (Fig. 4.13.B). I had difficulty in obtaining consistent number of cells due to variability in number and size of lung dLNs obtained from each mouse.

The kinetics of lung and dLN DCs over the course of infection were then assessed. Significant reduction of lung CD11b DC counts of CD169-DTR mice, but not that of CD103 DC, was observed on day 4 and 6 p.i (Fig. 4.14.B and C). In addition, significant reduction of lung pDCs was also observed on day 6 p.i (Fig. 4.16) due to unknown reason. Flow cytometry analysis of dLN DCs revealed some differences in CD103 DC and CD11b DC counts on day 6 p.i. (Fig. 4.15).

Moreover, I analyzed absolute numbers of neutrophils and monocytes by their expression of CD11b, Ly6G and Ly6C surface molecules. Increased number of neutrophils ($Ly6G^{+}Ly6C^{-}$ cells) was observed in CD169-DTR mice injected with DT even in the absence of PR8 infection (Fig. 4.17.C). Slight increase of monocytes ($Ly6G^{-}Ly6C^{+}$ cells) and $Ly6G^{+}Ly6C^{+}$ cells was also observed in the lung of CD169-DTR mice (Fig. 4.17.D-E). The $Ly6G^{+}Ly6C^{+}$ granulocytes have

been described in a number of studies [226, 227], although their specific roles are still unclear.

Next, I also monitored kinetics of lung AM and found that in WT mice, this population decreased gradually along the course of IAV infection (Fig. 4.18). I reasoned that reduction of AM number was caused by infection by IAV and subsequently apoptosis of infected AM. Future analysis at later time point is needed to find out if AM is restored after the inflammation is resolved.

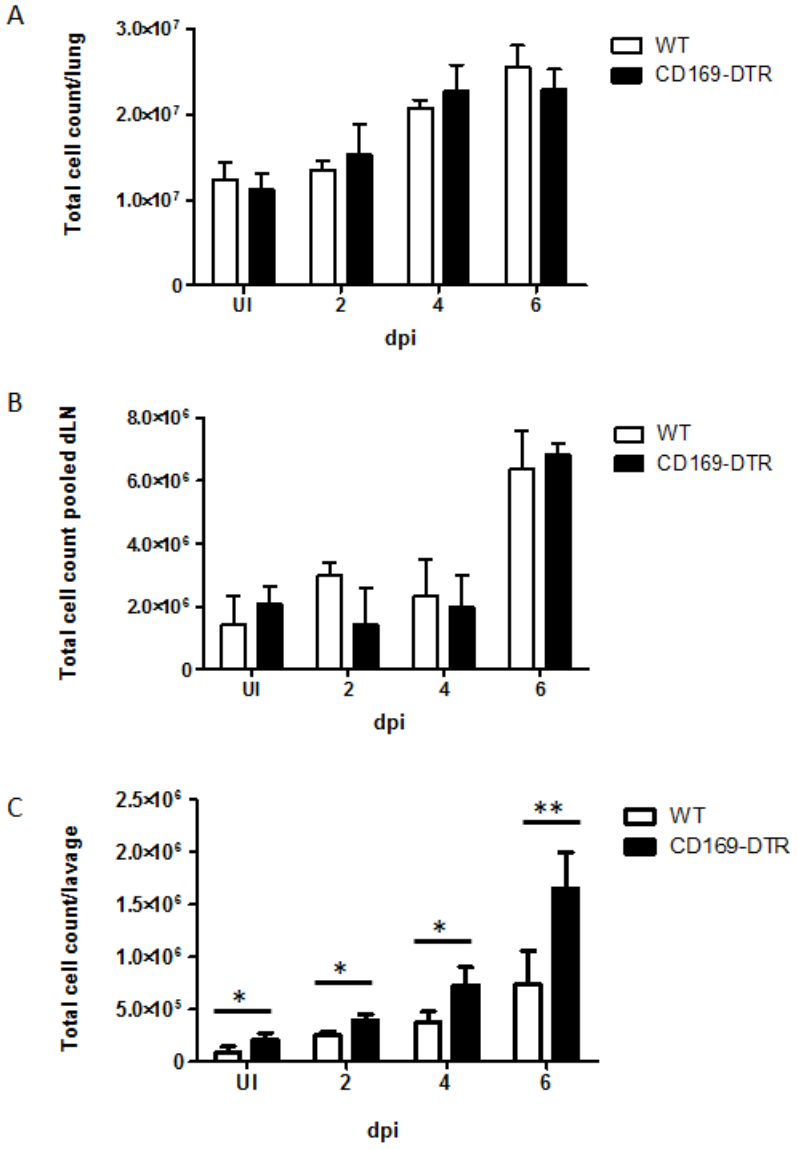

Figure 4.13. Cell counts of pulmonary organs in WT and CD169-DTR mice infected with 3 PFU of PR8. Total cell counts (mean±SD) of (A) lungs, (B) pooled dLNs, (C) BALF, and (D) lung dendritic cells at indicated time points after infection with 3 PFU of PR8. UI represents uninfected WT or DT-treated CD169-DTR mice. dpi: days post-infection. Results are representative of two experiments (n=3-5).

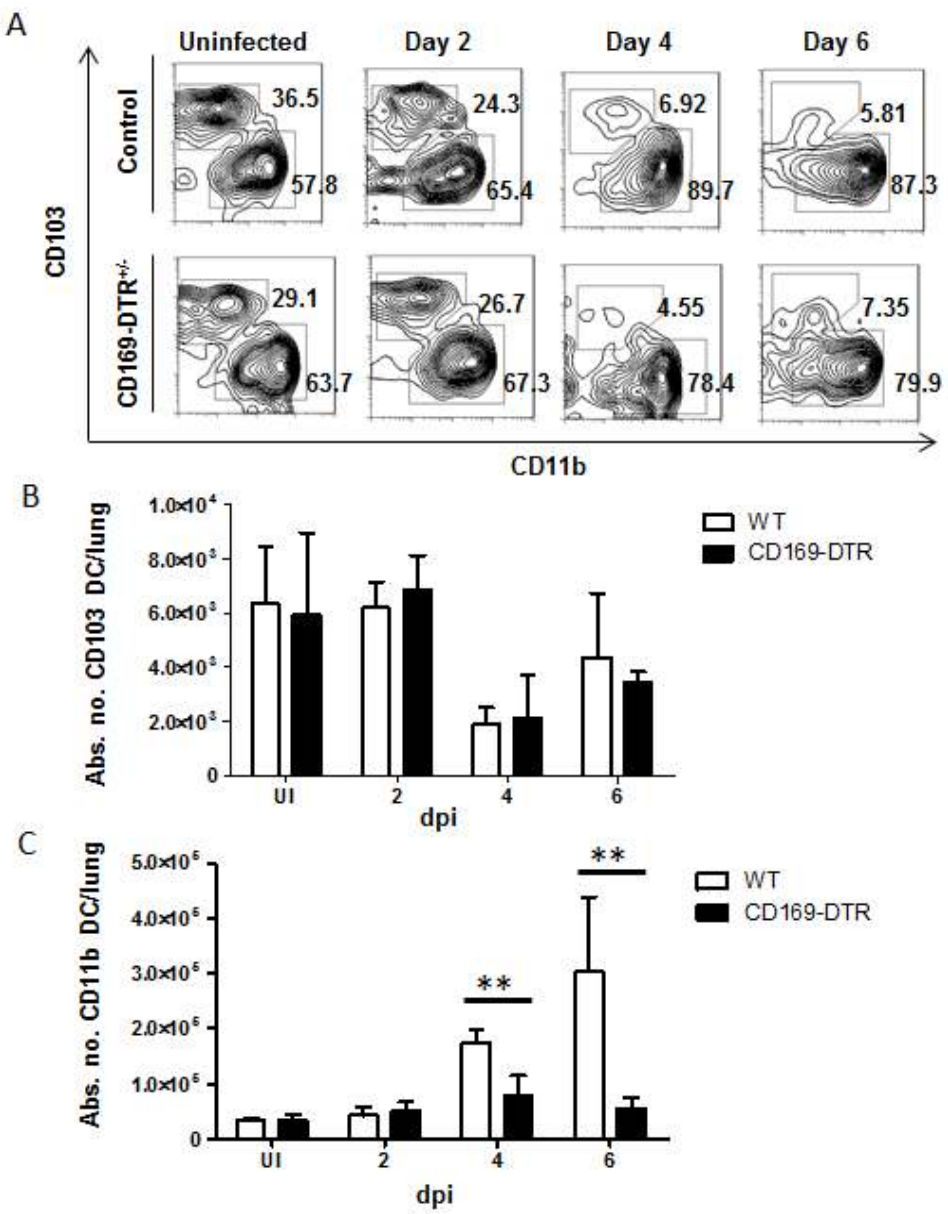

Figure 4.14. The kinetics of lung DC subsets in the course of IAV infection. (A) Representative flow cytometric analysis of lung DCs gated on CD11c^{hi}MHC-II^{hi} cells. Absolute numbers (mean±SD) of lung (B) CD103 and (C) CD11b DCs in WT and CD169-DTR mice at indicated time points. Gating strategy for flow cytometry analysis was shown in Fig. 4.4.B. Mice were infected with 3 PFU of PR8. UI represents uninfected WT or DT-treated CD169-DTR mice. Results are representative of two experiments (n=3-5).

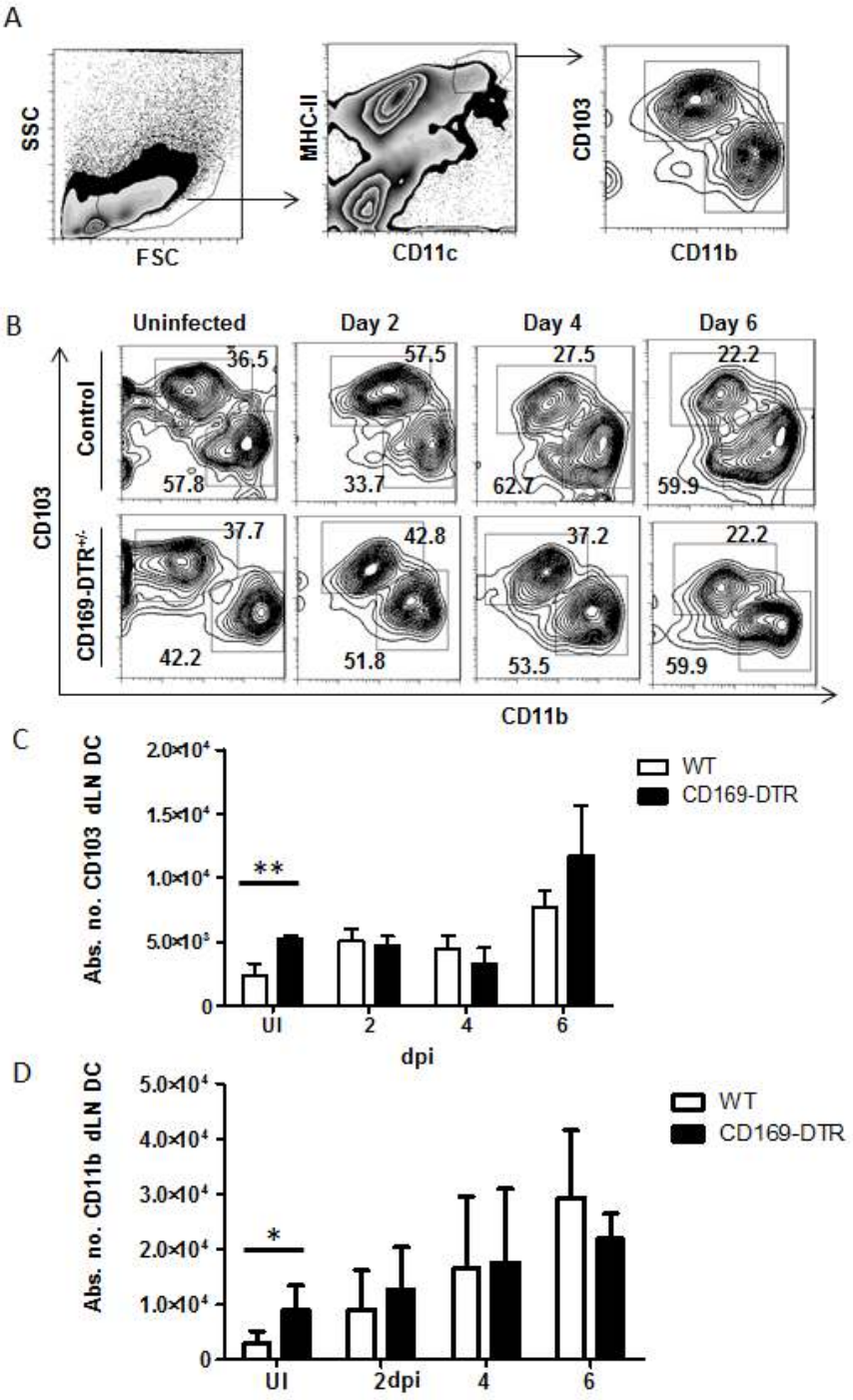

Figure 4.15. Kinetic of lung dLN DC subsets in the course of IAV infection. (A) Gating strategy, (B) representative flow cytometry analysis, and absolute no. (mean±SD) of lung dLN (C) CD103 or (D) CD11b dendritic cells in WT and CD169-DTR mice infected with 3 PFU of PR8. UI represents uninfected WT or DT-treated CD169-DTR mice. Lung draining lymph nodes from each mice were pooled for staining and counting. Results are representative of two experiments (n=3-5).

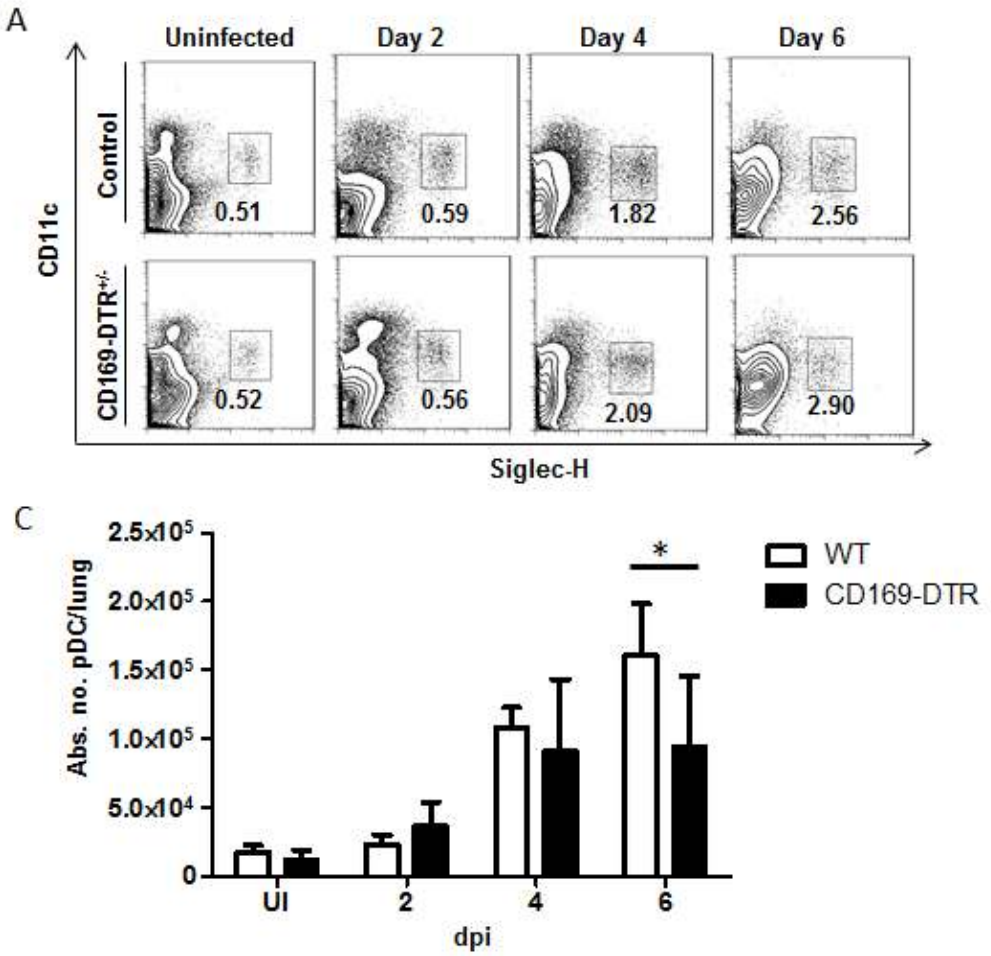

Figure 4.16. Kinetic of lung pDCs in the course of IAV infection. (A) representative flow cytometric analysis and (C) absolute numbers (mean±SD) of of lung pDCs in WT and CD169-DTR mice at indicated time points after infection with 3 PFU of PR8. Gating strategy for flow cytometry analysis was shown in Fig. 4.4.C. UI represents uninfected WT or DT-treated CD169-DTR mice. Results are representative of two experiments (n=3-5).

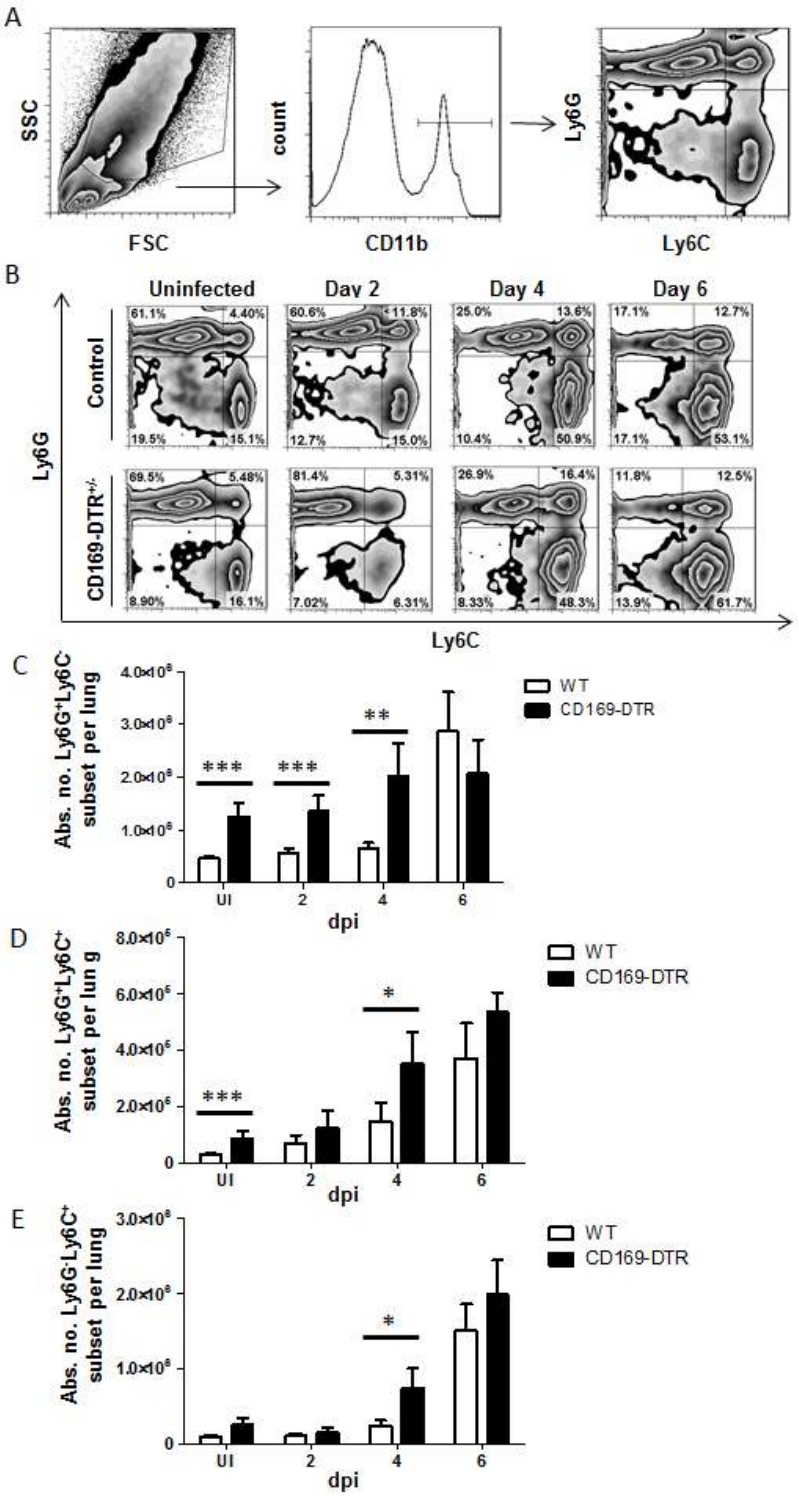

Figure 4.17. The kinetics of lung granulocyte subsets in the course of IAV infection. (A) Gating strategy and (B) representative flow cytometric analysis of indicated stainings are shown. Absolute numbers (mean±SD) of (C) $LyG^{+}Ly6C^{-}$ neutrophils, (D) $LyG^{+}Ly6C^{+}$ double positive granulocytes, and (E) $LyG^{-}Ly6C^{+}$ monocytes in WT or CD169-DTR mice at indicated time points after infection with 3 PFU of PR8. UI represents uninfected WT or DT-treated CD169-DTR mice. Results are representative of two experiments (n=3-5).

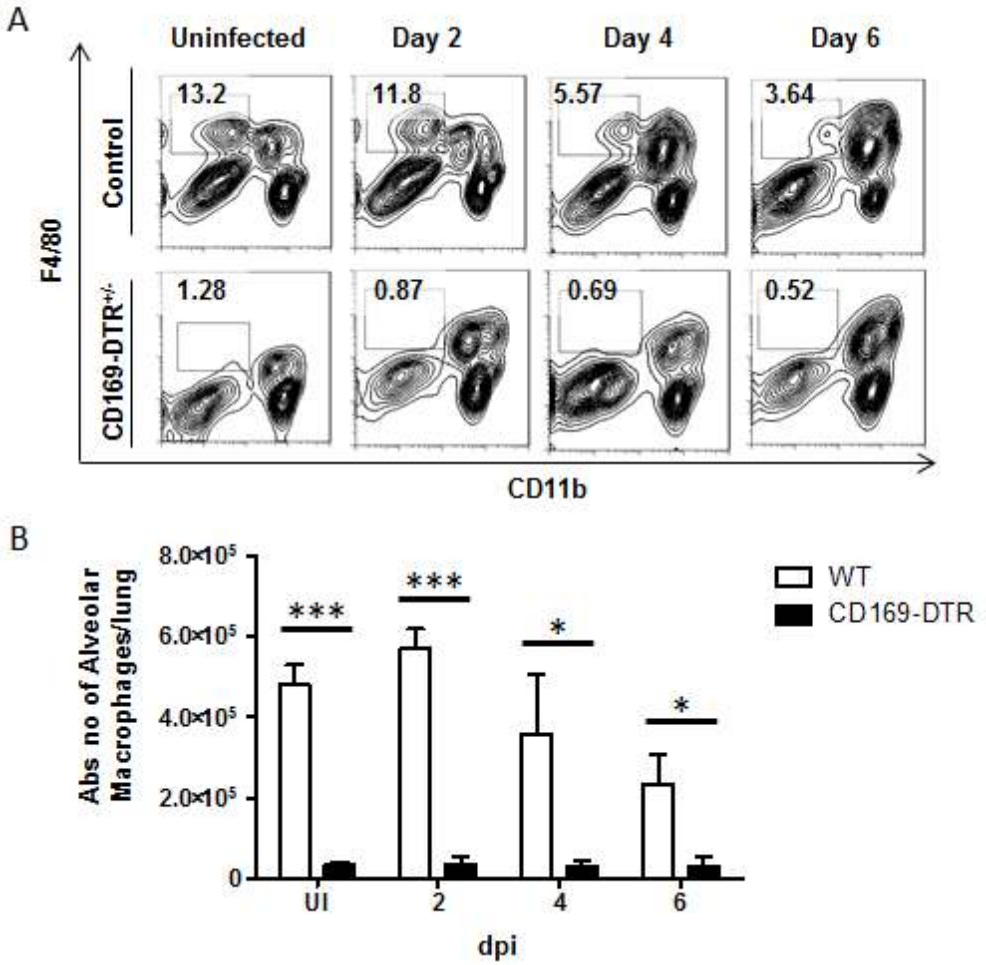

Figure 4.18. The kinetics of lung AMs in the course of IAV infection. (A) Representative flow cytometric analysis and (B) absolute numbers (mean±SD) of lung AMs in WT and CD169-DTR mice at indicated time points after infection with 3 PFU of PR8. Gating strategy for flow cytometry analysis was shown in Fig. 4.4.A. UI represents uninfected WT or DT-treated CD169-DTR mice. Results are representative of two experiments (n=3-5).

4.9. Increased lung pathology in the absence of alveolar macrophages

Histopathology analysis can help us in analyzing the disease severity of IAV infection. CD169-DTR mice and controls were sacrificed on day 6 post infection and lungs were subjected to haematoxylin and eosin staining for examining pathology. Infected CD169-DTR mice displayed more severe lung pathology, marked by increased infiltration of mononuclear cells and edema (Fig. 4.19). The extent of pathology might develop into difficulty in breathing and ultimately responsible for the mortality of AM-depleted mice.

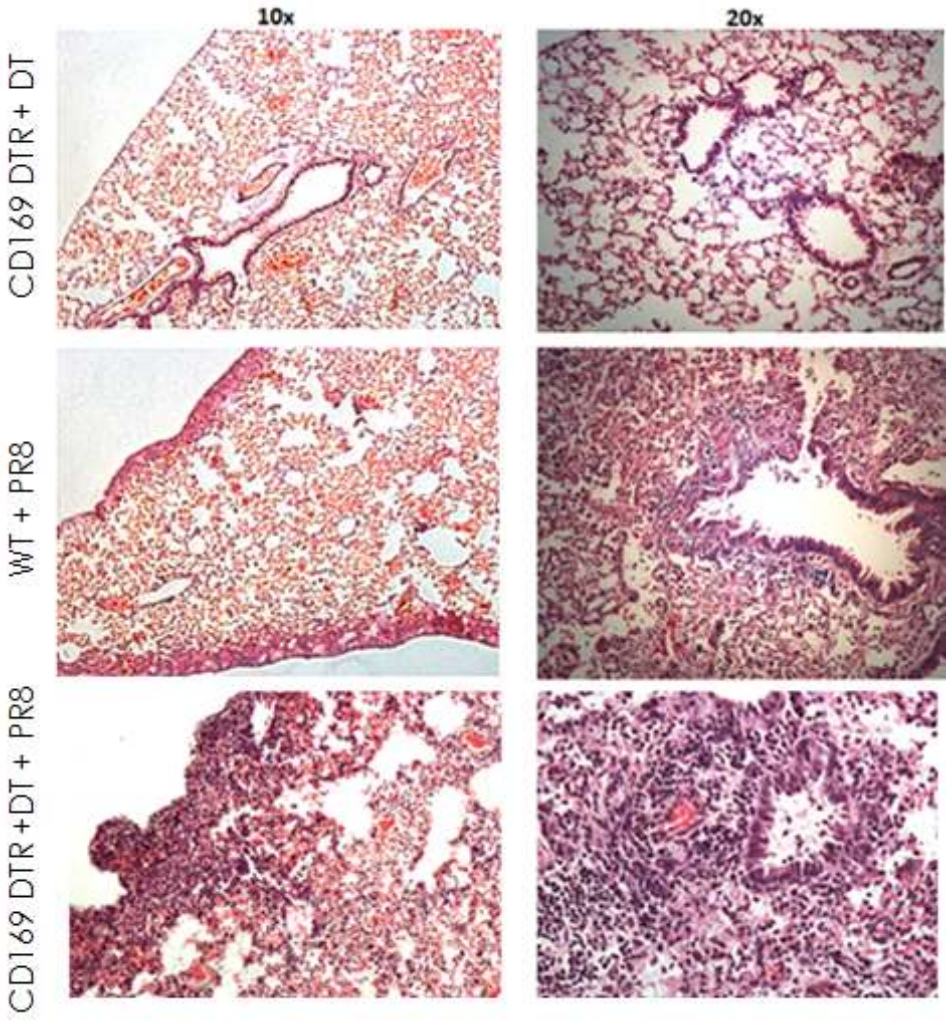

Figure 4.19. CD169-DTR mice exhibited more severe lung pathology upon infection with IAV. DT-treated CD169-DTR$^{+/-}$ mice or control mice were infected with 3 PFU of PR8 and lungs were harvested on day 6 for paraffin-embedded section and stained with haematoxylin and eosin. DT treated, but uninfected CD169-DTR$^{+/-}$ mice were included as control. Pictures were taken by 10x (left panel) or 20x objective (right panel).

4.10. Increased viral titer in the absence of alveolar macrophages

I then assessed the viral load of infected lungs by the means of qRT-PCR. This method could sensitively detect the amount of viral mRNA deposited in the infected tissue. I found significantly higher (>10 fold) viral load on lungs of AM-depleted mice on day 6 post-infection (Fig. 4.20). In addition, plaque assay was also conducted using MDCK cells to detect viable viral particles. I observed elevated viral burden in CD169-DTR mice, although the difference on day 8 was only ~4 fold. Note that for qRT-PCR, a small piece (1-2 mm) of lung tissue from the lower left lobe of each mouse was consistently used to

extract RNA. On the other hand, whole upper right lobe of the lung was used for the plaque assay.

These results suggest that AMs suppress influenza replication and/or spreading in the lung. Study of viral titer in more time points during the course of infection will help to draw better correlation between virus replication and weight loss.

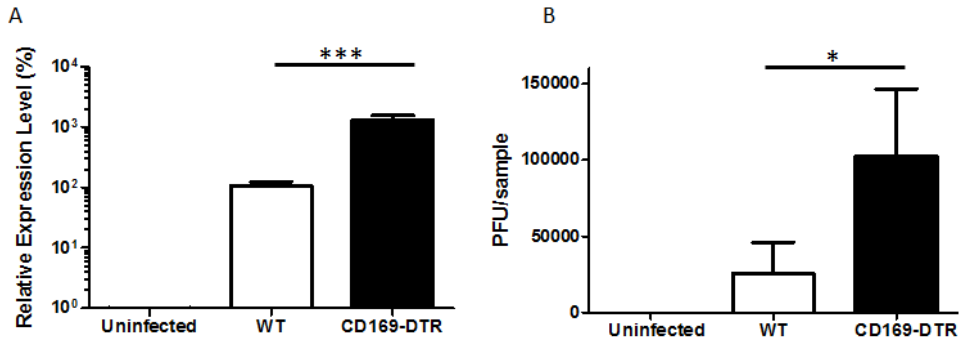

Figure 4.20. CD169-DTR mice displayed significantly higher lung viral load. DT-treated CD169-DTR$^{+/-}$ mice or control mice were infected with 3 PFU of PR8. Lungs were harvested and analysed for (A) Relative mRNA expression level of influenza M protein on day 6 p.i., and (B) Plaque assay from upper left lobe of the lungs on day 8 p.i. Values are expressed as mean±SD (n = 4 - 6).

4.11. Reduced CD8 T cell response in the absence of alveolar macrophages

CD8 T cells infiltrate lungs at later stage of the infection and are important for viral clearance. To determine CD8 T cell response in AM-depleted lungs, I used MHC Dextramer^{TM} reagent that allow detection of Influenza-specific CD8 T cells. Mice were infected with 3 PFU of PR8 and sacrificed for analysis on day 10 post infection. CD8 T cell response in the lung is predicted to be at its peak at 10 days after infection. Interestingly, there was a significant reduction of the number of flu-specific CD8 T cell in the CD169-DTR mice, in comparison to the WT control (Fig. 4.21).

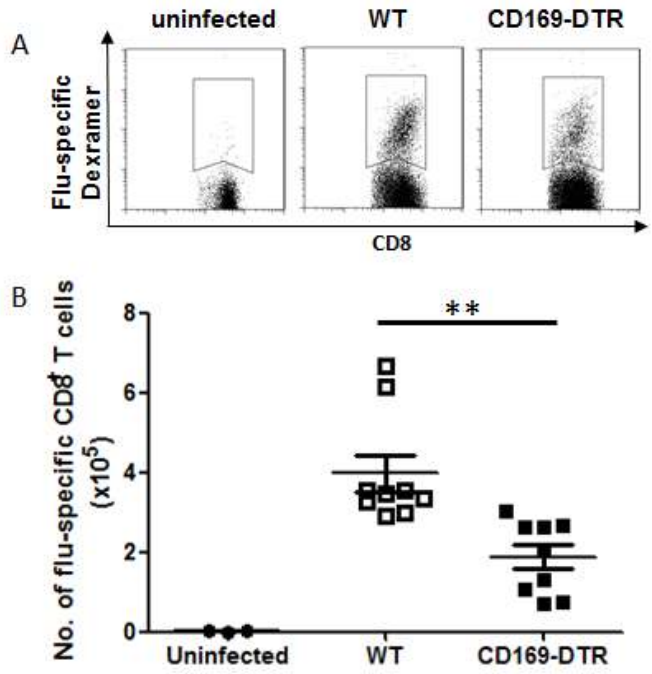

Figure 4.21. Reduced flu-specific CD8 T cell response in CD169-DTR mice. DT-treated CD169-DTR$^{+/-}$ mice or WT mice were infected with 3 PFU of PR8 and lymphocytes were purified from lung tissue on day 10 p.i. (A) Representative flow cytometric analysis and (B) absolute number (mean±SD) of CD8-positive T cells detected by flu-specific tetramer. Flow cytometry analysis was gated on CD8 positive cells. Results are summary of two experiments ($p<0.005$).

4.12. Protective role of alveolar macrophages in already established influenza A infection

It is unclear if depletion of alveolar macrophages after influenza infection will affect the morbidity and mortality against influenza A. To get a deeper understanding of AM roles at different stages of influenza infection, I studied the effect of AM depletion initiated on different time points post-infection. CD169-DTR mice were separated into groups, where DT treatment was initiated on indicated days post infection and with DT re-administration every 3 days afterwards (Table 4.1). In addition, one group of mice designated as 'pre DT only' group was injected with DT on day -2 and -1, but DT was not administered at any point post-infection (Table 4.1). Similar with the mice given repeated DT treatment starting from day -2, all mice in 'pre DT only' group also displayed severe mortality and morbidity (Fig. 4.22). All mice in the group treated with DT starting on day 2 p.i. also displayed 100% mortality by day 13 p.i (Fig. 4.22.B). Moreover, two out of three mice in the group treated with DT starting on day 5 died on day 13 p.i (Fig. 4.22.B). One mouse in this

group survived but was unable to recover its weight by 18 days p.i. (Fig. 4.22), thus was sacrificed. In contrast, no difference in weight loss or survival curve was observed between the control and mice treated with DT starting day 8 post infection (Fig. 4.22). These results demonstrated that AMs are essential for survival against IAV infection and are indispensable in the early stage of the infection.

Group\Day	-2	-1	0	1	2	3	4	5	6	7	8	10	11	12	13	14	15	16
CTRL			infect with PR8															
DT day -2	+DT	+DT			+DT			+DT			+DT			+DT			+DT	
DT day 2					+DT	+DT			+DT			+DT			+DT			+DT
DT day 5								+DT	+DT			+DT			+DT			+DT
DT day 8											+DT	+DT			+DT			+DT
Pre DT only	+DT	+DT																

Table 4.1. DT injection scheme for indicated groups of CD169-DTR mice infected with 3 PFU of PR8. CD169-DTR mice were treated with 10 ng/gr body weight DT on indicated days. All mice are infected with 3 PFU of PR8.

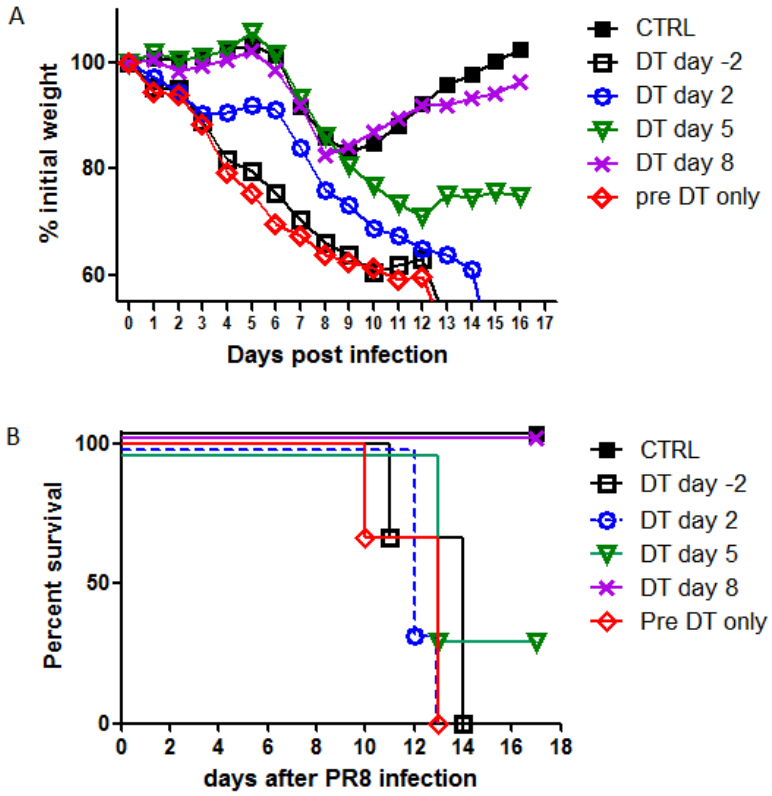

Figure 4.22. Effects of differential initiation of DT administration in CD169-DTR mice. All Mice were infected with 3 PFU of PR8. (A) Weight loss curve (mean) and (B) survival curve of WT (CTRL) or CD169-DTR DT-treated (DT) mice which repetitive DT treatment started on day -2, 2, 5, or 8 days p.i; as well as mice treated with DT prior to infection only (pre DT only). Results are representative of two experiments (n=3).

4.13. Discussion

Lung is a tissue environment where immune system is continuously challenged with both pathogens and harmless antigens. In such delicate tissue, maintaining a balanced immune response is very important. AM has been long accepted to be major immune cell population in the lung with primary access to the airway antigens. The large number and the strategic placement of these cells in naïve lungs suggest the ultimate role of this population in homeostasis and infection. In this chapter, by utilizing CD169-DTR mouse model that allow selective ablation of AMs, I have demonstrated that AMs are indispensable for survival against IAV infection.

To the best of my knowledge, there is no DTR mouse model that could deplete AMs specifically *in vivo* without causing non-specific ablation or lethality. In this chapter, I have demonstrated that specific ablation of AMs could be induced in CD169-DTR mice. Similar, if not better AMs depletion efficiency of >90% was achieved in the CD169-DTR mice in comparison to 60-85% efficiency by clodronate method [42, 139]. Immunohistology and flow cytometry analysis displayed that other immune cells such as DCs, granulocytes, and lymphocytes remained unaffected by the DT treatment (Figure 4.5). CD169-DTR line is thus better mouse model to study AMs than CD11c-DTR or Lysozyme M-DTR mice [152, 165]. The DTR method also has an advantage over clodronate method because DT treatment would not affect phagocytic DC or monocytes, unlike what clodronate treatment theoretically do [144].

Additionally, neutrophil infiltrations to the airways were observed after DT treatment (Fig. 4.3.C). Neutrophils are known as phagocytes, and they may infiltrate the airways to clear debris of apoptotic AMs post-DT treatment. Compensatory mechanism could be another reason for the observed mononuclear cell infiltration. Since monocytes serve as AM precursors, their infiltration is an attempt to repopulate the missing AM. In another light, AMs are also known to serve as suppressor cell, maintaining homeostasis in the airway environment. The absence of AMs could disrupt the balance, trigger inflammation signal, and subsequently cause the infiltration of neutrophils and monocytes. Nevertheless, other studies have also reported infiltration of neutrophils after DT administrations [168, 228]. Further study is needed to clarify the cause and effect of the observed neutrophilia.

Upon Influenza A infection, it was very clear that CD169-DTR mice displayed enhanced morbidity and mortality (Fig. 4.6). I attempted to determine the working dose of the PR8 virus, and 3 PFU seemed to work best for conducting experiments with the CD169-DTR BALB/c transgenic line. Given this dosage, WT mice displayed sub-lethal infection: they lost ~20% of their weight and then fully recovered. The DT-treated CD169-DTR mice infected with 3 PFU displayed 100% lethality but succumbed later (13-14 days p.i.) than those infected with 6 PFU (Fig. 4.6); thus giving us time to perform more analysis. All infected DT-treated CD169-DTR mice suffered from clinical signs such as hunched posture, ruffled fur, and lethargy. I also observed in the same experiment that CD169-DTR mice were starting to lose weight as early as day 1 post-infection. On the other hand, WT mice suffered from weight loss starting around day 5 post infections, where the virus titer was predicted to be at its peak. On the other hand, CD169-DTR mice treated with DT alone did not display signs of illness or mortality over time range studied (Fig. 4.6); implying that DT is nontoxic to CD169-DTR mice. Thus, DT treatment is unlikely to affect alveolar epithelial type II cells or other essential cells as reported to cause mortality in CD11c and Lysozyme M-DTR mice [168].

Since weight and gender of the mice could affect the infection outcome, female mice of 6-8 weeks old were always used for experiments. Thus, if any of these variables is altered in the future experimental settings, the flu working dosage may need to be adjusted accordingly. The virus dosage seemed little in comparison to PR8 dose of BALB/c mice used in other study whereby 10^2 PFU PR8 was indicated as 50% lethal dose (LD_{50}) for BALB/C mice [229]. This discrepancy might result from differences of animal health status, genetic background, or virus production.

Additional experiment with BM chimeric mice was conducted to rule out the effect of possible non-specific DT-mediated depletion of cells from non-haematopoietic origin. Indeed, the enhanced mortality and morbidity observed in CD169-DTR mice was reproduced in WT mice transplanted with CD169-DTR BM, and not vice versa (Fig. 4.12).

Intratracheal or intranasal route to administer depleting agents such as clodronate and DT has been harnessed in attempt to avoid systemic effect of ablation [42, 78, 139, 230]. Indeed, splenic macrophages were not affected by

i.t administration of DT (Fig. 4.7.D). Nevertheless, when IAV infection between i.t. and i.p. treated CD169-DTR mice were compared, no differences in weight loss and survival were observed in these experimental groups (Fig. 4.9). PR8 strain is not known to affect other organ or nervous system, unlike other more pathological IAV strains. Influenza infection and immunopathology caused by PR8 would thus is confined to the respiratory compartment. Therefore, depletion of $CD169^{+}$ macrophages in other organs caused by i.p. treatment is unlikely to contribute to disease prognosis or mortality of CD169-DTR mice. In addition, i.p. administration of DT caused less cellular infiltrations into the alveolar spaces and is more practical. I then proceeded with i.p. route of DT injection for the rest of the study.

Furthermore, I also assessed the depletion turnover kinetic of AM upon i.p injection of DT. In this scenario AM repopulated the lung within 14 days post-DT treatment (Fig. 4.10). It has been reported that under non-sterile condition, the half-life of AM is about 4 days [231]; and it might be longer in sterile condition. By generating chimeric mice through irradiation and bone marrow transplantation, researchers reported that the half-life of murine AMs are ranging between 10-30 days [232-235]. In tissue culture, AMs are even viable for more than 100 days [236]. Another study suggested that AM half-life in steady state can be longer than 4 months [237]. Hence, the life-span of this population is likely to depend on the functional demands. Here, the turnover of AM due to DT induced ablation is shorter than what has been reported in bone marrow chimeric experiments, or in studies conducted in steady-state by using non-invasive labeling methods. Differences in the state of bone marrow, blood-borne precursors, and lung environment result in the discrepancies of AM half-life observed in different settings.

I confirmed that lung AM depletion could be maintained in the CD169-DTR mice throughout the experimental time window of primary IAV infection (around 14 days, Fig. 4.11). Since possible generation of neutralizing antibody by the host may affect the depletion efficiency, the interval of DT injections has to be thoughtfully considered. For my experiments, repeated DT injection in every 3 days interval is sufficed to maintain efficient AM depletion during primary IAV infection in mouse.

Increased morbidity and mortality of CD169-DTR mice are likely to be caused by uncontrolled viral growth in the absence of AMs. Therefore, I measured viral titer by the means of qRT-PCR and plaque assay on day 6 and 8 p.i. respectively. Assessment of viral titer by qRT-PCR revealed significantly (~10 fold) higher viral genetic material in the lung of CD169-DTR mice on day 6 p.i (Fig. 4.20.A). Although qRT-PCR method is sensitive, specific, and rapid, it is unable to differentiate between nonviable from viable virus particles [214]. Hence, to confirm on the lung viral load, I also attempted plaque assay with MDCK cells and observed similar trend, although the difference on day 8 was only ~4 fold (Fig. 4.20.B). Similar observation whereby depletion of AMs induce significant increase of viral titer was also reported by other group who harnessed clodronate-mediated depletion method [42].

As AMs are known to phagocytose virus or infected cells [133], elimination of this population is likely to increase viral growth. In a study whereby phagocytosis inhibitors were introduced to the mice airway, increased in lethality was observed [131]. Infiltrating cells such as neutrophils, monocytes, exudate macrophages and inflammatory DC might as well carry out the phagocytic function. However, how much these cells are able to compensate for AM phagocytosis function remains to be determined.

I have shown that the enhanced disease severity observed in CD169-DTR mice was well correlated with high viral titer and reduced CD8 T cell response. However, I suspected that mortality of CD169-DTR mice was caused by pathology induced by excessive inflammation in the lung. Previous studies described monocyte-derived inflammatory DC, or often termed as TNF-iNOS DC (Tip DC), as the agents in inflammatory lung damage [86, 113]. Lin et al. demonstrated that monocyte-derived DCs and exudate macrophages were recruited to the lungs by C-C chemokine receptor 2 (CCR2), and both were the major producer of NOS2 and TNFα [86]. Subsequent studies with CCR2 deficient mice upon IAV infection revealed that decreased monocytes/macrophages recruitment to the lungs resulted in reduced pathology and mortality [118, 119, 238]. Others showed that IAV infection in NOS2 or TNF deficient mice decreased mortality rate [239-241]; confirming both cytokines contribution to pulmonary damage [242, 243]. In addition, Herold et al. described that exudate macrophages expressed elevated levels of TRAIL (tumor necrosis factor-related apoptosis-inducing ligand) upon IAV

infection [119]. The authors proposed that exudate macrophages promote epithelial cell apoptosis and lung immunopathology via TRAIL signaling [119]. Since I detected increased infiltration of cells in the airway and alveolar spaces as shown by cell count in BALF (Fig. 4.13.C) as well as lung histology (Fig. 4.19) on day 6 p.i., it is very likely that enhanced accumulation of inflammatory cells led to lung failure and mortality of CD169-DTR mice.

In addition, I also observed that CD11b DCs failed to accumulate in the lung on day 6 post infection (Fig. 4.14.C). Since CD11b DC is also responsible in priming and sustaining CD8 T cell response in the lung and dLNs, reduction of CD11b DC number is likely to affect the magnitude of flu-specific CD8 T cell response. Furthermore, although my staining data did not show that DT treatment affect $CD11b^{+}Ly6C^{+}$ monocytes (Fig. 4.17.E), several studies reported increased of CD169 expression in human inflammatory monocytes [185, 244-246]. Therefore, it is possible that reduction of CD11b DCs observed on day 6 p.i. in CD169-DTR mice was caused by the depletion of their monocyte precursors.

Furthermore, I attempted to initiate AM depletion at different time points with respect of infection to study the effect on mortality and morbidity of CD169-DTR mice (Fig. 4.22). I found that DT treatment initiated on day -2 to day 2 p.i. with or without repeated DT treatment resulted in severe weight loss and 100% mortality of the mice. On the other hand, two out of three mice died when DT treatment was initiated on day 5 p.i, and the only surviving mouse was unable to restore its weight on day 18 p.i. (Fig. 4.22.B). However, AMs are dispensable after day 8 post infection as the mice received DT starting day 8 p.i. were able to recover. These results indicate that AMs have critical role at the early stages of infection (up to day 6 p.i.), and the animals are unlikely to survive sublethal PR8 infection if AMs are absent during this period.

However, it has been suggested that depletion of macrophages before infection, but not when initiated at day 3 or 5 p.i., results in mortality and uncontrolled viral growth [247]. Yet, in the original study, Tumpey et al. infected the control and clodronate-treated groups with lethal 1918 HA/NA:Tx/91 IAV doses; thus even the control group could not survive the infection [42]. In this case, depletion of AMs initiated on day 3 or 5 could not make the disease any worse. Their original hypothesis was that the absence

of AM would alleviate, or rescue the pathology. After this observation, they conducted another experiment whereby sublethal dose of virus was administered and clodronate treatment was initiated prior to infection. In this experiment, indeed they observed that depletion of macrophages enhanced the severity of infection [42]. Collectively, it is clear from my results that AMs are essential during the early stage of IAV infection. A closer look to the effect on immunopathology and viral growth on experimental groups where depletion is manipulated at different time points will give us insights of the AM roles in different time period during influenza A infection.

I have not assessed whether the absence of dLN $CD169^+$ macrophages due to i.p. DT administration has any role in the enhanced pathology observed in CD169-DTR mice. Technically, it is very difficult to avoid depletion of $CD169^+$ cells of the dLNs since DT administration via i.p. or i.t. is likely to deplete them due to their close proximity to the lungs. One study stated that spleen and non-lung draining lymph nodes are not affected by i.t. administration of DT [78]; but they did not mention that lung dLNs were not affected. Another method claimed to be specifically targeting AM is the use of liposome clodronate . However, I do not favour this method because of the possibility of affecting other phagocytic cell in such as exudate macrophages and inflammatory DCs. Otherwise, a search for new regulatory elements which enables specific depletion of AMs but sparing other $CD169^+$ macrophages are needed to improve the targeting by DTR system. Transcriptional profiling will be necessary to explore for rare promoters or enhancers that are restricted to a single cell type. Alternatively, microRNA-based suppression can be utilized to narrow the transgene expression into certain tissue [142]. If a synthetic target site is engineered downstream of the DTR transgene, cell subsets in which the microRNA is expressed will suppress the transgene expression [248]. This ‘de-targeting’ approach can be a powerful mean to improve cell targeting such as the DTR transgenic system [249].

Collectively, the results described in this chapter suggest that AMs play an essential role in executing antiviral immune responses in the pulmonary environment. Knowledge provided by studying AMs in CD169-DTR mice will further our understanding in influenza immunity.

CHAPTER 5

FUTURE WORK AND CONCLUSION

5.1. Brief summary of findings

$CD169^+$ macrophages have emerged as a unique tissue macrophage population whose roles in antigen capture and initiation of innate/adaptive immunity have been emphasized in recent studies. I have generated CD169-DTR mouse model on BALB/c background, and characterized $CD169^+$ macrophages ablation patterns in the lymph nodes and spleen. With agreement to previous studies, SCS and MZM macrophages were depleted in our CD169-DTR mice.

In addition, AMs are known to express CD169. However, whether depletion of AMs can be induced in CD169-DTR mice has not been addressed previously. Here I demonstrated efficient (~90%) depletion of AMs upon i.p. DT treatment in CD169-DTR mice. More importantly, other immune populations such as DCs, granulocytes, and lymphocytes were not largely affected by DT treatment. DT treatment by itself was non-toxic and depletion could be maintained throughout the experimental time window of primary IAV infection. Hence, I propose CD169-DTR mice as a novel mice model to study roles of AMs during steady state or in pulmonary pathology settings, such as in IAV infection.

Furthermore, I conducted IAV infection in CD169-DTR mice; using PR8, a mice-adapted strain of IAV. While WT mice only experienced ~20% weight loss and survived the infection, CD169-DTR mice lost >30% of their weight and all succumbed by day 14 p.i. By harnessing BM chimeric mice, I confirmed that the mortality and morbidity of CD169-DTR mice was caused by ablation of cells derived from haematopoietic compartment, i.e. AM, and not by non-specific depletion of non-haematopoietic cells. In addition, I also observed enhanced lung pathology, increased viral titer, and reduced T cell responses in CD169-DTR mice. Moreover, by initiating DT treatment at different time point post infection, I found that AMs were essential for survival

in the early stage of IAV infection. Follow up studies are needed to unravel the mechanisms behind these observations.

5.2. Applicability to translational research

Human AMs have been recovered and cultured *in vitro* since the 1980s. AMs recovered from a smokers' broncho-alveolar lavage are larger, more granular, four times more in number, and often contain deposits of kaolinite and aluminum silicate [236].

However, getting access to healthy human lung tissue is one main limitation for human research. Virus infection study can only be conducted *in vitro*, and it is very difficult to assess the roles of immune cells like macrophages in such setting. Since human AMs are known to express CD169 [175], I expect that $CD169^{+}$ AMs in mice will behave similarly with their human counterpart. Hence, study of Influenza A infection in CD169-DTR mice may be relevant for translational or influenza vaccine research.

Nevertheless, there are undeniable differences between mouse and human immunology. For example, mice have different susceptibility to human pathogens; including Influenza A. Humanized mice will serve as a solution to conveniently study human immune response in influenza A and other settings. The generation of humanized mice involves reconstitution of human haematopoietic system in immunocompromised mice [142, 250]. Currently, the 'gold standard' humanized mice are derived by transplanting human CD34+ hematopoietic progrenitors to nonobese diabetic severe combined immunodeficiency (NOD/SCID) mice lacking the IL-2R chain [251]. However, these mice displayed poor development and function of myeloid cell subsets, including the AMs [250]. Knock-in of human cytokines such as IL-3 and GM-CSF was shown to improve development of human AMs [252]. Whether these humanized mice are sufficient to simulate human immune response in Influenza A infection remains to be determined.

5.3. Future work

Lung DCs have been described as the main population responsible for antigen presentation [78]. Early in infection CD103 DCs migrate to lung draining lymph node and stimulate T cells [78]. CD11b DCs also expand, carry antigen, and migrate to dLNs [85, 86]; although in per cell basis, CD103 DC are more potent in inducing CD8 T cell response [83]. GeurtsvanKessel et al. used CD11c-DTR and langerin-DTR mice and demonstrated the importance of DC in mediating protection against influenza virus. Ablation of $CD11c^{+}$ cells in CD11c-DTR mice, or $CD11c^{hi}Langerin^{+}CD103^{+}$ DC in langerin-DTR mice caused increased viral load, prominent weight loss, and abolished CD8 T cell response in comparison to control mice [78]. Upon adoptive transfer reconstitution experiment to DT treated CD11c-DTR mice, i.t. transfer of $2x10^{6}$ BM-derived DC, but not $2x10^{5}$ AMs restored antiviral immunity and viral clearance [78]. However, I suspect that the number of adoptive transferred AMs was not sufficient to alleviate the antiviral immunity; since my results demonstrated that AM do have crucial role in mounting immune response and antiviral clearance.

Since CD169-DTR mice displayed decreased flu-specific CD8 T cell response, I plan to research on the mechanism of how AM could directly or indirectly affect the T cell activation and/or proliferation. AMs were shown in a study published in 1983 vitro to stimulate T cell activation and proliferation [253]. There are also some evidences that AMs could transport antigens from lungs to draining lymph nodes very early in infection [83, 254]. Additionally, $CD169^{+}$ macrophages counterpart in spleen and lymph nodes are shown to play role in antigen delivery and induction of adaptive responses [180]. These CD169+ macrophages are suggested to prime CD8 T cells either by: (i) transferring antigen to CD8α DCs, or (ii) directly presenting antigen to CD8 T cells [182, 255]. However, there is no strong evidence showing APC capacity of AM to initiate or sustain adaptive immunity in the lung. In the near future, I plan to address on this matter by utilizing recombinant influenza virus expressing the ovalbumin epitope (PR8-OTI) together with OT-I CD8 T-cells to observe priming in CD169-DTR mice.

Moreover, AMs are known as the main type I IFNs producer in virus infection, which is the most important innate antiviral cytokines defense [97]. Production

of IFN-I by AM will activate neighboring cells to prepare for virus infection. Kumagai et al. utilized Ifna6^{gfp} mice, in which GFP expression is induced by Ifna6 promoter [97]. They infected the mice with Newcastle disease virus (NDV) intranasally and detected GFP$^+$ AMs at 24 hr; hence concluded that AM is the major IFN-α producers in NDV infection. When AMs were ablated by clodronate, pDCs seemed to compensate the IFN-I level as a backup mechanism, but pDC cannot control viral growth like AMs [97]. Their results also suggest that for AM to produce IFN-α, direct infection with viruses is required. Therefore, I plan to evaluate the IFN-I response in the absence of AMs in IAV infection. For this purpose, I plan to harness IFN-β reporter mice, whereby YFP expression is induced by Ifnb promoter [256].

Recently, an interesting mechanism whereby splenic marginal zone CD169$^+$ macrophages modulated type I interferon signalling to enforce VSV viral replication was described [189]. CD169$^+$ splenic macrophages upregulate Usp18 to downregulate IFN-I response and thus permit viral replication in these cells [189]. The authors proposed that availability of antigens needed to prime and maintain virus-specific T and B cells are ensured by this mechanism. As AM is CD169$^+$ and known to be highly susceptible to influenza infection [115], I will research in the near future if IAV infection also activate the regulation mechanism by Usp18 in AM.

Lastly, I also plan to compare the cytokines and chemokines levels of CD169-DTR and WT mice in future study. AMs have been reported as suppressive cells that control inflammatory responses in resting lung [257]. However, upon infection, they might produce both pro- and anti-inflammatory cytokines. Because of the observed lung pathology and increased accumulation of inflammatory cells observed in CD169-DTR mice, I predict that elevation of pro-inflammatory cytokines will be observed in CD169-DTR mice as the clinical signs worsen. Monitoring of cytokines and chemokines at the early stage of infection also will also be relevant because AM is suggested as cytokine and chemokine source during the early stages of infection [42]. Additionally, a lack of chemotactic cues for migration of effector T cells from the dLNs to the lung might result in reduced T cell response. Thus, it is also relevant to assess whether AM depletion affect the ability of T cell or DC migration.

5.4. Conclusion

AMs are the major population of phagocytes in the naive lung, and the first cells to encounter and exert responses against invading pathogens in the airway. For the first time, I demonstrated that lung AMs, but not other pulmonary immune cells, could be efficiently depleted upon DT treatment in CD169-DTR mice. Repeated DT injection is nontoxic to the mice, thus omits the requirement of bone marrow chimera as the case of CD11c-DTR mice. Hence, CD169-DTR line is an advanced mice model to study roles of AMs during steady state or in pulmonary pathology settings such as in IAV infection.

Upon infection with sublethal dose of PR8 influenza strain, CD169-DTR mice displayed increased morbidity and mortality. Additionally, more severe lung pathology, increased viral titers, and reduced CD8 T cell responses were also observed. By manipulating the initiation of DT treatment at different time points post infection I demonstrated that AMs are indispensable for survival in the early stage of IAV infection. Collectively, my results suggest that AM play an essential role in executing antiviral immune responses in the pulmonary environment. Future research will be conducted to understand the AM-control mechanisms over different components of antiviral immunity. Knowledge provided by studying AMs role using CD169-DTR mice will further our understanding in influenza immunity and benefit translational research.

REFERENCES

1. Fouchier, R.A., et al., *Characterization of a novel influenza A virus hemagglutinin subtype (H16) obtained from black-headed gulls.* Journal of virology, 2005. **79**(5): p. 2814-22.
2. Webster, R.G., et al., *Evolution and ecology of influenza A viruses.* Microbiological reviews, 1992. **56**(1): p. 152-79.
3. Nayak, D.P., E.K. Hui, and S. Barman, *Assembly and budding of influenza virus.* Virus research, 2004. **106**(2): p. 147-65.
4. Klenk, H.D., et al., *Activation of influenza A viruses by trypsin treatment.* Virology, 1975. **68**(2): p. 426-39.
5. Stegmann, T., et al., *The HA2 subunit of influenza hemagglutinin inserts into the target membrane prior to fusion.* The Journal of biological chemistry, 1991. **266**(27): p. 18404-10.
6. Bullough, P.A., et al., *Structure of influenza haemagglutinin at the pH of membrane fusion.* Nature, 1994. **371**(6492): p. 37-43.
7. Hale, B.G., R.A. Albrecht, and A. Garcia-Sastre, *Innate immune evasion strategies of influenza viruses.* Future microbiology, 2010. **5**(1): p. 23-41.
8. Horimoto, T. and Y. Kawaoka, *Influenza: lessons from past pandemics, warnings from current incidents.* Nature reviews. Microbiology, 2005. **3**(8): p. 591-600.
9. Nguyen-Van-Tam, J.S. and A.W. Hampson, *The epidemiology and clinical impact of pandemic influenza.* Vaccine, 2003. **21**(16): p. 1762-8.
10. Gani, R., et al., *Potential impact of antiviral drug use during influenza pandemic.* Emerging infectious diseases, 2005. **11**(9): p. 1355-62.
11. Tumpey, T.M. and J.A. Belser, *Resurrected pandemic influenza viruses.* Annual review of microbiology, 2009. **63**: p. 79-98.
12. Taubenberger, J.K. and D.M. Morens, *The pathology of influenza virus infections.* Annual review of pathology, 2008. **3**: p. 499-522.
13. Morens, D.M., J.K. Taubenberger, and A.S. Fauci, *Predominant role of bacterial pneumonia as a cause of death in pandemic influenza: implications for pandemic influenza preparedness.* The Journal of infectious diseases, 2008. **198**(7): p. 962-70.
14. Parvin, J.D., et al., *Measurement of the mutation rates of animal viruses: influenza A virus and poliovirus type 1.* Journal of virology, 1986. **59**(2): p. 377-83.
15. Boat, T.F., et al., *Human respiratory tract secretion. Mucous glycoproteins of nonpurulent tracheobronchial secretions, and sputum of patients with bronchitis and cystic fibrosis.* Archives of biochemistry and biophysics, 1976. **177**(1): p. 95-104.
16. Reading, P.C., et al., *Collectin-mediated antiviral host defense of the lung: evidence from influenza virus infection of mice.* Journal of virology, 1997. **71**(11): p. 8204-12.
17. Akira, S., S. Uematsu, and O. Takeuchi, *Pathogen recognition and innate immunity.* Cell, 2006. **124**(4): p. 783-801.
18. Meylan, E., J. Tschopp, and M. Karin, *Intracellular pattern recognition receptors in the host response.* Nature, 2006. **442**(7098): p. 39-44.

19. Der, S.D., et al., *Identification of genes differentially regulated by interferon alpha, beta, or gamma using oligonucleotide arrays.* Proceedings of the National Academy of Sciences of the United States of America, 1998. **95**(26): p. 15623-8.
20. Kolumam, G.A., et al., *Type I interferons act directly on CD8 T cells to allow clonal expansion and memory formation in response to viral infection.* The Journal of experimental medicine, 2005. **202**(5): p. 637-50.
21. Marrack, P., J. Kappler, and T. Mitchell, *Type I interferons keep activated T cells alive.* The Journal of experimental medicine, 1999. **189**(3): p. 521-30.
22. Wang, X., et al., *Influenza A virus NS1 protein prevents activation of NF-kappaB and induction of alpha/beta interferon.* Journal of virology, 2000. **74**(24): p. 11566-73.
23. Garcia-Sastre, A., et al., *Influenza A virus lacking the NS1 gene replicates in interferon-deficient systems.* Virology, 1998. **252**(2): p. 324-30.
24. Kochs, G., A. Garcia-Sastre, and L. Martinez-Sobrido, *Multiple anti-interferon actions of the influenza A virus NS1 protein.* Journal of virology, 2007. **81**(13): p. 7011-21.
25. Fernandez-Sesma, A., et al., *Influenza virus evades innate and adaptive immunity via the NS1 protein.* Journal of virology, 2006. **80**(13): p. 6295-304.
26. Ludwig, S., et al., *The influenza A virus NS1 protein inhibits activation of Jun N-terminal kinase and AP-1 transcription factors.* Journal of virology, 2002. **76**(21): p. 11166-71.
27. Lenschow, D.J., et al., *IFN-stimulated gene 15 functions as a critical antiviral molecule against influenza, herpes, and Sindbis viruses.* Proceedings of the National Academy of Sciences of the United States of America, 2007. **104**(4): p. 1371-6.
28. Koerner, I., et al., *Protective role of beta interferon in host defense against influenza A virus.* Journal of virology, 2007. **81**(4): p. 2025-30.
29. Demedts, I.K., et al., *Different roles for human lung dendritic cell subsets in pulmonary immune defense mechanisms.* American journal of respiratory cell and molecular biology, 2006. **35**(3): p. 387-93.
30. Chiorean, E.G. and J.S. Miller, *The biology of natural killer cells and implications for therapy of human disease.* Journal of hematotherapy & stem cell research, 2001. **10**(4): p. 451-63.
31. Mandelboim, O., et al., *Recognition of haemagglutinins on virus-infected cells by NKp46 activates lysis by human NK cells.* Nature, 2001. **409**(6823): p. 1055-60.
32. Arnon, T.I., et al., *Recognition of viral hemagglutinins by NKp44 but not by NKp30.* European journal of immunology, 2001. **31**(9): p. 2680-9.
33. Glasner, A., et al., *Elucidating the mechanisms of influenza virus recognition by Ncr1.* PloS one, 2012. **7**(5): p. e36837.
34. Gazit, R., et al., *Lethal influenza infection in the absence of the natural killer cell receptor gene Ncr1.* Nature immunology, 2006. **7**(5): p. 517-23.

35. Stein-Streilein, J. and J. Guffee, *In vivo treatment of mice and hamsters with antibodies to asialo GM1 increases morbidity and mortality to pulmonary influenza infection.* Journal of immunology, 1986. **136**(4): p. 1435-41.
36. Achdout, H., et al., *Killing of avian and Swine influenza virus by natural killer cells.* Journal of virology, 2010. **84**(8): p. 3993-4001.
37. Hashimoto, G., P.F. Wright, and D.T. Karzon, *Antibody-dependent cell-mediated cytotoxicity against influenza virus-infected cells.* The Journal of infectious diseases, 1983. **148**(5): p. 785-94.
38. Jegerlehner, A., et al., *Influenza A vaccine based on the extracellular domain of M2: weak protection mediated via antibody-dependent NK cell activity.* Journal of immunology, 2004. **172**(9): p. 5598-605.
39. Baumgarth, N. and A. Kelso, *In vivo blockade of gamma interferon affects the influenza virus-induced humoral and the local cellular immune response in lung tissue.* Journal of virology, 1996. **70**(7): p. 4411-8.
40. Graham, M.B., et al., *Response to influenza infection in mice with a targeted disruption in the interferon gamma gene.* The Journal of experimental medicine, 1993. **178**(5): p. 1725-32.
41. Szomolanyi-Tsuda, E. and R.M. Welsh, *T cell-independent antibody-mediated clearance of polyoma virus in T cell-deficient mice.* The Journal of experimental medicine, 1996. **183**(2): p. 403-11.
42. Tumpey, T.M., et al., *Pathogenicity of influenza viruses with genes from the 1918 pandemic virus: functional roles of alveolar macrophages and neutrophils in limiting virus replication and mortality in mice.* Journal of virology, 2005. **79**(23): p. 14933-44.
43. Fujisawa, H., *Inhibitory role of neutrophils on influenza virus multiplication in the lungs of mice.* Microbiology and immunology, 2001. **45**(10): p. 679-88.
44. Abbas, A.K., K.M. Murphy, and A. Sher, *Functional diversity of helper T lymphocytes.* Nature, 1996. **383**(6603): p. 787-93.
45. Sun, J., et al., *Effector T cells control lung inflammation during acute influenza virus infection by producing IL-10.* Nature medicine, 2009. **15**(3): p. 277-84.
46. Belz, G.T., et al., *Compromised influenza virus-specific CD8(+)-T-cell memory in CD4(+)-T-cell-deficient mice.* Journal of virology, 2002. **76**(23): p. 12388-93.
47. Riberdy, J.M., et al., *Diminished primary and secondary influenza virus-specific CD8(+) T-cell responses in CD4-depleted Ig(-/-) mice.* Journal of virology, 2000. **74**(20): p. 9762-5.
48. Homann, D., L. Teyton, and M.B. Oldstone, *Differential regulation of antiviral T-cell immunity results in stable CD8+ but declining CD4+ T-cell memory.* Nature medicine, 2001. **7**(8): p. 913-9.
49. Doherty, P.C., et al., *Effector CD4+ and CD8+ T-cell mechanisms in the control of respiratory virus infections.* Immunological reviews, 1997. **159**: p. 105-17.
50. Berke, G., *The CTL's kiss of death.* Cell, 1995. **81**(1): p. 9-12.
51. Price, G.E., et al., *Perforin and Fas cytolytic pathways coordinately shape the selection and diversity of CD8+-T-cell escape variants of influenza virus.* Journal of virology, 2005. **79**(13): p. 8545-59.

52. Johnson, B.J., et al., *Single-cell perforin and granzyme expression reveals the anatomical localization of effector CD8+ T cells in influenza virus-infected mice.* Proceedings of the National Academy of Sciences of the United States of America, 2003. **100**(5): p. 2657-62.
53. Bender, B.S., et al., *Transgenic mice lacking class I major histocompatibility complex-restricted T cells have delayed viral clearance and increased mortality after influenza virus challenge.* The Journal of experimental medicine, 1992. **175**(4): p. 1143-5.
54. Lawrence, C.W. and T.J. Braciale, *Activation, differentiation, and migration of naive virus-specific CD8+ T cells during pulmonary influenza virus infection.* Journal of immunology, 2004. **173**(2): p. 1209-18.
55. Tripp, R.A., S.R. Sarawar, and P.C. Doherty, *Characteristics of the influenza virus-specific CD8+ T cell response in mice homozygous for disruption of the H-2lAb gene.* Journal of immunology, 1995. **155**(6): p. 2955-9.
56. Lawrence, C.W., R.M. Ream, and T.J. Braciale, *Frequency, specificity, and sites of expansion of CD8+ T cells during primary pulmonary influenza virus infection.* Journal of immunology, 2005. **174**(9): p. 5332-40.
57. Cerwenka, A., T.M. Morgan, and R.W. Dutton, *Naive, effector, and memory CD8 T cells in protection against pulmonary influenza virus infection: homing properties rather than initial frequencies are crucial.* Journal of immunology, 1999. **163**(10): p. 5535-43.
58. Marshall, D.R., et al., *Measuring the diaspora for virus-specific CD8+ T cells.* Proceedings of the National Academy of Sciences of the United States of America, 2001. **98**(11): p. 6313-8.
59. Mintern, J.D., et al., *Cutting edge: Tissue-resident memory CTL down-regulate cytolytic molecule expression following virus clearance.* Journal of immunology, 2007. **179**(11): p. 7220-4.
60. Barber, D.L., E.J. Wherry, and R. Ahmed, *Cutting edge: rapid in vivo killing by memory CD8 T cells.* Journal of immunology, 2003. **171**(1): p. 27-31.
61. Ochsenbein, A.F. and R.M. Zinkernagel, *Natural antibodies and complement link innate and acquired immunity.* Immunology today, 2000. **21**(12): p. 624-30.
62. LeBien, T.W. and T.F. Tedder, *B lymphocytes: how they develop and function.* Blood, 2008. **112**(5): p. 1570-80.
63. Mozdzanowska, K., et al., *Roles of CD4+ T-cell-independent and -dependent antibody responses in the control of influenza virus infection: evidence for noncognate CD4+ T-cell activities that enhance the therapeutic activity of antiviral antibodies.* Journal of virology, 2005. **79**(10): p. 5943-51.
64. Sangster, M.Y., et al., *An early CD4+ T cell-dependent immunoglobulin A response to influenza infection in the absence of key cognate T-B interactions.* The Journal of experimental medicine, 2003. **198**(7): p. 1011-21.
65. Galli, G., et al., *Adjuvanted H5N1 vaccine induces early CD4+ T cell response that predicts long-term persistence of protective antibody*

levels. Proceedings of the National Academy of Sciences of the United States of America, 2009. **106**(10): p. 3877-82.
66. Graham, M.B. and T.J. Braciale, *Resistance to and recovery from lethal influenza virus infection in B lymphocyte-deficient mice.* The Journal of experimental medicine, 1997. **186**(12): p. 2063-8.
67. Mozdzanowska, K., K. Maiese, and W. Gerhard, *Th cell-deficient mice control influenza virus infection more effectively than Th- and B cell-deficient mice: evidence for a Th-independent contribution by B cells to virus clearance.* Journal of immunology, 2000. **164**(5): p. 2635-43.
68. Palladino, G., et al., *Virus-neutralizing antibodies of immunoglobulin G (IgG) but not of IgM or IgA isotypes can cure influenza virus pneumonia in SCID mice.* Journal of virology, 1995. **69**(4): p. 2075-81.
69. Mozdzanowska, K., et al., *A pulmonary influenza virus infection in SCID mice can be cured by treatment with hemagglutinin-specific antibodies that display very low virus-neutralizing activity in vitro.* Journal of virology, 1997. **71**(6): p. 4347-55.
70. Joo, H.M., Y. He, and M.Y. Sangster, *Broad dispersion and lung localization of virus-specific memory B cells induced by influenza pneumonia.* Proceedings of the National Academy of Sciences of the United States of America, 2008. **105**(9): p. 3485-90.
71. Lambrecht, B.N. and H. Hammad, *Lung dendritic cells in respiratory viral infection and asthma: from protection to immunopathology.* Annual review of immunology, 2012. **30**: p. 243-70.
72. Nussenzweig, M.C., et al., *Dendritic cells are accessory cells for the development of anti-trinitrophenyl cytotoxic T lymphocytes.* The Journal of experimental medicine, 1980. **152**(4): p. 1070-84.
73. Banchereau, J. and R.M. Steinman, *Dendritic cells and the control of immunity.* Nature, 1998. **392**(6673): p. 245-52.
74. Steinman, R.M. and Z.A. Cohn, *Identification of a novel cell type in peripheral lymphoid organs of mice. I. Morphology, quantitation, tissue distribution.* The Journal of experimental medicine, 1973. **137**(5): p. 1142-62.
75. Nussenzweig, M.C., et al., *Studies of the cell surface of mouse dendritic cells and other leukocytes.* The Journal of experimental medicine, 1981. **154**(1): p. 168-87.
76. D'Amico, A. and L. Wu, *The early progenitors of mouse dendritic cells and plasmacytoid predendritic cells are within the bone marrow hemopoietic precursors expressing Flt3.* The Journal of experimental medicine, 2003. **198**(2): p. 293-303.
77. Karsunky, H., et al., *Flt3 ligand regulates dendritic cell development from Flt3+ lymphoid and myeloid-committed progenitors to Flt3+ dendritic cells in vivo.* The Journal of experimental medicine, 2003. **198**(2): p. 305-13.
78. GeurtsvanKessel, C.H., et al., *Clearance of influenza virus from the lung depends on migratory langerin+CD11b- but not plasmacytoid dendritic cells.* The Journal of experimental medicine, 2008. **205**(7): p. 1621-34.
79. Sung, S.S., et al., *A major lung CD103 (alphaE)-beta7 integrin-positive epithelial dendritic cell population expressing Langerin and tight junction proteins.* Journal of immunology, 2006. **176**(4): p. 2161-72.

80. Ginhoux, F., et al., *The origin and development of nonlymphoid tissue CD103+ DCs.* The Journal of experimental medicine, 2009. **206**(13): p. 3115-30.
81. Bursch, L.S., et al., *Identification of a novel population of Langerin+ dendritic cells.* The Journal of experimental medicine, 2007. **204**(13): p. 3147-56.
82. del Rio, M.L., et al., *CD103- and CD103+ bronchial lymph node dendritic cells are specialized in presenting and cross-presenting innocuous antigen to CD4+ and CD8+ T cells.* Journal of immunology, 2007. **178**(11): p. 6861-6.
83. Kim, T.S. and T.J. Braciale, *Respiratory dendritic cell subsets differ in their capacity to support the induction of virus-specific cytotoxic CD8+ T cell responses.* PloS one, 2009. **4**(1): p. e4204.
84. Raymond, M., et al., *Selective control of SIRP-alpha-positive airway dendritic cell trafficking through CD47 is critical for the development of T(H)2-mediated allergic inflammation.* The Journal of allergy and clinical immunology, 2009. **124**(6): p. 1333-42 e1.
85. GeurtsvanKessel, C.H., et al., *Both conventional and interferon killer dendritic cells have antigen-presenting capacity during influenza virus infection.* PloS one, 2009. **4**(9): p. e7187.
86. Lin, K.L., et al., *CCR2+ monocyte-derived dendritic cells and exudate macrophages produce influenza-induced pulmonary immune pathology and mortality.* Journal of immunology, 2008. **180**(4): p. 2562-72.
87. Bhardwaj, N., et al., *Influenza virus-infected dendritic cells stimulate strong proliferative and cytolytic responses from human CD8+ T cells.* The Journal of clinical investigation, 1994. **94**(2): p. 797-807.
88. Jakubzick, C., et al., *Blood monocyte subsets differentially give rise to CD103+ and CD103- pulmonary dendritic cell populations.* Journal of immunology, 2008. **180**(5): p. 3019-27.
89. Varol, C., et al., *Monocytes give rise to mucosal, but not splenic, conventional dendritic cells.* The Journal of experimental medicine, 2007. **204**(1): p. 171-80.
90. Hohl, T.M., et al., *Inflammatory monocytes facilitate adaptive CD4 T cell responses during respiratory fungal infection.* Cell host & microbe, 2009. **6**(5): p. 470-81.
91. Leon, B., M. Lopez-Bravo, and C. Ardavin, *Monocyte-derived dendritic cells formed at the infection site control the induction of protective T helper 1 responses against Leishmania.* Immunity, 2007. **26**(4): p. 519-31.
92. Randolph, G.J., C. Jakubzick, and C. Qu, *Antigen presentation by monocytes and monocyte-derived cells.* Current opinion in immunology, 2008. **20**(1): p. 52-60.
93. Kamphorst, A.O., et al., *Route of antigen uptake differentially impacts presentation by dendritic cells and activated monocytes.* Journal of immunology, 2010. **185**(6): p. 3426-35.
94. Hashimoto, D., J. Miller, and M. Merad, *Dendritic cell and macrophage heterogeneity in vivo.* Immunity, 2011. **35**(3): p. 323-35.
95. von Garnier, C., et al., *Anatomical location determines the distribution and function of dendritic cells and other APCs in the respiratory tract.* Journal of immunology, 2005. **175**(3): p. 1609-18.

96. Kool, M., et al., *An anti-inflammatory role for plasmacytoid dendritic cells in allergic airway inflammation.* Journal of immunology, 2009. **183**(2): p. 1074-82.
97. Kumagai, Y., et al., *Alveolar macrophages are the primary interferon-alpha producer in pulmonary infection with RNA viruses.* Immunity, 2007. **27**(2): p. 240-52.
98. Shortman, K. and Y.J. Liu, *Mouse and human dendritic cell subtypes.* Nature reviews. Immunology, 2002. **2**(3): p. 151-61.
99. Gordon, S., *The macrophage: Past, present and future.* European Journal of Immunology, 2007. **37**(SUPPL. 1).
100. Hume, D.A., *The mononuclear phagocyte system.* Current Opinion in Immunology, 2006. **18**(1): p. 49-53.
101. Gordon, S. and P.R. Taylor, *Monocyte and macrophage heterogeneity.* Nature reviews. Immunology, 2005. **5**(12): p. 953-64.
102. Mosser, D.M. and J.P. Edwards, *Exploring the full spectrum of macrophage activation.* Nature Reviews Immunology, 2008. **8**(12): p. 958-969.
103. Taylor, P.R., et al., *Marophage Receptors and Immune Recognition.* Annual review of immunology, 2005. **23**: p. 901-944.
104. Harmsen, A.G., et al., *The role of macrophages in particle translocation from lungs to lymph nodes.* Science, 1985. **230**(4731): p. 1277-80.
105. Holt, P.G., *Inhibitory activity of unstimulated alveolar macrophages on T-lymphocyte blastogenic response.* The American review of respiratory disease, 1978. **118**(4): p. 791-3.
106. Holt, P.G., et al., *Downregulation of the antigen presenting cell function(s) of pulmonary dendritic cells in vivo by resident alveolar macrophages.* The Journal of experimental medicine, 1993. **177**(2): p. 397-407.
107. Strickland, D.H., et al., *Regulation of T-cell function in lung tissue by pulmonary alveolar macrophages.* Immunology, 1993. **80**(2): p. 266-72.
108. Bilyk, N. and P.G. Holt, *Cytokine modulation of the immunosuppressive phenotype of pulmonary alveolar macrophage populations.* Immunology, 1995. **86**(2): p. 231-7.
109. Thepen, T., N. Van Rooijen, and G. Kraal, *Alveolar macrophage elimination in vivo is associated with an increase in pulmonary immune response in mice.* The Journal of experimental medicine, 1989. **170**(2): p. 499-509.
110. Broug-Holub, E., et al., *Alveolar macrophages are required for protective pulmonary defenses in murine Klebsiella pneumonia: elimination of alveolar macrophages increases neutrophil recruitment but decreases bacterial clearance and survival.* Infection and immunity, 1997. **65**(4): p. 1139-46.
111. Nathan, C.F., *Secretory products of macrophages.* The Journal of clinical investigation, 1987. **79**(2): p. 319-26.
112. Sibille, Y. and H.Y. Reynolds, *Macrophages and polymorphonuclear neutrophils in lung defense and injury.* The American review of respiratory disease, 1990. **141**(2): p. 471-501.
113. Aldridge, J.R., Jr., et al., *TNF/iNOS-producing dendritic cells are the necessary evil of lethal influenza virus infection.* Proceedings of the

National Academy of Sciences of the United States of America, 2009. **106**(13): p. 5306-11.
114. Holt, P.G., et al., *Regulation of immunological homeostasis in the respiratory tract.* Nature reviews. Immunology, 2008. **8**(2): p. 142-52.
115. Hofmann, P., et al., *Susceptibility of mononuclear phagocytes to influenza A virus infection and possible role in the antiviral response.* Journal of leukocyte biology, 1997. **61**(4): p. 408-14.
116. Rodgers, B. and C.A. Mims, *Interaction of influenza virus with mouse macrophages.* Infection and immunity, 1981. **31**(2): p. 751-7.
117. Jenkins, S.J., et al., *Local macrophage proliferation, rather than recruitment from the blood, is a signature of TH2 inflammation.* Science, 2011. **332**(6035): p. 1284-8.
118. Dawson, T.C., et al., *Contrasting effects of CCR5 and CCR2 deficiency in the pulmonary inflammatory response to influenza A virus.* The American journal of pathology, 2000. **156**(6): p. 1951-9.
119. Herold, S., et al., *Alveolar epithelial cells direct monocyte transepithelial migration upon influenza virus infection: impact of chemokines and adhesion molecules.* Journal of immunology, 2006. **177**(3): p. 1817-24.
120. Perrone, L.A., et al., *H5N1 and 1918 pandemic influenza virus infection results in early and excessive infiltration of macrophages and neutrophils in the lungs of mice.* PLoS pathogens, 2008. **4**(8): p. e1000115.
121. Wareing, M.D., et al., *Chemokine regulation of the inflammatory response to a low-dose influenza infection in CCR2-/- mice.* Journal of leukocyte biology, 2007. **81**(3): p. 793-801.
122. Wareing, M.D., et al., *CXCR2 is required for neutrophil recruitment to the lung during influenza virus infection, but is not essential for viral clearance.* Viral immunology, 2007. **20**(3): p. 369-78.
123. Bilyk, N. and P.G. Holt, *Inhibition of the immunosuppressive activity of resident pulmonary alveolar macrophages by granulocyte/macrophage colony-stimulating factor.* The Journal of experimental medicine, 1993. **177**(6): p. 1773-7.
124. Taut, K., et al., *Macrophage Turnover Kinetics in the Lungs of Mice Infected with Streptococcus pneumoniae.* American journal of respiratory cell and molecular biology, 2008. **38**(1): p. 105-13.
125. Gordon, S., *Alternative activation of macrophages.* Nature reviews. Immunology, 2003. **3**(1): p. 23-35.
126. Sica, A. and A. Mantovani, *Macrophage plasticity and polarization: in vivo veritas.* The Journal of clinical investigation, 2012. **122**(3): p. 787-95.
127. Martinez, F.O., et al., *Macrophage activation and polarization.* Frontiers in bioscience : a journal and virtual library, 2008. **13**: p. 453-61.
128. Wilson, H.M., et al., *Inhibition of macrophage nuclear factor-kappaB leads to a dominant anti-inflammatory phenotype that attenuates glomerular inflammation in vivo.* The American journal of pathology, 2005. **167**(1): p. 27-37.
129. Janssen, W.J., et al., *Fas determines differential fates of resident and recruited macrophages during resolution of acute lung injury.*

American journal of respiratory and critical care medicine, 2011. **184**(5): p. 547-60.
130. Duan, M., et al., *Distinct macrophage subpopulations characterize acute infection and chronic inflammatory lung disease.* Journal of immunology, 2012. **189**(2): p. 946-55.
131. Watanabe, Y., et al., *Augmentation of fatality of influenza in mice by inhibition of phagocytosis.* Biochemical and biophysical research communications, 2005. **337**(3): p. 881-6.
132. Kim, H.M., et al., *Alveolar macrophages are indispensable for controlling influenza viruses in lungs of pigs.* Journal of virology, 2008. **82**(9): p. 4265-74.
133. Hashimoto, Y., et al., *Evidence for phagocytosis of influenza virus-infected, apoptotic cells by neutrophils and macrophages in mice.* Journal of immunology, 2007. **178**(4): p. 2448-57.
134. Huber, V.C., et al., *Fc receptor-mediated phagocytosis makes a significant contribution to clearance of influenza virus infections.* Journal of immunology, 2001. **166**(12): p. 7381-8.
135. van Rooijen, N. and R. van Nieuwmegen, *Elimination of phagocytic cells in the spleen after intravenous injection of liposome-encapsulated dichloromethylene diphosphonate. An enzyme-histochemical study.* Cell and tissue research, 1984. **238**(2): p. 355-8.
136. Van Rooijen, N. and A. Sanders, *Liposome mediated depletion of macrophages: mechanism of action, preparation of liposomes and applications.* Journal of immunological methods, 1994. **174**(1-2): p. 83-93.
137. Zhang, Y., et al., *APCs in the liver and spleen recruit activated allogeneic CD8+ T cells to elicit hepatic graft-versus-host disease.* Journal of immunology, 2002. **169**(12): p. 7111-8.
138. van Rooijen, N. and E. van Kesteren-Hendrikx, *Clodronate liposomes: perspectives in research and therapeutics.* Journal of liposome research, 2002. **12**(1-2): p. 81-94.
139. McGill, J., N. Van Rooijen, and K.L. Legge, *Protective influenza-specific CD8 T cell responses require interactions with dendritic cells in the lungs.* The Journal of experimental medicine, 2008. **205**(7): p. 1635-46.
140. Mircescu, M.M., et al., *Essential role for neutrophils but not alveolar macrophages at early time points following Aspergillus fumigatus infection.* The Journal of infectious diseases, 2009. **200**(4): p. 647-56.
141. Traeger, T., et al., *Selective depletion of alveolar macrophages in polymicrobial sepsis increases lung injury, bacterial load and mortality but does not affect cytokine release.* Respiration; international review of thoracic diseases, 2009. **77**(2): p. 203-13.
142. Chow, A., B.D. Brown, and M. Merad, *Studying the mononuclear phagocyte system in the molecular age.* Nature reviews. Immunology, 2011. **11**(11): p. 788-98.
143. Burnett, S., et al., *Conditional macrophage ablation in transgenic mice expressing a Fas-based suicide gene.* Journal of Leukocyte Biology, 2004. **75**.
144. Bennett, C.L. and B.E. Clausen, *DC ablation in mice: promises, pitfalls, and challenges.* Trends in immunology, 2007. **28**(12): p. 525-31.

145. Paine, R., 3rd, et al., *Impaired functional activity of alveolar macrophages from GM-CSF-deficient mice.* American journal of physiology. Lung cellular and molecular physiology, 2001. **281**(5): p. L1210-8.
146. Jung, S., et al., *In vivo depletion of CD11c+ dendritic cells abrogates priming of CD8+ T cells by exogenous cell-associated antigens.* Immunity, 2002. **17**(2): p. 211-20.
147. Naglich, J.G., et al., *Expression cloning of a diphtheria toxin receptor: identity with a heparin-binding EGF-like growth factor precursor.* Cell, 1992. **69**(6): p. 1051-61.
148. Mitamura, T., et al., *Structure-function analysis of the diphtheria toxin receptor toxin binding site by site-directed mutagenesis.* The Journal of biological chemistry, 1997. **272**(43): p. 27084-90.
149. Saito, M., et al., *Diphtheria toxin receptor-mediated conditional and targeted cell ablation in transgenic mice.* Nature biotechnology, 2001. **19**(8): p. 746-50.
150. Pappenheimer Jr, A.M., et al., *Diphtheria toxin and related proteins: Effect of route of injection on toxicity and the determination of cytotoxicity for various cultured cells.* Journal of Infectious Diseases, 1982. **145**(1): p. 94-102.
151. Bennett, C.L., et al., *Inducible ablation of mouse Langerhans cells diminishes but fails to abrogate contact hypersensitivity.* Journal of Cell Biology, 2005. **169**(4): p. 569-576.
152. Miyake, Y., et al., *Protective role of macrophages in noninflammatory lung injury caused by selective ablation of alveolar epithelial type II Cells.* Journal of immunology, 2007. **178**(8): p. 5001-9.
153. Thorburn, J., A.E. Frankel, and A. Thorburn, *Apoptosis by leukemia cell-targeted diphtheria toxin occurs via receptor-independent activation of Fas-associated death domain protein.* Clinical cancer research : an official journal of the American Association for Cancer Research, 2003. **9**(2): p. 861-5.
154. Cailhier, J.F., et al., *Conditional macrophage ablation demonstrates that resident macrophages initiate acute peritoneal inflammation.* Journal of Immunology, 2005. **174**(4): p. 2336-2342.
155. Duffield, J.S., et al., *Selective depletion of macrophages reveals distinct, opposing roles during liver injury and repair.* The Journal of clinical investigation, 2005. **115**(1): p. 56-65.
156. Duffield, J.S., et al., *Conditional ablation of macrophages halts progression of crescentic glomerulonephritis.* American Journal of Pathology, 2005. **167**(5): p. 1207-1219.
157. Stoneman, V., et al., *Monocyte/macrophage suppression in CD11b diphtheria toxin receptor transgenic mice differentially affects atherogenesis and established plaques.* Circulation research, 2007. **100**(6): p. 884-93.
158. Lahl, K., et al., *Selective depletion of Foxp3⁺ regulatory T cells induces a scurfy-like disease.* Journal of Experimental Medicine, 2007. **204**(1): p. 57-63.
159. Kim, J.M., J.P. Rasmussen, and A.Y. Rudensky, *Regulatory T cells prevent catastrophic autoimmunity throughout the lifespan of mice.* Nature Immunology, 2007. **8**(2): p. 191-197.

160. Walzer, T., et al., *Identification, activation, and selective in vivo ablation of mouse NK cells via NKp46.* Proceedings of the National Academy of Sciences of the United States of America, 2007. **104**(9): p. 3384-3389.
161. Chow, A., et al., *Bone marrow CD169+ macrophages promote the retention of hematopoietic stem and progenitor cells in the mesenchymal stem cell niche.* The Journal of experimental medicine, 2011. **208**(2): p. 261-71.
162. Hatori, M., et al., *Inducible ablation of melanopsin-expressing retinal ganglion cells reveals their central role in non-image forming visual responses.* PloS one, 2008. **3**(6): p. e2451.
163. Bennett, C.L., et al., *Inducible ablation of mouse Langerhans cells diminishes but fails to abrogate contact hypersensitivity.* The Journal of cell biology, 2005. **169**(4): p. 569-76.
164. Vallon-Eberhard, A., et al., *Transepithelial pathogen uptake into the small intestinal lamina propria.* Journal of immunology, 2006. **176**(4): p. 2465-9.
165. van Rijt, L.S., et al., *In vivo depletion of lung CD11c+ dendritic cells during allergen challenge abrogates the characteristic features of asthma.* The Journal of experimental medicine, 2005. **201**(6): p. 981-91.
166. Probst, H.C., et al., *Histological analysis of CD11c-DTR/GFP mice after in vivo depletion of dendritic cells.* Clinical and experimental immunology, 2005. **141**(3): p. 398-404.
167. Zaft, T., et al., *CD11chigh dendritic cell ablation impairs lymphopenia-driven proliferation of naive and memory CD8+ T cells.* Journal of immunology, 2005. **175**(10): p. 6428-35.
168. Meredith, M.M., et al., *Expression of the zinc finger transcription factor zDC (Zbtb46, Btbd4) defines the classical dendritic cell lineage.* The Journal of experimental medicine, 2012. **209**(6): p. 1153-65.
169. Jones, C., V. M, and P.R. Crocker, *Recognition of sialylated menigococcal lipopolysaccharide by siglecs expressed on myeloid cells leads to enhanced bacterial uptake.* Molecular Microbiology, 2003. **49**: p. 1213-1225.
170. Crocker, P.R. and S. Gordon, *Properties and distribution of a lectin-like hemagglutinin differentially expressed by murine stromal tissue macrophages.* The Journal of experimental medicine, 1986. **164**(6): p. 1862-75.
171. Crocker, P.R. and S. Gordon, *Mouse macrophage hemagglutinin (sheep erythrocyte receptor) with specificity for sialylated glycoconjugates characterized by a monoclonal antibody.* The Journal of experimental medicine, 1989. **169**(4): p. 1333-46.
172. Crocker, P.R., et al., *Sialoadhesin, a macrophage sialic acid binding receptor for haemopoietic cells with 17 immunoglobulin-like domains.* The EMBO journal, 1994. **13**(19): p. 4490-503.
173. Crocker, P.R., J.C. Paulson, and A. Varki, *Siglecs and their roles in the immune system.* Nature reviews. Immunology, 2007. **7**(4): p. 255-66.
174. Crocker, P.R. and P. Redelinghuys, *Siglecs as positive and negative regulators of the immune system.* Biochemical Society transactions, 2008. **36**(Pt 6): p. 1467-71.

175. Hartnell, A., et al., *Characterization of human sialoadhesin, a sialic acid binding receptor expressed by resident and inflammatory macrophage populations.* Blood, 2001. **97**(1): p. 288-96.
176. Martinez-Pomares, L. and S. Gordon, *Antigen presentation the macrophage way.* Cell, 2007. **131**(4): p. 641-3.
177. Martinez-Pomares, L., et al., *Fc chimeric protein containing the cysteine-rich domain of the murine mannose receptor binds to macrophages from splenic marginal zone and lymph node subcapsular sinus and to germinal centers.* The Journal of experimental medicine, 1996. **184**(5): p. 1927-37.
178. Linehan, S.A., et al., *Mannose receptor and its putative ligands in normal murine lymphoid and nonlymphoid organs: In situ expression of mannose receptor by selected macrophages, endothelial cells, perivascular microglia, and mesangial cells, but not dendritic cells.* The Journal of experimental medicine, 1999. **189**(12): p. 1961-72.
179. Taylor, P.R., S. Gordon, and L. Martinez-Pomares, *The mannose receptor: linking homeostasis and immunity through sugar recognition.* Trends in immunology, 2005. **26**(2): p. 104-10.
180. Martinez-Pomares, L. and S. Gordon, *CD169+ macrophages at the crossroads of antigen presentation.* Trends in immunology, 2012. **33**(2): p. 66-70.
181. Backer, R., et al., *Effective collaboration between marginal metallophilic macrophages and CD8+ dendritic cells in the generation of cytotoxic T cells.* Proceedings of the National Academy of Sciences of the United States of America, 2010. **107**(1): p. 216-21.
182. Asano, K., et al., *CD169-positive macrophages dominate antitumor immunity by crosspresenting dead cell-associated antigens.* Immunity, 2011. **34**(1): p. 85-95.
183. Crocker, P.R. and A. Varki, *Siglecs in the immune system.* Immunology, 2001. **103**(2): p. 137-145.
184. Müerköster, S., et al., *Sialoadhesin-positive host macrophages play an essential role in graft-versus-leukemia reactivity in mice.* Blood, 1999 **93**(12): p. 4375-4386.
185. van der Kuyl, A.C., et al., *Sialoadhesin (CD169) Expression in CD14+ Cells Is Upregulated Early after HIV-1 Infection and Increases during Disease Progression.* PLoS ONE, 2007. **2**(2): p. e257.
186. Iannacone, M., et al., *Subcapsular sinus macrophages prevent CNS invasion on peripheral infection with a neurotropic virus.* Nature, 2010. **465**(7301): p. 1079-83.
187. Junt, T., et al., *Subcapsular sinus macrophages in lymph nodes clear lymph-borne viruses and present them to antiviral B cells.* Nature, 2007. **450**(7166): p. 110-4.
188. Barral, P., et al., *CD169(+) macrophages present lipid antigens to mediate early activation of iNKT cells in lymph nodes.* Nature immunology, 2010. **11**(4): p. 303-12.
189. Honke, N., et al., *Enforced viral replication activates adaptive immunity and is essential for the control of a cytopathic virus.* Nature immunology, 2012. **13**(1): p. 51-7.

190. Moseman, E.A., et al., *B cell maintenance of subcapsular sinus macrophages protects against a fatal viral infection independent of adaptive immunity.* Immunity, 2012. **36**(3): p. 415-26.
191. Miyake, Y., et al., *Critical role of macrophages in the marginal zone in the suppression of immune responses to apoptotic cell-associated antigens.* The Journal of clinical investigation, 2007. **117**(8): p. 2268-78.
192. Muyrers, J.P., et al., *Rapid modification of bacterial artificial chromosomes by ET-recombination.* Nucleic acids research, 1999. **27**(6): p. 1555-7.
193. de Felipe, P., et al., *E unum pluribus: multiple proteins from a self-processing polyprotein.* Trends in biotechnology, 2006. **24**(2): p. 68-75.
194. Ruedl, C., H.J. Khameneh, and K. Karjalainen, *Manipulation of immune system via immortal bone marrow stem cells.* International immunology, 2008. **20**(9): p. 1211-8.
195. Morita, S., T. Kojima, and T. Kitamura, *Plat-E: an efficient and stable system for transient packaging of retroviruses.* Gene therapy, 2000. **7**(12): p. 1063-6.
196. Hansson, G.K., *Advanced information: gene modification in mice.* The Nobel Assembly at Karolinska Institutet, 2007.
197. Xu, L., J. Sandoval, and A.C. Young, *Purification of BAC DNA.* Focus, 1999. **21**(2).
198. Zhang, Y., et al., *A new logic for DNA engineering using recombination in Escherichia coli.* Nature genetics, 1998. **20**(2): p. 123-8.
199. Muyrers, J.P.P., Y. Zhang, and A.F. Stewart, *Techniques: Recombinogenic engineering - New options for cloning and manipulating DNA.* Trends Biochem. Sci., 2001. **26**(5): p. 325-331.
200. Losch, S., S. Braatsch, and H. Kranz, *Red/ET recombination lambda against Mu: Base-specific modification of the E. coli genome.* Bio Spektrum, 2007. **13**(5): p. 516-518.
201. Chan, W.I., et al., *A recombineering based approach for high-throughput conditional knockout targeting vector construction.* Nucleic Acids Res., 2007. **35**(8).
202. Copeland, N.G., N.A. Jenkins, and D.L. Court, *Recombineering: A powerful new tool for mouse functional genomics.* Nat. Rev. Genet., 2001. **2**(10): p. 769-779.
203. Haurogne, K., J.M. Bach, and B. Lieubeau, *Easy and rapid method of zygosity determination in transgenic mice by SYBR Green real-time quantitative PCR with a simple data analysis.* Transgenic research, 2007. **16**(1): p. 127-31.
204. Oetke, C., G. Kraal, and P.R. Crocker, *The antigen recognized by MOMA-I is sialoadhesin.* Immunology letters, 2006. **106**(1): p. 96-8.
205. Szymczak, A.L. and D.A. Vignali, *Development of 2A peptide-based strategies in the design of multicistronic vectors.* Expert opinion on biological therapy, 2005. **5**(5): p. 627-38.
206. Tang, W., et al., *Faithful expression of multiple proteins via 2A-peptide self-processing: a versatile and reliable method for manipulating brain circuits.* The Journal of neuroscience : the official journal of the Society for Neuroscience, 2009. **29**(27): p. 8621-9.

207. Donnelly, M., et al., *Analysis of the aphthovirus 2a/2B polyprotein 'cleavage' mechanism indicates not a proteolytic reaction, but a novel translational effect: a putative ribosomal 'skip'.* Journal of general Virology, 2001. **82**: p. 1013-1025.
208. Trichas, G., J. Begbie, and S. Srinivas, *Use of the viral 2A peptide for bicistronic expression in transgenic mice.* BMC Biology, 2008. **6**.
209. Shaner, N.C., et al., *Improved monomeric red, orange and yellow fluorescent proteins derived from Discosoma sp. red fluorescent protein.* Nature Biotechnology, 2004. **22**(12): p. 1567-1572.
210. Campbell, R.E., et al., *A monomeric red fluorescent protein.* Proceedings of the National Academy of Sciences of the United States of America, 2002. **99**(12): p. 7877-7882.
211. Hoshino, Y., et al., *Maximal HIV-1 replication in alveolar macrophages during tuberculosis requires both lymphocyte contact and cytokines.* Journal of Experimental Medicine, 2002. **195**(4): p. 495-505.
212. Van Keuren, M.L., et al., *Generating transgenic mice from bacterial artificial chromosomes: transgenesis efficiency, integration and expression outcomes.* Transgenic research, 2009. **18**(5): p. 769-85.
213. Watanabe, H., et al., *Innate immune response in Th1- and Th2-dominant mouse strains.* Shock, 2004. **22**(5): p. 460-6.
214. Matsuoka, Y., E.W. Lamirande, and K. Subbarao, *The mouse model for influenza.* Current protocols in microbiology, 2009. **Chapter 15**: p. Unit 15G 3.
215. Bouvier, N.M. and A.C. Lowen, *Animal Models for Influenza Virus Pathogenesis and Transmission.* Viruses, 2010. **2**(8): p. 1530-1563.
216. Grimm, D., et al., *Replication fitness determines high virulence of influenza A virus in mice carrying functional Mx1 resistance gene.* Proceedings of the National Academy of Sciences of the United States of America, 2007. **104**(16): p. 6806-11.
217. Tumpey, T.M., et al., *The Mx1 gene protects mice against the pandemic 1918 and highly lethal human H5N1 influenza viruses.* Journal of virology, 2007. **81**(19): p. 10818-21.
218. Ibricevic, A., et al., *Influenza virus receptor specificity and cell tropism in mouse and human airway epithelial cells.* Journal of virology, 2006. **80**(15): p. 7469-80.
219. Shinya, K., et al., *Avian flu: influenza virus receptors in the human airway.* Nature, 2006. **440**(7083): p. 435-6.
220. Shope, R.E., *The Infection of Mice with Swine Influenza Virus.* The Journal of experimental medicine, 1935. **62**(4): p. 561-72.
221. Majde, J.A., et al., *Detection of mouse-adapted human influenza virus in the olfactory bulbs of mice within hours after intranasal infection.* Journal of neurovirology, 2007. **13**(5): p. 399-409.
222. Subbarao, K., B.R. Murphy, and A.S. Fauci, *Development of effective vaccines against pandemic influenza.* Immunity, 2006. **24**(1): p. 5-9.
223. Charles A. Janeway, J., Paul Travers, Mark Walport, Mark Shlomchik ed. *Immunobiology, Sixth Edition*. 2005, Garland Science Publishing.
224. Barnard, D.L., *Animal models for the study of influenza pathogenesis and therapy.* Antiviral research, 2009. **82**(2): p. A110-22.

225. Bedoret, D., et al., *Lung interstitial macrophages alter dendritic cell functions to prevent airway allergy in mice.* The Journal of clinical investigation, 2009. **119**(12): p. 3723-38.
226. Seo, S.U., et al., *Type I interferon signaling regulates Ly6C(hi) monocytes and neutrophils during acute viral pneumonia in mice.* PLoS pathogens, 2011. **7**(2): p. e1001304.
227. Kowanetz, M., et al., *Granulocyte-colony stimulating factor promotes lung metastasis through mobilization of Ly6G+Ly6C+ granulocytes.* Proceedings of the National Academy of Sciences of the United States of America, 2010. **107**(50): p. 21248-55.
228. Tittel, A.P., et al., *Functionally relevant neutrophilia in CD11c diphtheria toxin receptor transgenic mice.* Nature methods, 2012. **9**(4): p. 385-90.
229. Quan, F.S., et al., *A bivalent influenza VLP vaccine confers complete inhibition of virus replication in lungs.* Vaccine, 2008. **26**(26): p. 3352-61.
230. Bosio, C.M. and S.W. Dow, *Francisella tularensis induces aberrant activation of pulmonary dendritic cells.* Journal of immunology, 2005. **175**(10): p. 6792-801.
231. Bowden, D.H. and I.Y. Adamson, *Role of monocytes and interstitial cells in the generation of alveolar macrophages I. Kinetic studies of normal mice.* Laboratory investigation; a journal of technical methods and pathology, 1980. **42**(5): p. 511-7.
232. Godleski, J.J. and J.D. Brain, *The origin of alveolar macrophages in mouse radiation chimeras.* The Journal of experimental medicine, 1972. **136**(3): p. 630-43.
233. Maus, U.A., et al., *Resident alveolar macrophages are replaced by recruited monocytes in response to endotoxin-induced lung inflammation.* American journal of respiratory cell and molecular biology, 2006. **35**(2): p. 227-35.
234. van oud Alblas, A.B. and R. van Furth, *Origin, Kinetics, and characteristics of pulmonary macrophages in the normal steady state.* The Journal of experimental medicine, 1979. **149**(6): p. 1504-18.
235. Coggle, J.E. and J.D. Tarling, *Cell kinetics of pulmonary alveolar macrophages in the mouse.* Cell and tissue kinetics, 1982. **15**(2): p. 139-43.
236. Bowden, D.H., *The alveolar macrophage.* Environmental health perspectives, 1984. **55**: p. 327-41.
237. Murphy, J., et al., *The prolonged life-span of alveolar macrophages.* American journal of respiratory cell and molecular biology, 2008. **38**(4): p. 380-5.
238. Herold, S., et al., *Lung epithelial apoptosis in influenza virus pneumonia: the role of macrophage-expressed TNF-related apoptosis-inducing ligand.* The Journal of experimental medicine, 2008. **205**(13): p. 3065-77.
239. Peper, R.L. and H. Van Campen, *Tumor necrosis factor as a mediator of inflammation in influenza A viral pneumonia.* Microbial pathogenesis, 1995. **19**(3): p. 175-83.

240. Karupiah, G., et al., *Identification of nitric oxide synthase 2 as an innate resistance locus against ectromelia virus infection.* Journal of virology, 1998. **72**(9): p. 7703-6.
241. Jayasekera, J.P., et al., *Enhanced antiviral antibody secretion and attenuated immunopathology during influenza virus infection in nitric oxide synthase-2-deficient mice.* The Journal of general virology, 2006. **87**(Pt 11): p. 3361-71.
242. Akaike, T. and H. Maeda, *Nitric oxide and virus infection.* Immunology, 2000. **101**(3): p. 300-8.
243. Davis, I. and S. Matalon, *Reactive species in viral pneumonitis: lessons from animal models.* News in physiological sciences : an international journal of physiology produced jointly by the International Union of Physiological Sciences and the American Physiological Society, 2001. **16**: p. 185-90.
244. Biesen, R., et al., *Sialic acid-binding Ig-like lectin 1 expression in inflammatory and resident monocytes is a potential biomarker for monitoring disease activity and success of therapy in systemic lupus erythematosus.* Arthritis and rheumatism, 2008. **58**(4): p. 1136-45.
245. Ashokkumar, C., et al., *Increased monocyte expression of sialoadhesin during acute cellular rejection and other enteritides after intestine transplantation in children.* Transplantation, 2012. **93**(5): p. 561-4.
246. Coombes, Janine L., et al., *Infection-Induced Regulation of Natural Killer Cells by Macrophages and Collagen at the Lymph Node Subcapsular Sinus.* Cell Reports, 2012.
247. McGill, J., J.W. Heusel, and K.L. Legge, *Innate immune control and regulation of influenza virus infections.* Journal of leukocyte biology, 2009. **86**(4): p. 803-12.
248. Brown, B.D. and L. Naldini, *Exploiting and antagonizing microRNA regulation for therapeutic and experimental applications.* Nature reviews. Genetics, 2009. **10**(8): p. 578-85.
249. Gentner, B., et al., *Identification of hematopoietic stem cell-specific miRNAs enables gene therapy of globoid cell leukodystrophy.* Science translational medicine, 2010. **2**(58): p. 58ra84.
250. Willinger, T., et al., *Improving human hemato-lymphoid-system mice by cytokine knock-in gene replacement.* Trends in immunology, 2011. **32**(7): p. 321-7.
251. Pearson, T., D.L. Greiner, and L.D. Shultz, *Humanized SCID mouse models for biomedical research.* Current topics in microbiology and immunology, 2008. **324**: p. 25-51.
252. Willinger, T., et al., *Human IL-3/GM-CSF knock-in mice support human alveolar macrophage development and human immune responses in the lung.* Proceedings of the National Academy of Sciences of the United States of America, 2011. **108**(6): p. 2390-5.
253. Daughety, T.W., et al., *The capacity of murine alveolar macrophages to stimulate antigen-dependent T-lymphocyte activation and proliferation.* Cellular immunology, 1983. **79**(2): p. 374-82.
254. Kirby, A.C., M.C. Coles, and P.M. Kaye, *Alveolar macrophages transport pathogens to lung draining lymph nodes.* Journal of immunology, 2009. **183**(3): p. 1983-9.

255. Chtanova, T., et al., *Dynamics of T cell, antigen-presenting cell, and pathogen interactions during recall responses in the lymph node.* Immunity, 2009. **31**(2): p. 342-55.
256. Scheu, S., P. Dresing, and R.M. Locksley, *Visualization of IFNbeta production by plasmacytoid versus conventional dendritic cells under specific stimulation conditions in vivo.* Proceedings of the National Academy of Sciences of the United States of America, 2008. **105**(51): p. 20416-21.
257. Spiteri, M.A., et al., *Alveolar macrophage-induced suppression of peripheral blood mononuclear cell responsiveness is reversed by in vitro allergen exposure in bronchial asthma.* The European respiratory journal : official journal of the European Society for Clinical Respiratory Physiology, 1994. **7**(8): p. 1431-8.

APPENDIX

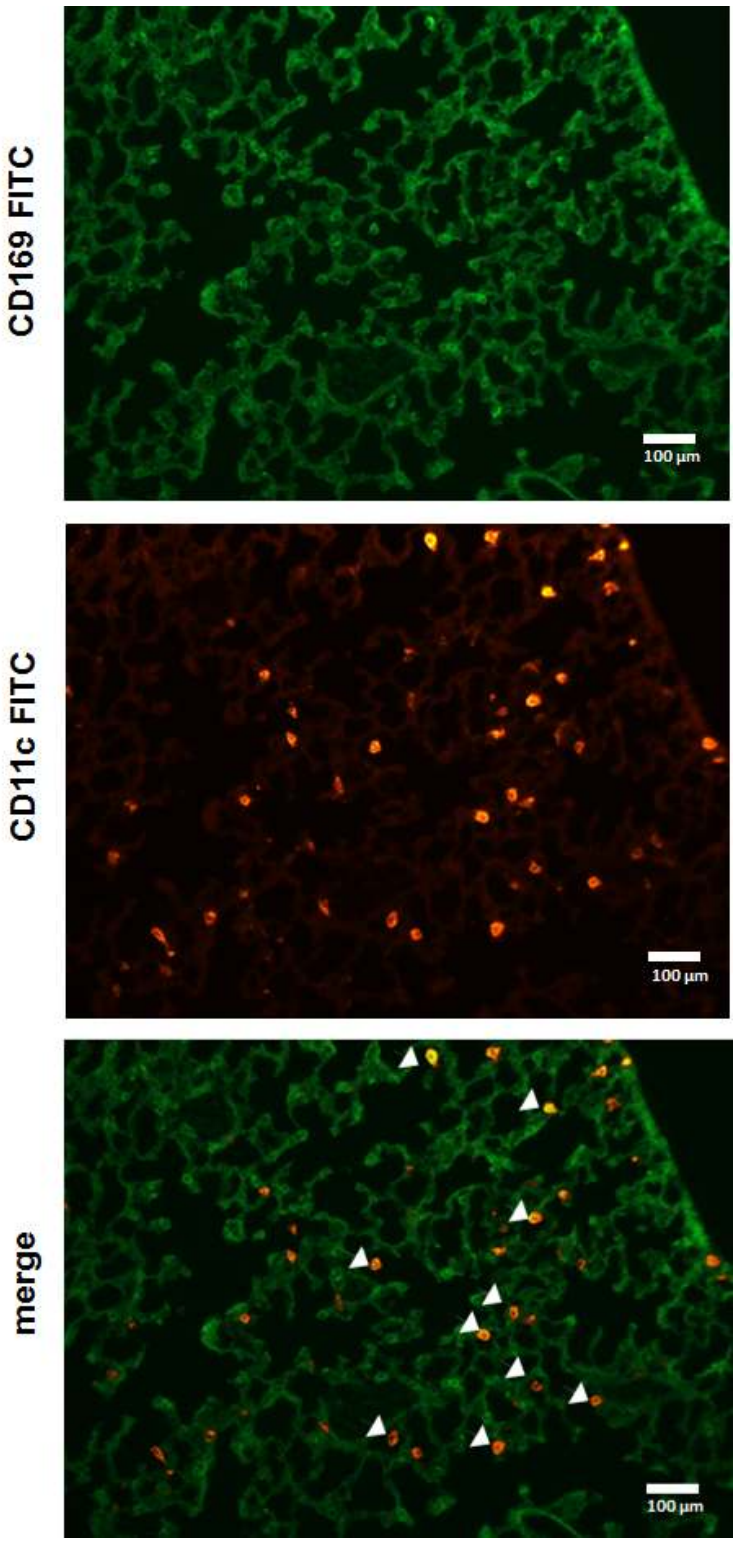

Appendix A. Alveolar Macrophages immunohistology in WT mice. Lungs were inflated with PBS/OCT (1:1) and were snap-frozen en bloc. Cryosections were performed and 6µm thick sections were fixed in acetone and then stained with antibodies against indicated markers.